An Evaluation of the Observational Capabilities of A Scanning 95-GHz Radar in Studying the 3D Structures of Marine Stratocumulus Clouds

Kevin Bowley

Master of Science

Supervised by Professor Pavlos Kollias

Department of Atmospheric and Oceanic Sciences

McGill University

Montreal, Quebec

2012

A thesis submitted to McGill University in partial fulfillment of the requirements of the degree of Master of Science

Acknowledgements

I would like to acknowledge all who have assisted me or lent support in the completion of this thesis. I first and foremost acknowledge the contibutions of my supervisor, Professor Pavlos Kollias, whose invaluable guidance to this project has been greatly appreciated. I also acknowledge Aleksandra Tatarevic and Ieng Jo for the processing and gridding of the scanning cloud radar data, and the sharing of their knowledge involving the techniques used. I would like to thank Dr. John Gyakum, Dr. Eyad Atallah, and Melissa Gervais for their assistance with edits, Jasmine Rémillard for translating my abstract into French, and Ariaan Purich for her assistance with LaTeX formatting. I was graciously provided funding from a Principal's Graduate Fellowship, and Provost's Graduate Fellowship, and the financial support of Professor Pavlos Kollias, for all of which I am most thankful. Finally, my most sincere thanks to my friends and family for all the support and for their patience when needed most.

Abstract

Marine stratocumulus clouds play a critical role in Earth's radiative balance primarily due to the role of their high albedo reflecting incoming solar radiation, causing a cooling effect, while weakly reflecting outgoing infrared radiation. Characterization of the 3-Dimensional (3D) structure of these cloud systems over scales of 20-40 km is required to accurately account for the role of cloud inhomogeneity and structure on their shortwave forcing and lifetime, which has important applications for Global Climate Models. For the first time, such 3D measurements in clouds were made available from a scanning cloud radar during the U.S. Department of Energy (DOE) Atmospheric Radiation Measurement (ARM) programs Clouds, Aerosol, and Precipitation in the Marine Boundary Layer (CAP-MBL) field campaign in the Azores Islands. The scanning radar observations were complemented by a suite of zenith-pointing active and passive remote sensors that were deployed to provide a detailed description of marine stratus over a long-term observation period in the ideal marine environment commonly found at the Azores. The scanning cloud radar observations present a shift from a multi-instrument, vertically pointing soda-straw observation technique to a radar-only, radar-centric observation technique. The scanning radar observations were gridded using a nearest-neighbor type scheme devised to take the natural variability of the observed field into account. The ability of the scheme to capture primary cloud properties (cloud fraction, cloud boundaries, drizzle detection) was assessed using measurements from the vertically pointing sensors. Despite the great sensitivity of the scanning cloud radar (-42.66 dBZ at 1 km range), the drop in sensitivity with range resulted in an artificial thinning of clouds with range from the radar. Drizzle-free cloud structures were undetectable beyond 5 km from the radar. Cloud fields containing drizzle were generally detectable to ranges exceeding 10 km from the radar. Well-defined streaking patterns in the drizzle field

(reflectivity greater than -15 dBZ) at cloud base were concluded to be concomitant with the formation of boundary layer rolls. Sounding data for these well-defined (unbroken) rolls revealed a mean sub-cloud layer wind exceeding 3.9 ms^{-1}, sub-cloud layer shear exceeding 7.5 x 10^{-3} s^{-1}, and a majority of streaks oriented within 20° of the mean sub-cloud layer wind, satisfying many boundary layer roll criteria proposed in past studies. Attempts to reconstruct the 3D cloud liquid water content and 2D column liquid water path across the scanning radar domain using Z (Reflectivity) vs. LWC (Liquid Water Content) regressions trained using the zenith measurements were proved ineffective due to the overall extent of drizzle at Graciosa, and errors associated with sensitivity loss at range. Despite some difficulties, the SWACR satisfied ARM metrics for success by proving effective at detecting weak clouds for extended time periods across a 10 km plane, and drizzle across a 20 km range, at high spatial resolutions. Difficulties in resolving accurate vertical velocity patterns also suggest the need for an adaptive sampling strategy to most effectively remove horizontal wind components.

Résumé

Les nuages stratocumulus marins jouent un rôle essentiel dans l'équilibre radiatif de la Terre en raison, principalement, de leur albédo élevé réfléchissant le rayonnement solaire, provoquant un effet de refroidissement, tout en ayant peu d'effet thermique. La caractérisation de la structure tridimensionnelle (3D) de ces systèmes nuageux sur des échelles de 20-40 km est requise pour tenir compte, avec exactitude, du rôle de l'hétérogénéité et de la structure des nuages sur leur forçage dans les ondes courtes et leur cycle de vie, ce qui a des applications importantes pour les modèles climatiques globaux. Pour la première fois, de telles mesures 3D dans les nuages ont été rendues disponibles grâce à un radar de nuages à balayage (le SWACR) pendant la campagne de terrain dans les Açores ≪ Clouds, Aerosol, and Precipitation in the Marine Boundary Layer ≫ (CAP-MBL) du programme ≪ Atmospheric Radiation Measurement ≫ (ARM) du ≪ Department of Energy ≫ (DOE) américain. Les observations du radar à balayage ont été complémentées par une suite dinstruments de télédétection actifs et passifs pointant vers le zénith ayant été déployée pour fournir une description détaillée des stratus marins au cours d'une longue période d'observation dans l'environnement marin idéal couramment trouvé dans les Açores. Les observations du radar de nuages à balayage présentent le passage d'une technique d'observation ≪ paille ≫, utilisant plusieurs instruments pointant verticalement, à une technique d'observation ≪ radar-centrique ≫, utilisant uniquement un radar. Les observations du radar à balayage ont été quadrillées en utilisant une technique du plus proche voisin conçue pour prendre en compte la variabilité naturelle du champ observé. La capacité du régime à capturer les propriétés primaires des nuages (fraction nuageuse, limites des nuages, détection de bruine) a été évaluée en utilisant les mesures des détecteurs pointant verticalement. Malgré la grande sensibilité du radar de nuages à balayage (-42,66 dBZ à une distance de 1 km), la diminution de la

sensibilité avec la distance a entraîné un amincissement artificiel des nuages avec la distance du radar. Les structures nuageuses sans bruine étaient indétectables au delà de 5 km du radar. Les domaines de nuages contenant de la bruine étaient généralement détectables à des distances excédant 10 km du radar. Des stries bien définies dans le domaine de bruine (réflectivité (Z) supérieure á -15 dBZ) á la base des nuages ont été associées avec la formation de rouleaux dans la couche limite. Des données de sondage pour ces rouleaux bien définis (ininterrompus) ont révélé un vent moyen dans la sous-couche nuageuse dépassant 3,9 ms^{-1}, un cisaillement dans la sous-couche nuageuse supérieur à 7,5 x 10^{-3} s^{-1} et une majorité des stries orientées dans les 20° du vent moyen de la sous-couche nuageuse, satisfaisant de nombreux critères des rouleaux de couche limite proposés dans des études antérieures. Les tentatives visant à reconstruire la teneur 3D en eau liquide (LWC) et la colonne 2D d'eau liquide des nuages dans le domaine du radar à balayage utilisant des régressions de Z vs LWC formées à partir des mesures en zénith se sont avérées inefficaces en raison de l'étendue générale de la bruine sur Graciosa et les erreurs associées à la perte de sensibilité avec la distance. Malgré quelques difficultés, le SWACR satisfait les métriques de réussite de ARM en s'avérant efficace pour détecter les nuages faibles pendant de longues périodes à travers un plan de 10 km et la bruine sur une distance de 20 km, à haute résolution spatiale. Des difficultés à résoudre les structures précises de vitesse verticale suggèrent également la nécessité d'une stratégie d'échantillonnage adaptatif pour éliminer plus efficacement les composantes du vent horizontal.

Table of Contents

List of Tables

List of Figures

Chapter 1
Introduction

Marine stratocumulus clouds have a major impact on Earths climate, especially on the net radiative energy budget due to an enhanced shortwave albedo effect as compared with ocean surface albedo values (Ramanathan et al. 1989; Harrison et al. 1990; Klein and Hartmann 1993). These low-level stratiform clouds are seasonally prevalent in the eastern basins of large oceanic regions, where the combination of low sea-surface temperatures due to oceanic upwelling and large-scale synoptic subsidence from subtropical high-pressure systems results in ideal (statically-stable) conditions for stratocumulus formation (*Figure 2.1*; Klein and Hartmann (1993)). Their high shortwave albedo, near surface cloud layer temperature, and large area of coverage in the subtropical oceans make marine stratocumulus clouds one of the most important cloud types in terms of a net cooling-effect on the atmosphere.

Although synoptic-scale meteorology can explain a large percent of the variance associated with the frequency of occurrence, overall persistence, and cloud fraction of marine stratocumulus (Wood and Bretherton 2006), cloud-scale processes still play a critical role in the determination on the microphysical and radiative properties of marine stratocumulus. The 3-Dimensional (3D) characterization of the cloud structure and dynamics over a large domain (e.g. 20-40 km) of marine stratocumulus can provide insights on the complex interplay of microphysics, dynamics and radiation at cloud-scales. For example, cloud inhomogeneity can have a significant impact on the shortwave forcing of stratocumulus clouds. Furthermore, mesoscale organization (e.g., open cellular convection) can affect the lifecycle of these cloud systems (e.g., Stevens et al. (2005)). Thus, to provide more realistic future

climate simulations, a 3D documentation of the cloud structure is needed to accurately account for these processes and represent them in Global Climate Models (Harrison et al. 1990).

The development of short-wavelength radars and their synergistic use with other sensors during the last 20 years has improved our ability to study cloud structure (Kropfli and Hildebrand 1980; Clothiaux et al. 1995; White et al. 1996; Moran et al. 1998; White et al. 2000; Wang and Geerts 2003; Kollias and Albrecht 2000; Kollias et al. 2007, 2011). These observational studies utilize millimeter wavelength radars that are used in a profiling mode due to their sensitivity to small cloud droplets, and their high-resolution measurements are supplemented by additional observations from microwave radiometers and lidars. Such synergistic column measurements are the signature of the US Department of Energy (DOE) Atmospheric Radiation Measurement (ARM, www.arm.gov) program. However, the characterization of the 3D cloud structure requires a scanning sensor, a limitation of prior vertically point instruments. One such cloud radar system is the Scanning W-Band ARM Cloud Radar (SWACR). The use of scanning cloud radars for marine stratocumulus studies represents a shift in the approach to surface-based radar cloud studies, from a multi-instrument single column technique to a radar-centric 3D observational strategy. However, the spatial increase of the observational domain (1D to 3D) brings several challenges associated with the objective determination of cloud structure properties, such as cloud fraction and cloud boundaries, due to the decrease in radar sensitivity and resolution with range. These challenges can directly conflict with the ARM-determined metrics of success for cloud radars, in which a radar should exhibit excellent sensitivity to detect weak clouds and should demonstrate high reliability for long-term, unattended operations (Moran et al. 1998).

The purpose of this study is to assess these challenges using SWACR observations collected in November 2009 during the ARM Mobile Facility (AMF) deployment at Graciosa

Island, Azores for the study of marine stratocumulus clouds. The SWACR observations are compared against the observations from a collocated vertically pointing radar (W-band ARM Cloud Radar, WACR), and we assess the ability of the gridded scanning cloud radar observations to represent the measured cloud properties such as reflectivity, cloud fraction, and cloud boundaries in the 3D gridded domain. The ability to document some of these basic properties is key to demonstrating the ability of the instrument to document weak clouds for an extended observation period. Furthermore, as a first application of such measurements, the ability of the SWACR to document roll-like structures in the boundary layer cloud field is demonstrated. Finally, the shortcomings of this new radar system are discussed to understand the present limitations of the SWACR.

Chapter 2
Background

2.1 Previous Observations of Marine Stratocumulus Clouds

Several field campaigns have focused on the study of marine stratocumulus. During June and July of 1987, the First International Satellite Cloud Climatology Project Regional Experiment (FIRE) was conducted in the northeastern Pacific basin, using satellite, aircraft, and surface instruments to provide the first field-based stratocumulus study for analysis (Albrecht et al. 1988). The first Atlantic-based stratocumulus field study, the Atlantic Stratocumulus Transition Experiment (ASTEX), was conducted in June 1992 with the goal of documenting the transition from marine stratocumulus clouds to fair weather cumulus clouds (Albrecht et al. 1995a). Both of these campaigns primarily focused on building a dataset that expanded from the cloud-scale up to the grid spacing of a GCM model (Albrecht et al. 1995a). These two campaigns were similar in many facets of their experimental approach; however they sampled two distinctly different cloud regimes, with FIRE documenting a more continuous unbroken cloud field while ASTEX experienced a more broken cloud field (Albrecht et al. 1995a).

Following ASTEX, the focus of marine-stratocumulus field campaigns shifted to the eastern Pacific basin. The aircraft-based Dynamics and Chemistry of Marine Stratocumulus II (DYCOMS-II) campaign in July 2001 consisted of nine flights through nearly uniform cloud fields off the California coast (vanZanten et al. 2005). During October 2001, the Eastern Pacific Investigation of Climate (EPIC) project targeted the physical processes of coupled atmosphere-ocean interactions in the tropical eastern Pacific basin. The specific goal of the

EPIC field project, amongst other scientific objectives, was to use ship and surface observations to determine the impacts of the planetary boundary layer on stratocumulus albedo (Bretherton et al. 2004). The installation and maintenance of the Stratus Ocean Reference Station (Stratus ORS) in the southeast Pacific resulted in Pan American Climate Studies (PACS) research cruises through regions of dense stratocumulus in 2003 and 2004 (Kollias et al. 2004; Serpetzoglou et al. 2008). These three campaigns (EPIC 2001, PACS 2003, and PACS 2004) utilized several instruments to study marine stratocumulus off the South American coast including but not limited to millimeter wavelength cloud radars, microwave radiometers, laser ceilometer, and wind profilers (Serpetzoglou et al. 2008).

Despite the multitude of field studies over the past two decades focusing on marine stratocumulus clouds, little focus has been put on the eastern Atlantic basin, where daytime marine stratocumulus make up roughly 23% of the annual cloud type (*Figure 2.1*).

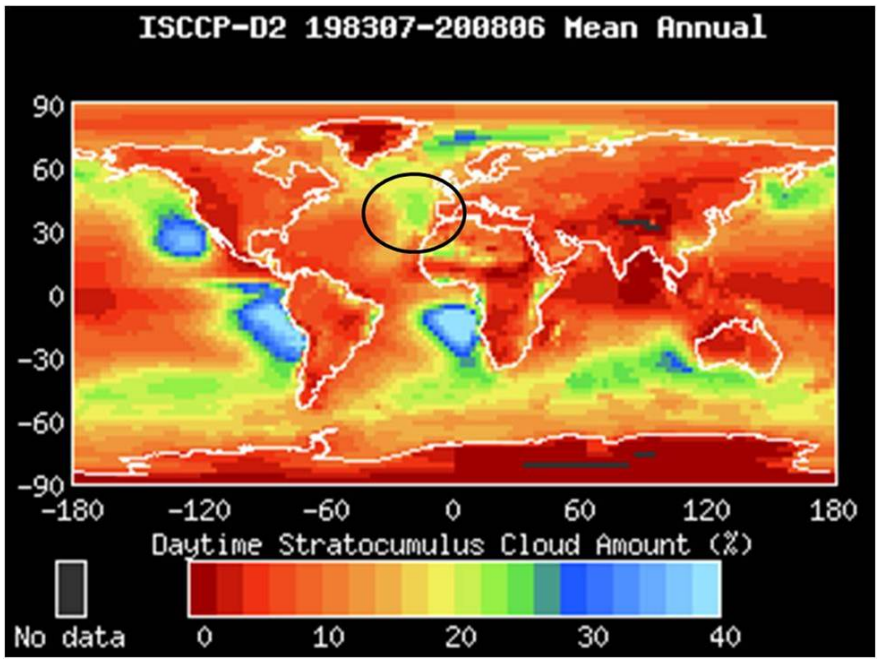

Figure 2.1: ISCCP-D2 July 1983-June 2008 global annual mean daytime stratocumulus cloud percentage. Outlined circle highlights the region around the Azores island chain. (isccp.giss.nasa.gov).

Although the Azores island chain is located in an ideal region for stratocumulus formation (Klein and Hartmann 1993), the ASTEX campaign has been the only major field study to focus on these clouds far offshore (Albrecht et al. 1995a). In addition, the majority of field projects have focused predominantly on understanding unbroken stratocumulus cloud fields, while little has been done to understand broken stratocumulus decks and deep marine boundary layers (Albrecht et al. 1995a). Also, previous campaigns have been relatively short-lived, spanning only 2-4 weeks, which does not lend well to statistically robust climatological studies.

2.2 Profiling cloud radar measurements of marine stratocumulus clouds

Vertically pointing millimeter cloud radars have been demonstrated to be able to successfully measure cloud properties and to better understand the dynamics of clouds throughout the troposphere (e.g. Clothiaux et al. (1995); Kollias and Albrecht (2000); Serpetzoglou et al. (2008); Kollias et al. (2007)). In a profiling configuration, cloud radars are often coupled with other vertically pointing instruments, such as lidars and microwave radiometers, in a synergistic manner to better understand the hydrometeor distribution in the overlaying atmospheric column. The study of clouds with either stand-alone vertically pointing cloud radars or multi-instrument approaches has resulted in a strong enhancement in our understanding of cloud dynamics and microphysics. One prime example of such facilities is the US DOE ARM program (Stokes and Schwartz 1994; Ackerman and Stokes 2003).

Several efforts have been made to improve the ability of cloud radars to document weak clouds for extended observation periods. Clothiaux et al. (1995) describes a 94-GHz vertically-pointing cloud radar with a 0.24° beamwidth and demonstrated a minimum detectable signal (MDS) of -50 dBZ at 1 km away from the radar assuming no atmospheric attenuation gases or other particles. Moran et al. (1998) describes the performance of the first

generation ARM 35-GHz millimeter cloud radar (MMCR). This radar has a 0.2° beamwidth and a 45-90 meter gate-spacing resolution. The radar is operated in 4 observation modes, resulting in unambiguous ranges of 18.9 km to 10.8 km, and MDSs ranging from -47 dBZ to -30 dBZ at 5 km, respectively. Recently, a 95-GHz radar developed in Japan demonstrated a very high spatial resolution with a 0.2° beamwidth and 9 m gate-spacing resolution, and a 5 km MDS of -34 dBZ (Takano et al. 2010). The aforementioned ground-based profiling systems have typical characteristics of cloud radars: higher frequency systems devised to have greater sensitivity to cloud particles, relatively high-resolution gate spacing with a narrow beamwidth and robust operations that make them suitable form long-term cloud and precipitation observations (Kollias et al. 2007).

Cloud radars, with a sensitivity of -50 to +20 dBZ, afford the ability to study a range of atmospheric phenomena including clouds, drizzle, and light precipitation (Kollias et al. 2005). The most important macroscopic cloud measurement is the cloud fraction. In column measurements, the cloud fraction is defined as the fractional occurrence of cloud detection over a fixed time period of observations (typically one hour intervals). The cloud fraction of marine stratocumulus is integral to understanding their impact on Earths radiation budget (Albrecht 1989). Clothiaux et al. (1995) showed that key cloud boundaries and parameters are detectable using millimeter cloud radars, essential for the computation of cloud fraction. The ASTEX campaign focused on several different cloud regimes: for marine stratocumulus, a campaign cloud fraction of 0.83 was measured, while for the transition of stratocumulus to fair weather cumulus, a cloud fraction of 0.4-0.67 was measured (Albrecht et al. 1995b). EPIC 2001 documented diurnal variations in fractional cloudiness, with cloud fraction statistically varying between 0.65 during the day to 1.0 at night (Bretherton et al. 2004). During the PACS 2003 cruise, Kollias et al. (2004) documented a cloud fraction of 0.8 using a laser

ceilometer, while measuring a cloud fraction of 0.68 using an 8.6 mm cloud radar.

Another important parameter in marine stratocumulus derived from radars is the measurement of drizzle, defined qualitatively through the use of a radar reflectivity threshold and quantitatively in terms of rain rate (Sauvageot and Omar 1987; Albrecht 1989; Fox and Illingworth 1997; vanZanten et al. 2005). Using data from the CALIPSO satellite observation system, Leon et al. (2008) suggest drizzle occurs near the Azores in the North Atlantic 37% of the time, suggesting the likelihood of drizzle in the Azores region. Several column techniques have been used in an attempt to adequately identify drizzle in radar measurements of stratocumulus clouds mainly through the use of a radar reflectivity (dBZ) threshold. Several values have been proposed: -20 dBZ (Frisch et al. 1995), -18 dBZ (Wang and Geerts 2003; Leon et al. 2008), -15 dBZ (Sauvageot and Omar 1987; Löhnert et al. 2001), and -14 dBZ (Kollias et al. 2004). The lack of agreement on a radar reflectivity threshold is likely due to varying cloud properties (e.g. total number concentration of cloud droplets, see Liu et al. (2008)). In addition to reflectivity thresholds, the presence of radar echoes below the ceilometer-defined cloud base is often used as an indicator of drizzle presence. Identification of drizzle is important, as a primary drawback of cloud radars is that they suffer from significant attenuation associated with atmospheric gases and hydrometeor, leading to substantial attenuation of the radar signal in certain situations (Clothiaux et al. 1995).

Though cloud radars offer several advances over other instruments with regard to cloud observations, there are also disadvantages associated with their application to cloud research. In addition to the issues addressed above with a radar reflectivity threshold for identifying drizzle, vertically-pointing radars are well documented in losing a sensitivity to cloud base in cases of precipitation (Clothiaux et al. 1995). Radar measurements are more sensitive

to large droplets than small droplets by the D^6 relationship, where D is the droplet diameter. In the case of droplets falling below cloud base, the radar-indicated cloud base will routinely be lower than the actual cloud base. In addition, sensitivity loss with range leads to a lack of sensitivity to weak radar returns at range (Clothiaux et al. 1995). These two distinct problems are the backbone behind why a multi-instrument approach has been used for cloud studies involving cloud radars, and must be addressed when considering the shift to a radar-centric scanning observation technique.

2.3 Scanning cloud radar observations

The shift toward 3D cloud radar observations offers the potential for key improvements in our existing knowledge on cloud structure and cloud lifetime. Cloud variability provides key details to the radiative characteristics of a marine stratocumulus cloud; broken clouds will have different influences on the radiative budget when compared to a continuous cloud field. Previous studies have utilized the high temporal resolution provided by static vertically pointing radars. However, these studies, having utilized satellites and vertically pointing cloud radars in an attempt to understand cloud structures and variability, are limited by spatial resolution and spatial extent, respectively.

Historically, applications of scanning atmospheric radars have come primarily from the weather research community and focused on longer wavelength radars (Baeck and Smith 1998; Keenan 2003; Harrison et al. 2000; White et al. 1996, 2000; Anagnostou et al. 2001). Longer wavelength radars offer a great range of spatial observation, and due to their longer wavelength, are substantially less attenuated by precipitation. Two scanning patterns that are commonly utilized by scanning weather radars are the Plan Position Indicator (PPI) pattern and the Range Height Indicator scan (RHI). A PPI scans with a varying azimuth angle (between 1° and 360°) while holding a constant elevation angle, and continues these

azimuthal scans over several different elevation angles. An RHI scan, on the other hand holds a constant azimuth angle, while increasing the elevation angle (between 1° and 180°). The advantage of this scanning technique is that it does not have the low temporal frequency needed to fill a full volume of measurements (e.g. Baeck and Smith (1998); Harrison et al. (2000); Keenan (2003)), but instead scans along a single azimuth from near horizon to near horizon, resulting in a high temporal and spatial frequency. In addition, the issues caused by data gaps between elevation scans (Baeck and Smith 1998) are generally not applicable given the nature of the scan pattern. These gaps can pose great challenges in the development of 3D gridded cloud radar observation since clouds are often limited in vertical extent.

As a result, RHI-based volume scan strategies were preferred during the SWACR deployment at Graciosa. This pattern, repeated over a 5-60 minute period, provided a gain over the snapshot-type temporal resolution obtained by most low earth orbit satellites. By adding a scanning capability, the observed data from the radar offers greater potential toward understanding the variability of cloud features over a plane while retaining many of the radar characteristics of the W-Band ARM Cloud Radar (Widener and Johnson 2006). In doing so, the high radar sensitivity to small targets and high spatial resolution remains similar to those of prior cloud radars (e.g. Clothiaux et al. (1995); Moran et al. (1998); Takano et al. (2010)), key for detecting smaller clouds. Despite the radar system still being subject to atmospheric attenuation issues due to the choice in wavelength (95 GHz), and the prevalent issue of cloud base biasing by drizzle and large particles below cloud base, the SWACR utilizes some of the more ideal characteristics of many scanning and vertically-pointing radars to provide a new and unique view of the cloud field.

The SWACR was developed to deal with some of the instrumental limitations associated with scanning long wavelength radars, vertically pointing short wavelength radars,

and satellite-borne radars and remote sensors. To test whether the SWACR successfully addressed the shortcomings of other observational systems, and to understand the limitations of the instrument itself, we studied the ability of the radar to document cloud structures across the observational domain. In particular, determining the ranges to which the instrument can accurately document cloud properties is essential to understanding the advantages provided by the scanning radar over a vertically pointing system such as the WACR. Demonstrating the ability to accurately document cloud boundaries and fractional cloudiness at range is one of the principal goals of this new instrument, and as such it is the primary focus of this study. Furthermore, some of the primary drawbacks of satellite-based observation systems (temporal resolution), vertically-pointing cloud radar systems (spatial range), and scanning weather radar systems (sensitivity to small targets) were addressed by examining the ability of the SWACR to document cloud and drizzle properties across a 20 km plane for an extended period of time. By first understanding the ability of the SWACR to overcome the some of the limitations of other remote sensing platforms, we can identify specific experiments that best utilize the instrument, such as studying boundary layer cloud and drizzle properties, and the mapping of cloud liquid water properties.

2.4 Boundary Layer Rolls and Associated Cloud Structures

The organization of vertical motions into organized rolls or streaks in the planetary boundary layer (PBL) is considered to be a function of two primary mechanisms: convective instability and dynamic instability (e.g. Kuettner (1971); LeMone (1973); Brown (1980)). Instances of pure convective instability, wherein there is a thermal instability within the PBL, have been shown to result in convective roll circulations that are close to parallel with the mean flow in the PBL (Brown 1980). In a static environment, Rayleigh-Benard convective cells have been demonstrated to form, which tend to align in a 2D roll-pattern when perturbed by the mean flow in the PBL (Kuettner 1971; Brown 1980). Instances

of pure dynamic instability can also lead to the formation of rolls. Rolls formed through dynamic instability are associated with regions of relatively strong shear, where localized maxima in vorticity can result in positive and negative perturbations in the vertical velocity field (Brown 1980). Brown (1980) also demonstrated the importance of the type of shear involved, wherein pure speed shear results in Kelvin-Helmholtz waves with cloud rows orientated perpendicular to the wind, pure rotational shear results in Faller-Lilly Ekman layer instabilities and Keuttner cloud streets oriented parallel to the mean PBL flow, and mixed (speed and rotational) shear results in a solution between the two extremes. Observed rolls in the atmosphere are often, but not always, a conglomerate of both effects (e.g. Kuettner (1971); LeMone (1973); Brown (1980)). The rolls tend to form into counter-rotating helical rolls, oriented in such a manner that the updraft region of one roll will interact with the updraft region of the roll paralleling it, and vice versa (e.g. LeMone (1973); Brown (1980); Schumann and Moeng (1991)).

Boundary layer rolls have been well documented using a variety of observational platforms including radars (surface, airborne, and satellite), wind profiling towers, and satellite observations. These studies have generally been devised to determine the atmospheric thermodynamic and dynamic variables that can be used to characterize the likelihood of streak phenomena occurring. These characteristic factors include, but are not limited to, roll alignment with PBL winds, strength of shear in the PBL, and the aspect ratio (AR) of roll wavelength to PBL depth. Additional theoretical studies have been conceived to further test these variables in a controlled model environment. LeMone (1973) documented roll structures situated between -5° and 19° (+/- 10°) to the left of the mean geostrophic wind in the PBL using tower wind observations coupled with aircraft data. In addition, LeMone (1973) noted an AR of roughly 3:1 with wind speeds exceeding 7 ms^{-1}. Utilizing dual-Doppler snapshots of the PBL along with surface observations, Frisch et al. (1976) documented PBL

rolls and their corresponding surface pressure perturbations moving with the same speed and direction of the mean flow within a 5 km x 5 km x 1 km domain. Using X-Band and C-Band radars situated in a tri-doppler orientation measuring chaff, Kropfli and Hildebrand (1980) documented clear-air roll alignments that were roughly aligned with the 3 ms-1 horizontal flow, with an AR of roughly 3:1. Wackerman et al. (1996) utilized the ERS-1 Synthetic Aperture Radar (SAR) system to document cloud rows in associated with wind rolls in the PBL over the ocean. The updraft/downdraft structure of these rolls often can lead to momentum transfer to the sea surface, which essentially roughens the sea surface when strong enough. These perturbations to the background sea surface can be documented by SAR algorithms, allowing the identification of streak structures in the PBL. Using these rows, they were able to estimate the surface wind direction within 11° (+/- 19°) of wind rows measured on the sea surface. Two surface radars, two aircraft, and several other surface-based instruments were used as part of the Convection and Precipitation/Electrification (CaPE) project to document a correlation factor of greater than 0.95 between the mean wind direction and roll orientation, while a required PBL mean speed of 5.5 ms^{-1} and shear of 2 x 10^{-3} s^{-1} was needed for roll formation (Weckwerth et al. 1997). Using surface and airborne Doppler radar measurements in the Turbulence Radar Aircraft cells (TRAC) experiment, Lohou et al. (1998) remarked that roll vorticies measured in the experiment were roughly aligned with the mean PBL wind. Zecchetto et al. (1998) used an airborne SAR over the northern Adriatic Sea to document a SAR wind row that was roughly 10° offset from the mean surface wind direction, while experiencing a mean surface wind speed of 3.8 ms^{-1} and an average sea temperature 4° C warmer than the average air temperature.

It can generally be summarized that longitudinal rolls in the PBL are often aligned within 5° to 20° of different layer winds in the PBL, though the mean wind throughout the layer is often used for comparison. In addition, rolls tend to align when the layer wind speed

exceeds 3.5 ms^{-1}, and there is some component of surface instability occurring at the surface. These studies, however, were often limited by the observational capabilities of the platforms used, including short temporal durations (flight and satellite-based projects), sensitivity to boundary layer cloud motions (non-cloud scanning radars), and difficulties in retrievals from oceanic conditions (SAR-based studies). The ability of the SWACR, with high sensitivity to cloud and drizzle targets, to scan across a 20km horizontal plane in the boundary layer for an extended period of time makes it an ideal instrument for addressing the shortcomings of previous boundary layer roll experiments.

Chapter 3
Methodology

3.1 The CAP-MBL Field Campaign at Graciosa Island, Azores

The US Department of Energy (DOE) Atmospheric Radiation Measurements (ARM) program is part of one of the worlds largest climate research programs. Its primary mission is to better the understanding of the influence of clouds on the environment and in particular the role of cloud radiative feedbacks in the climate system, in hopes of improving model parameterization schemes (Stokes and Schwartz 1994; Ackerman and Stokes 2003). The primary ARM observations are conducted at climate research facilities that use a combination of active and passive sensors to provide a comprehensive view of the atmospheric column over the ARM sites. The ARM sites are a combination of permanent long-term observation sites and temporary field campaign sites, and are located at many strategic locations worldwide. The ARM program has targeted the Azores region as a potential area of long-term study as far back as the early 1990s (Stokes and Schwartz 1994), with the goal of creating a surface-based observation site to study marine stratus clouds throughout the year. From April 2009 to December 2010, the ARM program finally realized this goal by deploying one of its ARM Mobile Facilities (ARM) at Graciosa Island in the Azores island chain (29° 5' 28"N, 28° 1' 45"W). The deployment was part of the ARM Clouds, Aerosol, and Precipitation in the Marine Boundary Layer (CAP-MBL) field campaign. The location was selected for its frequent occurrence of low marine stratocumulus clouds, and the pristine environment offered by its distance from Europe and North America. In addition, the islands small profile was chosen to reduce land effects as much as possible, with the goal of sampling a pristine

oceanic environment (Wood 2009).

3.2 Instrumentation

The underlying goal of the campaign was to construct a detailed climatology of cloud and precipitation structure in low clouds using a variety of remote and in-situ instruments. It involved over 15 active and passive remote sensing instruments, including the first Scanning W-Band ARM Cloud radar (SWACR). This instrument, along with the W-Band ARM Cloud Radar (WACR), Vaisala Ceilometer, and the Balloon-Borne Sounding System (SONDE), were the primary instruments used in this study.

3.2.1 Scanning W-Band ARM Cloud Radar

The SWACR is one of the latest additions to the ARM cloud radar array, and was first deployed for research purposes in October 2009 at Graciosa Island (*Figure 3.1*).

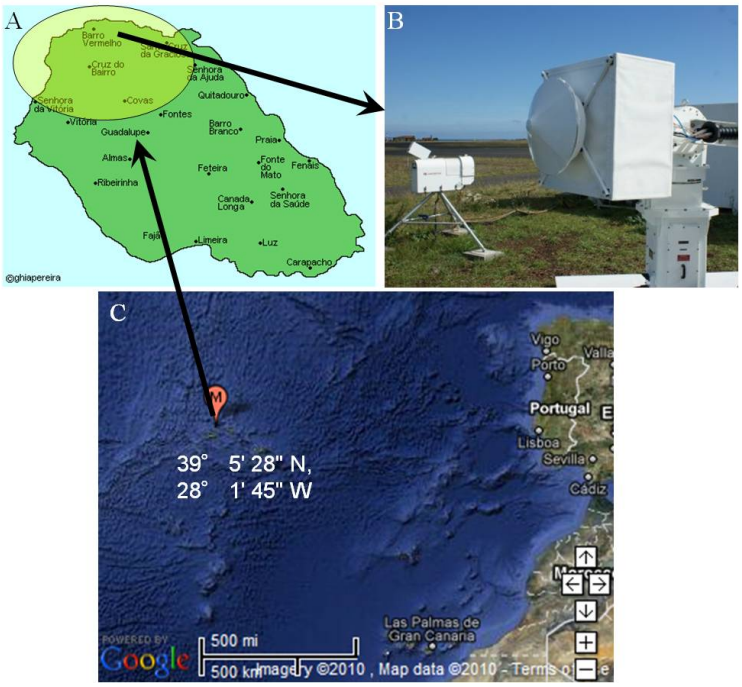

Figure 3.1: Location of the ARM AMF-GRW Field Campaign at Graciosa Island, Azores (a,b), along with the Scanning W-Band ARM Cloud Radar (SWACR)(c). (www.arm.gov)

This 95 GHz (3 mm) radar was used in a variety of scanning strategies, of which the cross-wind range height indicator (CW-RHI) was used for this study. The antenna beamwidth of the SWACR is 0.4° and the scan rate is 6-12 degrees per second. Owing to the narrow beamwidth of the SWACR, a volumetric scanning strategy based on a series of PPI scans at different elevations will lead to large vertical gaps. In particular, the SWACR scan strategy used in this study is a cross-wind RHI scanning pattern. The CW-RHI scanning strategy was designed such that the radar scans perpendicular to the wind; for the Graciosa Island campaign, an estimated climatological wind of 315° (NW) was used. This resulted in a near-horizon to horizon scanning pattern, with scans following a plane from 225° (SW) to 45° (NE), which was repeated for a 5-60 minute period. When compiled together over time, this results in a zigzag-type pattern (*Figure 3.2*), where the maximum distance between scan-to-scan points at the same range from the radar (*Figure 3.2*, vector a) varies depending on the horizontal component of the mean in-cloud wind. The scan-to-scan distances are compiled in Table 1, where the distances at 21 km (*Figure 3.2*, vector a) can be up to 560 meters apart for a 28 second scanning strategy in a 10 ms^{-1} wind.

Wind Speed	**A (56 sec)**	**B (36 sec)**	**C (28 sec)**	**D (20 sec)**	**E (0.5 sec)**
5 m/s	280 m	180 m	140 m	100 m	2.5 m
10 m/s	560 m	360 m	280 m	200 m	5 m
15 m/s	840 m	540 m	420 m	300 m	7.5 m
20 m/s	1120 m	720 m	560 m	400 m	10 m
25 m/s	1400 m	900 m	700 m	500 m	12.5 m
30 m/s	1680 m	1080 m	840 m	600 m	15 m

Table 1: Distances for vectors a-e in SWACR schematic cross-wind scanning strategy for ARM-GRW Field Campaign, Graciosa Island, Azores. Distances are determined from average time between radar beam passage over a point n-distance from the radar, and multiplied by an average wind speed.

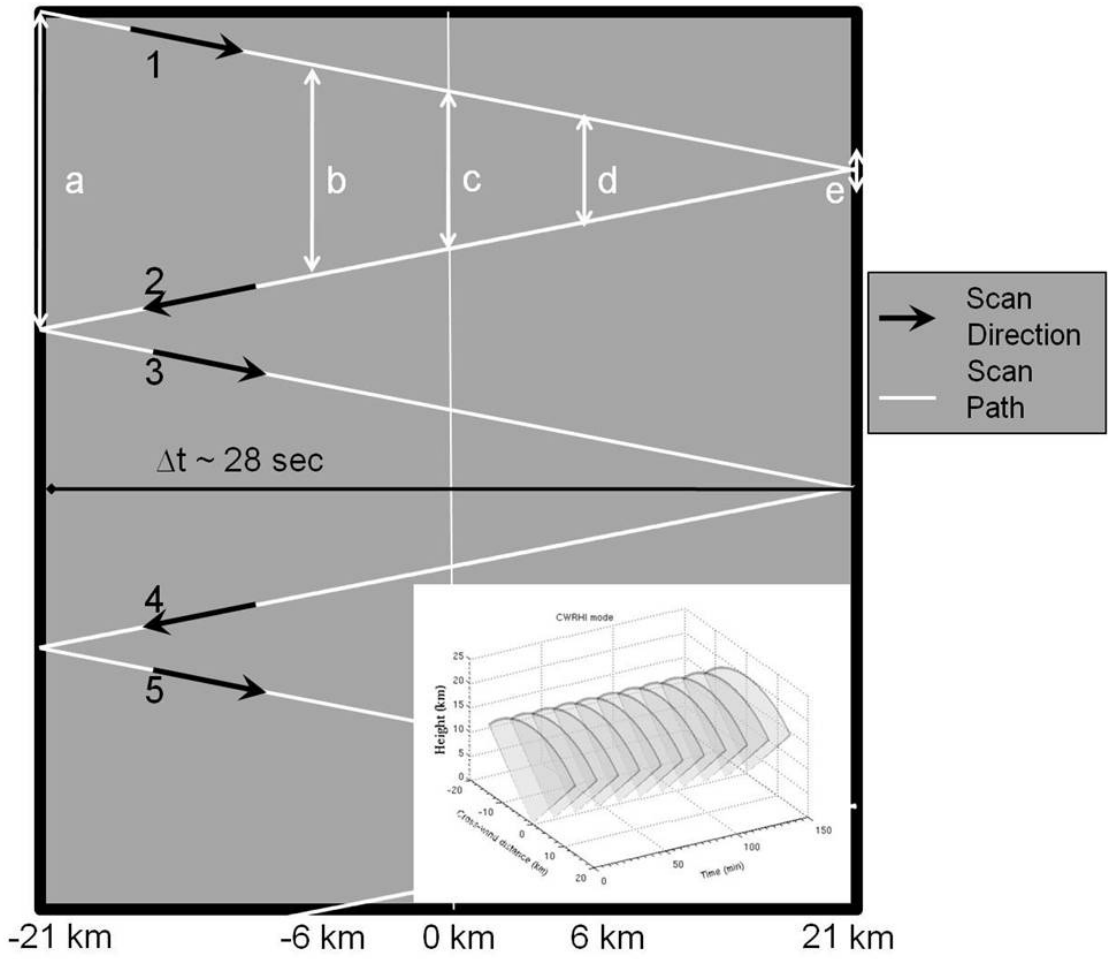

Figure 3.2: Sample schematic SWACR Cross-Wind range height indicator scanning strategy utilized during ARM-GRW Field Campaign. Distances for a-e for a given mean wind speed are provided in table 1.

In this campaign, the repeat time at zenith (*Figure 3.2*, vector c) for the radar is 28-29 seconds, with the maximum time gap between back-to-back scans around 56 seconds (*Figure 3.2*, vector a), and as short as near-instantaneous at range maxima (*Figure 3.2*, vector e). Using the Signal-to-Noise Ratio (SNR) measurements of the radar at each range-gate (the range-gate estimate of the noise is based on Fast Fourier Transform (FFT) processing), a baseline for radar receiver noise generated by the radar is estimated and used to determine SWACR range gates with hydrometeors (Clothiaux et al. 1995). In addition, the same SNR

measurements were used to find potential floating points, or measurements that did not make physical sense given their location in the radar volume because of their isolated nature; these points were also removed from the data. Such points potentially included ground clutter, areas of insects, and other isolated non-meteorological radar targets. In addition to the cleaning of the data, a correction was applied to attenuation errors due to water vapor and other gases. This correction followed the work of Liebe (1985) and the corresponding Interactive Data Language (IDL) coded version from John Haynes (personal communication), which accounts for one-way attenuation of a 95 GHz signal. This code was altered to double the one-way attenuation to account for two-way attenuation in the radar volume.

The minimum detectable signal in unit of received power (mW) of a radar system can be estimated if the radar constant and the radar receiver noise are well known (Doviak and Zrnic 1993). In term of radar reflectivity, the minimum detected radar reflectivity decreases with the square of the range from the radar. The SWACR gridded data used here include only radar reflectivities that are above the radar receiver noise (using the threshold technique outlined in Clothiaux et al. (1995)). Thus, if we fix the range (1 km from the SWACR) we can compute the probability distribution function (pdf) of significant detections in dBZ. The radar reflectivity values at 1 km vary from -52 dBZ to -17 dBZ (*Figure 3.3*). The high end of the distribution can be simply attributed to the lack of weak echoes in certain SWACR profiles (attributable to drizzle and strong cloud returns). The low end of the distribution gives a sense of the absolute sensitivity of the radar at 1 km (-50 dBZ). Although the absolute minimum detectable signal (MDS) is less than -50 dBZ, we consider the statistical mode of the distribution at 1 km to be the minimum detectable signal for computation of the radar constant for the SWACR. Applying this 1 km statistical mode of -42.66 dBZ as our MDS to the radar equation:

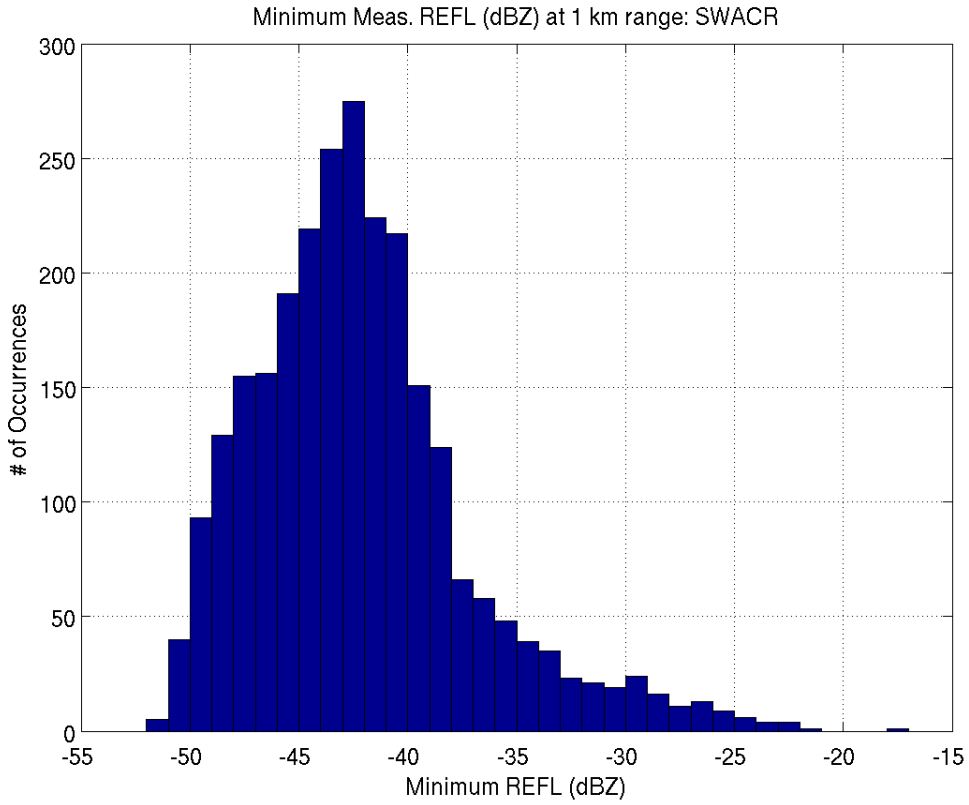

Figure 3.3: Gridded minimum radar reflectivity (dBZ) probability distribution function at 1 km distance from SWACR for all available SWACR CW-RHI scanning periods for November 2009.

$$MDS = RC + 20log10(R) \tag{3.1}$$

such that R is the range (in km) and RC is the radar constant (in dBZ), we resolve a radar constant for the SWACR of -42.66 dBZ.

3.2.2 W-Band ARM Cloud Radar

The WACR has been integral to the ARM cloud radar program since 2005 (Widener and Johnson 2006). This 95 GHz (3 mm) radar is a vertically pointing system, and offers the same radar characteristics of the SWACR, providing for key inter-comparisons between the radars. With a scan-to-scan time scale of 2.14 seconds and a vertical range-gate resolution of

42 meters, the WACR is valuable tool for not only understanding cloud variability on small spatial and temporal scales, but also for long-term climatology studies. The data was limited vertically to elevations between 350 m and 3000 m to account for radar antenna-induced artifacts and mid to high level clouds. WACR data were cleaned using the same SNR techniques as the SWACR; though for this study attenuation corrections were not made given the close proximity of the measured field (less than 2.5 km). The radar was alternating between a co-pol and a cross-pol (collection of Linear Depolarization Ratio (LDR) measurements) sampling mode. In this study, only the co-pol data were used, resulting in a degradation of the temporal scan from 2.14 seconds to 4.28 seconds. Finally, as with the SWACR, radar reflectivity was limited to a range of returns between -50 dBZ to +10 dBZ (Kollias et al. 2005). WACR radar data were collected for an extended period throughout the campaign, and 56 days of marine stratocumulus cases were isolated from the roughly 550 days of data available. These days of stratocumulus were broken down into 24 one-hour periods of observation for analysis purposes. An additional focus was placed on the November 2009 cases that matched to the SWACR, providing a matching WACR column scanning period for each SWACR regional scanning period.

3.2.3 Vaisala Ceilometer

The model CT25K Vaisala Ceilometer deployed for the Graciosa campaign can detect multiple cloud bases, and has a range of 7,620 m above ground level. It is an active remote sensor that transmits a pulse of near-infrared energy vertically and scans for reflected energy indicating cloud base heights at a temporal frequency of 15 seconds. No corrections were made to the data, and measured cloud bases were either matched to the closest temporal step of radar data, or averaged out to 75-second mean cloud base intervals. Data were available for the full field campaign, and were either allocated into 1-hour increments to match the

WACR cases, or specifically dissected to match the SWACR scanning periods.

3.2.4 Balloon-Borne Sounding System (Sonde)

Balloon soundings were launched from Graciosa Island every 6 hours during the campaigns, double the temporal resolution of typical meteorological convention. Of particular interest to this study were the lower tropospheric winds concomitant to each radar scan period. Using the closest balloon launch time to match to the radar scan period, were computed cloud mean winds. Determining the elevation of mid-cloud using ceilometer measured cloud bases and radar indicated cloud tops directly above the radar, the closest matching vertical elevation of measurement from the balloon launch to mid-cloud was determined. This measurement, in addition to the two measurement levels above and below mid-cloud, were averaged to calculate the mean mid-cloud wind speed and direction for each given measurement interval. Hourly mean winds were determined by averaging the hourly mid-cloud mean winds. These mean winds were then combined with the time interval between scans ($\sim$28 seconds) to determine the advective speed of the cloud field passing over the radar location. Additional cases that involved potential roll-structures in the atmosphere were further isolated, and surface to cloud top hodographs were computed using the closest sounding launch that correlated to the SWACR scan. All sondes from November 2009 were considered for this study.

3.3 SWACR Gridding Scheme

Gridding radar data schemes typically implemented a Cressman Gridding Scheme (Cressman 1959), which utilizes a weighting function W such that:

$$W = (N^2 - d^2)/(N^2 + d^2) \tag{3.2}$$

where N is the distance from a gridpoint at which W goes to zero, and d is the distance between the grid point and observation. The SWACR data gridding scheme, however, is more conservative given the difference in cloud and precipitation structures. The radar first measures individual radial radar reflectivity measurements across the observation medium, which are bound by the volume constrained to an individual range bin and the radar 3-dB (0.4°) beam width. The SWACR data gridding scheme initially assigns these maximum radar reflectivity values to grid boxes (25m x 25m) directly overlapped by the radar observations. In the case of multiple observations overlapping at the same grid point, the maximum value of the measured observations was assigned to the full grid point. Finally, some grid points could not be populated due to a lack of overlap with measured data. A binary cloud-no cloud (-50 dBZ threshold) cloud mask was assigned to the full gridded field, and if a point with no data was surrounded by three grid points (75 m) vertically above and below that were masked as cloud, it was determined to be a cloud point. The missing point was then populated with the mean value of these six vertically surrounding data points. If a point is not surrounded by three cloud masked points above and below, the point was populated as an 'empty' non-cloud point.

This gridding scheme resulted in a spatially-limited domain of 42 km horizontal by 3 km vertical with 25m x 25m resolution. In additional, the lowest 325 m of observations were removed to address potential ground clutter and antenna artifacts, resulting in an effective 2.675 km by 42 km region for each gridded scanning period ($\sim$28 seconds), with the number of slices corresponding to the number of full scans in the scanning period (ranging between 15 and 133). Additional limitations to the horizontal domain were implemented for some analysis, limiting the effective horizontal domain to 12-24 km. Furthermore, these data were also limited to a radar reflectivity range of -50 dBZ to +10 dBZ, reasonably corresponding to the limits proposed by Kollias et al. (2005) and our sensitivity study. Good stratocumulus

conditions were present during 10 particular daily periods of SWACR scanning at Graciosa Island: November 1, 3, 7, 21, 22, 23, 24, 25, 28, and 29. During these days, 7 to 45 individual periods of scanning were gridded into 3D regimes, lasting between 8 minutes and 1 hour. These dates were selectively chosen due to their relatively extensive marine stratocumulus cloud decks and, perhaps more importantly, relative lack of heavy precipitation.

The quality of the gridded data depends on the initial resolution of the observations, the desirable grid resolution, the gridding scheme used, and the preliminary quality control of the radar observations associated with the removal of spurious effects (e.g., ground clutter). The SWACR has the same characteristic along-beam spatial resolution of these vertically pointing radars (20-45 m). This high resolution in the along-beam sense allows for the use of a high-resolution grid (25m x 25m) for gridding the data. The SWACR oversamples along the plane of scanning, thus, no gaps are anticipated in this plane. However, the zigzag pattern creates gaps in the along wind direction of variable time which translate to gaps in the along-wind distance between measurements. The spatial gaps created by this pattern were not addressed for this preliminary study; instead, each individual scan was gridded side-by-side with no corrections for the zigzag spatial gaps. Future studies will eventually have to address this issue and devise a gridding technique to account for the spatial gaps inherent to the scanning technique. Similar uneven radar data spacing occurs if other scans are used (e.g., sequence of RHI's at different azimuths, or sequences of PPIs at different elevations). This is one of the challenges of scanning radar observations: the degradation of sensitivity and resolution at range from the radar.

The decisions made by a gridding scheme can have major impacts on the 3D cloud and drizzle statistics. If a scheme provides an observation more influence beyond the boundaries of the radar sampling volume as defined by the 3-dB antenna and range weighting functions

to radar measurements in an effort to occupy many nearby grid points, there is a danger of stretching and smearing cloud features and subsequent statistics. The alternate (under-representation) will occur if not enough weight is given to these variables and artificial gaps and boundaries are created. In addition, when multiple measurements are impacting a single grid-box in the domain, the choice of gridding technique (e.g. maximum, mean, random, etc.) can either over or under-represent anomalously strong or weak returns relative to the field surrounding it.

The schemes applied to regions where no data are measured in a grid box also present a challenge to the gridding scheme. The technique applied for the SWACR was devised in a manner such that only the vertical column of data around a missing point is considered. This is done because there should, in theory, be less advectively driven variation in a vertical column than in the corresponding horizontal points around a missing point. In addition, the consideration of the cloud mask into the scheme is important, as a cloud is more likely to have naturally-occurring gaps closer to cloud edges than in mid-cloud. However, this can still create artificial gaps that may not be occurring naturally in the field, which may adversely diminish cloud boundaries and negatively bias cloud characteristics by introducing false regions of non-cloudy gridded observation.

3.3.1 SWACR Gridding Scheme Evaluation using WACR Data

To better assess potential errors in the SWACR gridded data, a series of tests were performed utilizing the WACR vertical-column measured data. WACR data for all days with well-established marine stratocumulus during the field campaign are used, comprised of 56 days of radar data. Each day is broken into 24 one-hour intervals for analysis. Two tests were devised to understand the potential impacts of the following two scenarios of inherent gridding issues: 1) multiple observations within a grid box, and (2) no observations within

a grid box.

For the 1D multiple observations test, WACR observations were obtained for mid-cloud, where mid-cloud was determined to be the mid-point between the ceilometer-indicated cloud base and the WACR indicated cloud top. The data were allocated into groups of five measurements, serving as a proxy of five measurements occurring in one single SWACR grid box. These five observations represent a 20 seconds observation period (4.28 seconds/observation), removing many (but not all) advective effects in the data and providing a reasonable synthetic multiple-observation point. Two methods were tested for the groupings of data: selecting the maximum value of the group to represent the grid point (i.e. the SWACR/maximum method), and selecting one of the five points randomly to represent the grid point (random method). Cloud fraction (*Figure 3.4*), hourly-mean Reflectivity in dBZ (*Figure 3.5*), and the standard deviation of the hourly Reflectivity field (*Figure 3.6*) are considered.

Overall, both methods performed very well when compared to the original field. In examining the cloud fraction, we found that the maximum method is biased slightly high when compared with the actual data (*Figure 3.4*). This highlights the expected issues of utilizing a maximum method near cloud edges, where cloud boundaries can be over-extended. This occurs because if both cloud and non-cloud observations are present, this method will always assign a cloud to the grid box. The random method, on the other hand, results in a nearly unbiased cloud fraction when compared with the actual field. In a random method, there is an equal probability of assigning a cloud or non-cloud measurement to the grid point. With a large enough sample size, it is expected that the random sampling will retain the characteristic cloud fraction of the actual field, as a large sample size will allow the random method to mirror the statistics of the physical field.

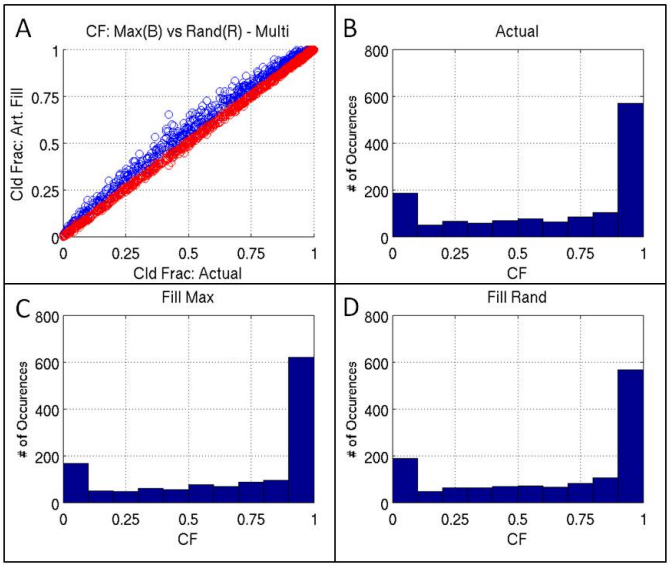

Figure 3.4: Computed hourly cloud fraction for 1-D mid-cloud WACR field and WACR multiple-observation gridded field. The maximum value scheme (blue) and the randomly selected value scheme (red) are plotted (A) comparing observed cloud fraction from observations to estimated cloud fraction from gridded field; PDF of the corresponding cloud fractions for the measured (B), maximum scheme-filled (C), and random scheme-filled (D) fields are presented.

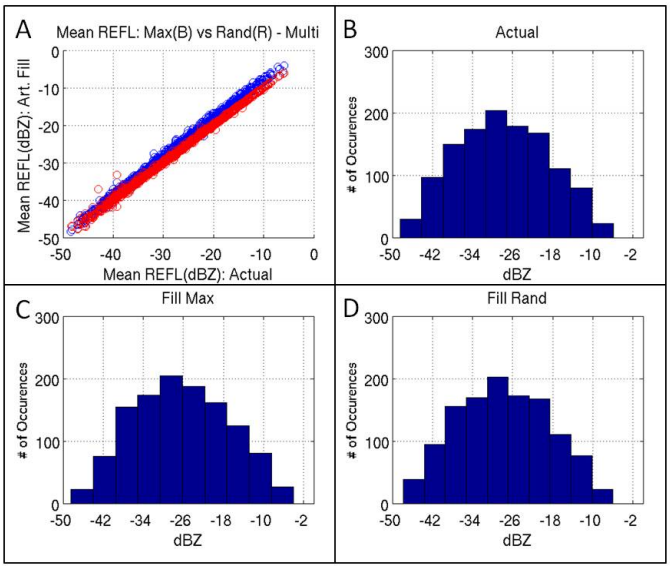

Figure 3.5: Computed hourly mean radar refelctivity for 1-D mid-cloud WACR field and WACR multiple-observation gridded field. The maximum value scheme (blue) and the randomly selected value scheme (red) are plotted (A) comparing observed mean reflectivity from observations to estimated mean reflectivity from gridded field; PDF of the corresponding cloud fractions for the measured (B), maximum scheme-filled (C), and random scheme-filled (D) fields are presented.

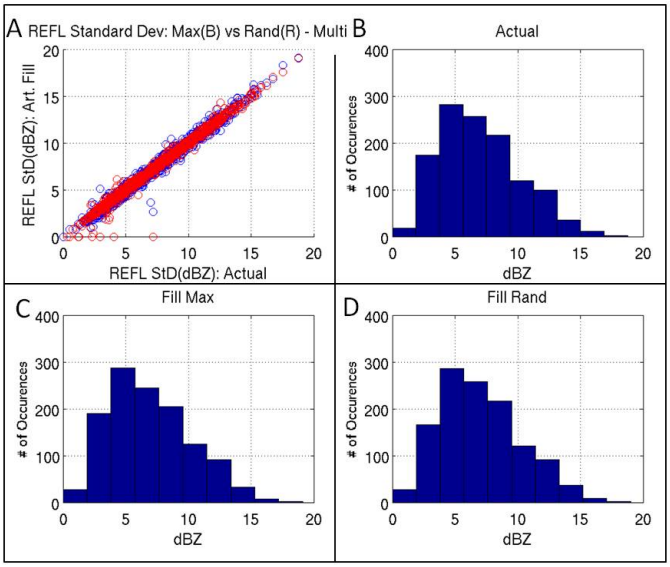

Figure 3.6: Computed hourly mean radar refelctivity standard deviation for 1-D mid-cloud WACR field and WACR multiple-observation gridded field. The maximum value scheme (blue) and the randomly selected value scheme (red) are plotted (A) comparing observed reflectivity standard deviation from observations to estimated reflectivity standard deviation from gridded field; PDF of the corresponding cloud fractions for the measured (B), maximum scheme-filled (C), and random scheme-filled (D) fields are presented.

Regarding the mean reflectivity (*Figure 3.5*), the maximum method was also biased slightly high, which is expected when assigning the strongest observation to the grid box. No bias was found in the random method when compared with the observation field. As with the cloud fraction, by randomly selecting points, and with a large sample size, one would expect to resolve the reflectivity characteristics of the actual field. Finally, both methods retained the standard deviation and the characteristic error of the observational field well (*Figure 3.6*). These results allow us to conclude that, although a random method performed better than a maximum method when considering multiple observations in a single grid box, the errors introduced by the maximum method (used by the SWACR) are small enough that we find it to be adequate at resolving the measured cloud field and its statistical characteristics.

The full 2D WACR observed cloud field for stratocumulus cases in November 2009 were considered when testing the importance of the SWACR gridding method applied to empty grid points in the gridded field. Using the WACR data as a proxy for a 2D gridded field (similar to a single 2D SWACR slice), we first apply a binary cloud mask to the full hourly field, wherein all measurements greater than -50 dBZ were masked as cloud, and all less than -50 dBZ as no-cloud. After masking the field, ∼10% of the data points in each vertical column (6 points of 66 observations) were randomly selected for artificial removal and assigned as a missing point. This created a field with simulated gaps in the data akin to what may be seen in a gridded field. Closely mimicking the method utilized for the SWACR, if a missing point was imbedded in the cloud field, and the 2 points (∼84 m) vertically above and below the missing value were all masked as cloud, the missing point was deemed a cloud point. The value for this cloud point was determined using either the mean of these four vertically bordering observations (SWACR/mean method), or one of the four values was randomly assigned to the missing point (random method). If the missing point was not imbedded in the cloud field, it was considered no-cloud. Also, if the missing point was imbedded in the cloud field but did not have the requisite four surrounding cloud-masked observations, then it was also considered non-cloud.

Both the mean and random methods performed well in retaining the reflectivity characteristics of the initial field. The mean and random method both retained the cloud mean reflectivity field without bias (*Figure 3.7*). The random method also retained a non-biased standard deviation of the cloud reflectivity; the mean method, however, resulted in a slightly higher standard deviation when compared with the full observed field (*Figure 3.8*), though the differences are between the full observational field and the gap-filled field are minimal for the mean method. This difference was unexpected however, in that it would be expected that if a grid point is filled using the mean value of the four vertically surrounding points, it

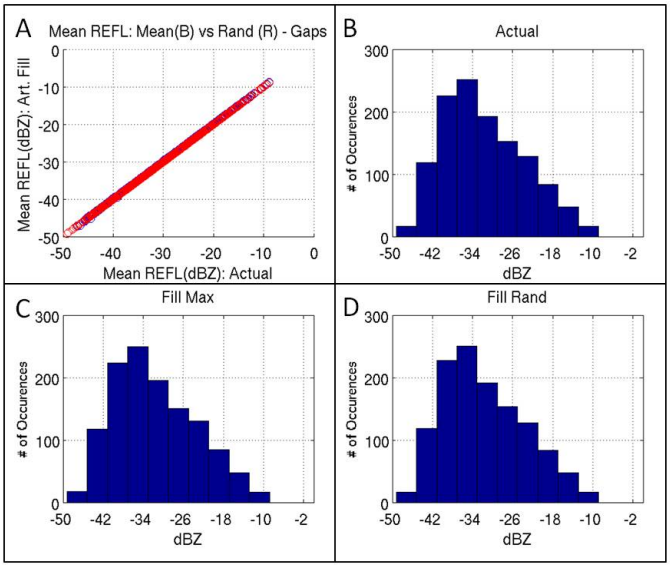

Figure 3.7: Computed hourly mean radar reflectivity (dBZ) for full 2-D WACR field and WACR artificially degraded (10% removal) gridded field. The mean value scheme (blue) and the randomly selected value scheme (red) are plotted (A) comparing observed mean reflectivity from observations to estimated mean reflectivity from gridded field; PDF of the corresponding mean reflectivity for Actual (B), Mean (C), and Random (D) fields are presented.

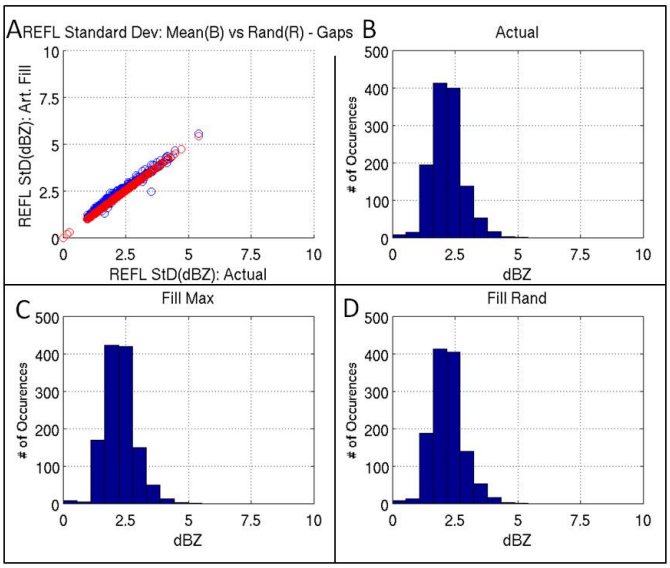

Figure 3.8: Computed hourly mean radar reflectivity standard deviation (dBZ) for full 2-D WACR field and WACR artificially degraded (10% removal) gridded field. The mean value scheme (blue) and the randomly selected value scheme (red) are plotted (A) comparing observed reflectivity standard deviation from observations to estimated reflectivity standard deviation from gridded field; PDF of the corresponding mean reflectivity for Actual (B), Mean (C), and Random (D) fields are presented.

will be more representative of the mean reflectivity in the cloud, and should therefore lead to a lower standard deviation. In this case, however, a randomly selected value amongst the four instead resolved a much more accurate standard deviation with respect to the original field. This may be due to the relatively thin nature of the clouds, which may be resolved by as few as 5-10 vertical observations. This small of a sample size for determining a mean and standard deviation may be heavily skewed by the existence of two identical points (as by the random method) as opposed to a distribution of points (as by the mean method). If this is the case, then the standard deviation would be more accurate for the random method.

To test the impacts of cloud-no cloud determination based for filling data gaps, we look at the measurement of cloud thickness using two different definitions of thickness. Cloud thickness was computed in two forms, using the same criteria as the SWACR: 1) Cloud thickness defined as the longest length of unbroken cloud observations in a vertical column (type 1), and 2) Cloud thickness defined as the vertical distance between the lowest and highest detected significant radar returns (exceeding -50 dBZ), a method that includes both the cloud thickness and any penetration of drizzle below cloud base (type 2). The selection of scheme for cloud thickness resolves the same results, as the thickness is independent of the strength of the reflectivity observation; instead, it is dependent on the gridding scheme determination of whether or not a missing point will be populated or left empty (cloud or no cloud, respectively). It is expected that the type 1 cloud thickness will be more sensitive to data gaps than type 2 by simple odds. If a missing point occurs within 2 grid points of the actual cloud boundary, the point will not be populated and the type 1 thickness will perceive this missing point as the cloud boundary (decreasing the cloud thickness). However, type 2 thickness values will only decrease if the actual cloud-edge measurement is one of the missing points. For a column of 66 measurements, therefore, type 1 is sensitive to 4 grid points (2 at each cloud boundary), or 6% of the field, while type 1 is just sensitive to 2 grid points, or

3% of the field.

Figures 3.9 (mean cloud thickness) and *3.10* (standard deviation of the mean cloud thickness) show the ability of the gridding scheme to resolve an accurate cloud thickness for both definitions of cloud thickness for clouds thinner than 500 meters. In general, the scheme performed exceptionally well for type 2 cloud thickness (red), resolving both the mean thickness and standard deviation of the observed cloud field at a near 1:1 ratio. For a 10% loss in data, there is a relatively low likelihood of removal for the two observations that make up the cloud top and bottom, and therefore an accurate type 2 cloud thickness is almost always retained. However, degradation in type 1 cloud thickness (blue) occurred with a 10% loss in data. Mean cloud thickness was relatively well-resolved for observed thicknesses up to 500 m (*Figure 3.9*). For an observed thickness exceeding 500 m, the degraded field was biased low, such that for an observed thickness of 1000 m, the type 1 thickness for the degraded field was closer to 950 m. Furthermore, the standard deviation of the type 1 thickness field (*Figure 3.10*) demonstrated a higher standard deviation than the actual field for lower variance periods, and a lower standard deviation than the actual field for higher variance periods. This suggests that the degradation of the data for low variance cases (steady-state cloud fields) had a greater impact on the observations generating more error, while highly varying cases (i.e. drizzle and transitional cloud fields) were generally standardized by the observation degradation, resulting in less overall error. These results are interesting in that the scheme has varying skill that is associated with the natural variance within the cloud field. *Figures 3.11* and *3.12* show the same two fields as *Figures 3.9* and *3.10*, but with a 50% removal of data, further exemplifying the impacts of data gaps on the computations of two types of cloud thickness.

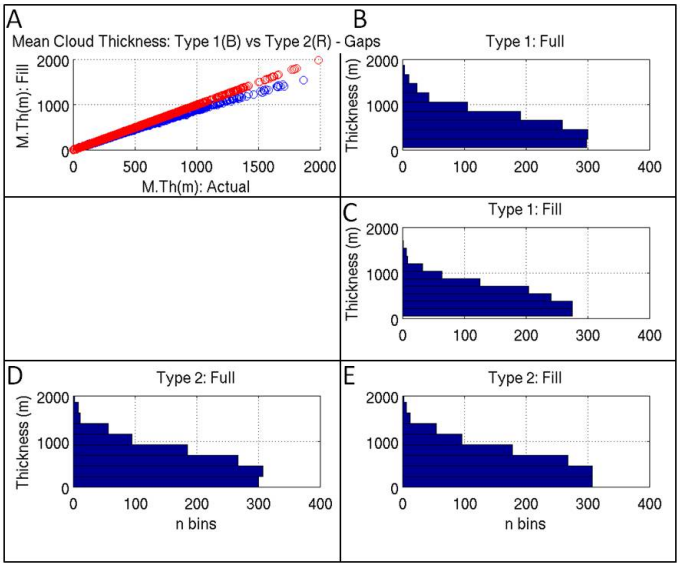

Figure 3.9: Mean hourly type 1 (blue) and 2 (red) cloud thickness computed from observed 2-D WACR field (x-axis) and degraded (10% removal) WACR gridded field (y-axis) (A); PDF of the corresponding type 1 cloud thickness for measured (B) and degraded (C) fields, and type 2 cloud thickness for measured (D) and degraded (E) fields, are presented.

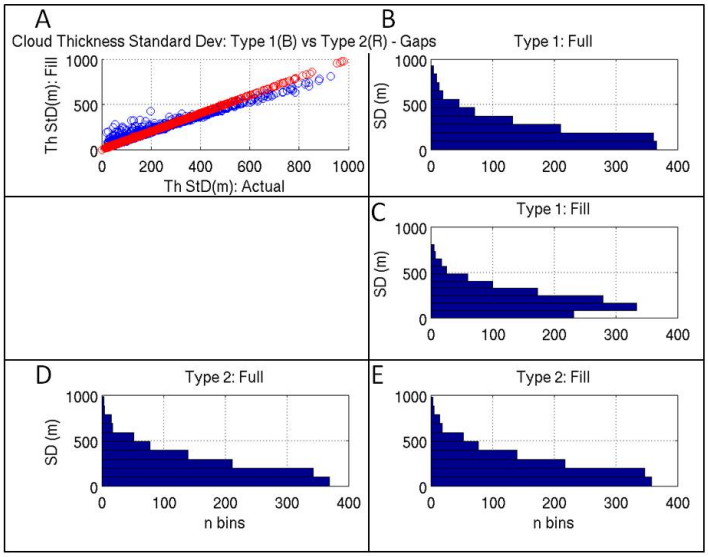

Figure 3.10: Mean hourly type 1 (blue) and 2 (red) cloud thickness standard deviation computed from observed 2-D WACR field (x-axis) and degraded (10% removal) WACR gridded field (y-axis) (A); PDF of the corresponding type 1 cloud thickness for measured (B) and degraded (C) fields, and type 2 cloud thickness for measured (D) and degraded (E) fields, are presented.

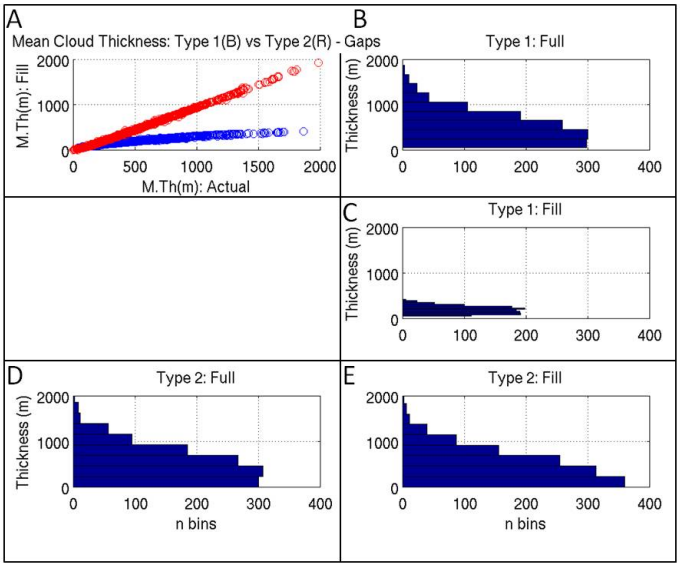

Figure 3.11: Mean hourly type 1 (blue) and 2 (red) cloud thickness computed from observed 2-D WACR field (x-axis) and degraded (50% removal) WACR gridded field (y-axis) (A); PDF of the corresponding type 1 cloud thickness for measured (B) and degraded (C) fields, and type 2 cloud thickness for measured (D) and degraded (E) fields, are presented.

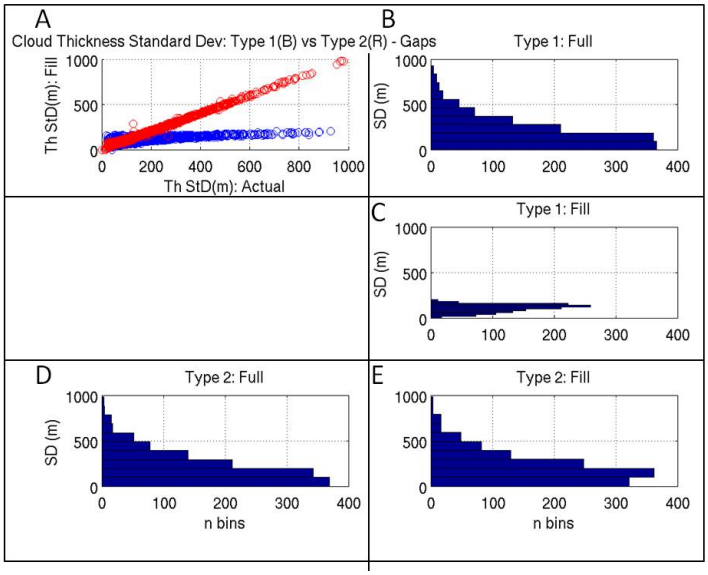

Figure 3.12: Mean hourly type 1 (blue) and 2 (red) cloud thickness standard deviation computed from observed 2-D WACR field (x-axis) and degraded (50% removal) WACR gridded field (y-axis) (A); PDF of the corresponding type 1 cloud thickness for measured (B) and degraded (C) fields, and type 2 cloud thickness for measured (D) and degraded (E) fields, are presented.

Overall, we can conclude that for the computation of type 1 cloud thickness, it is important to utilize a scanning strategy that results in as few spatial gaps in the observation field as possible. However, the computation of type 2 cloud thickness is generally moreforgiving based off simple statistics, suggesting that a faster scanning technique (which results in a more gap-ridden field) will not have exceptionally detrimental effects on mean hourly thickness values. We can also conclude that the random method performs better than the mean method in resolving the statistics of the reflectivity field, though the errors of the mean method are minimal enough that both methods are adequate for gridding SWACR observations.

The objective determination of cloud boundaries is one of the key measurements associated with cloud radars. Several techniques have been devised to resolve cloud boundaries, many of which attempt to overcome the errors inherent using a radar that is highly sensitive to larger particles such as drizzle, aerosols, and insects that can occur on a routine basis below the physical cloud base. The majority of these techniques have been devised around a multi-instrument approach (e.g., Clothiaux et al. (2000)), thus, presenting a challenge to determining the cloud boundaries using SWACR observations alone.

Cloud boundaries in gridded data are typically identified by sharp transitions in the reflectivity field for neighboring grid points, with one indicating cloud (signal above the radar reciever noise floor) and one indicating hydrometeor-free area (radar receiver noise). In a column, these transitions are used to determine the hydrometeor layer base and top. The presence of drizzle particles near and below the cloud base in form of precipitation can create an artificial cloud base that is substantially below the actual cloud base. Here, the cloud base is estimated using the column data from the ceilometer and the WACR. The SWACR-indicated cloud base (at zenith) can be used in conjunctions with the ceilometer-estimated

cloud base to estimate the column penetration depth of drizzle particles below cloud base. More specifically, the penetration depth of drizzle below cloud base was computed by taking the difference between the ceilometer-indicated cloud base height and the lowest measured radar reflectivity from hydrometeors (SWACR-indicated cloud base height). The comparison of the cloud base estimated using the profiling sensors and the SWACR observations verifies that SWACR-indicated cloud base is often biased lower than the physical cloud base. This agrees with previous studies (e.g. Clothiaux et al. (1995); Moran et al. (1998)). This also has major implications at range from the radar, where cloud base is estimated from the lowest altitude significant radar return (reflectivity greater than -50 dBZ). Therefore, errors in cloud base can occur not only from radar sensitivity loss at range, but also from hydrometeors falling below the physical cloud base.

Cloud top boundaries are generally more accurate to determine from cloud radar data when studying marine stratocumulus clouds because these clouds are often capped by a temperature inversion that restricts upward motions within the cloud. Cloud top is computed by finding a reflectivity value at Z that is greater than -50 dBZ, and a value at Z+δZ (wherein Z+δZ is at a higher altitude than Z) that is less than -50 dBZ. Cloud thickness values using only radar data were determined by subtracting the height of the cloud base from the height of the cloud top.

Finally, the SWACR data were used to determine the fractional cloudiness in the gridded domain. At each vertical column of gridded SWACR data, if there is at least one grid point with radar reflectivity from hydrometeors, the column is considered cloudy. Area-averaged cloud fraction was computed by dividing the total the number of cloudy columns into the total number of columns overall. This was calculated for each 25 m gridded interval in the domain from -21 km to 21 km, or southwest to northeast for the radar orientation in this

field experiment.

3.4 Drizzle Identification Schemes

In this study, drizzle presence is classified in the SWACR and WACR observations for two purposes: to determine where pockets/clusters of drizzle were occurring near the cloud base, and to determine the relative strength of a drizzle event for separation into drizzle and non-drizzle regimes. The cloud base drizzle threshold scheme at cloud base followed prior research in determining a minimum reflectivity value at which drizzle is likely occurring (e.g. Sauvageot and Omar (1987); Frisch et al. (1995); Kollias et al. (2004)). For this study, the minimum reflectivity for drizzle to be occurring was selected to be -15 dBZ (Sauvageot and Omar 1987; Löhnert et al. 2001). Cloud base was determined in the column directly above the radar using ceilometer data, and the ceilometer value was extrapolated to the full width of the gridded observational field for each time step. This is a reasonable approximation given the small change in Lifting Condensation Level (LCL) expected within 10-20 km, and the relatively small observational domain of the radar. All reflectivity measurements at this height above ground level were analyzed in a binary drizzle-no drizzle algorithm where all grid points with radar reflectivity values greater than -15 dBZ were considered containing drizzle, and all grid points with radar reflectivity values less than -15 dBZ were considered non-drizzling.

The analysis of gridded SWACR observations near the cloud base revealed the presence of exhibited streak-like spatial organization of the drizzle field in November 2009. These streaks were structured such that a long axis and short axis of orientation could describe the length and width of the streak, respectively. The orientation of the long axis was measured along the drizzle-non drizzle boundary (i.e. edge) of each streak, resulting in an axis angle with respect to north. The CW-RHI scanning pattern for this campaign was designed

to capture advections of clouds along the climatological mean wind (315°). However, the wind motions throughout the campaign varied, as expected, from this climatological mean, introducing both along-wind (perpendicular to the radar scanning volume) and cross-wind (parallel to the radar scanning volume) advections of the cloud field. The along-wind advection of the streaks is initially taken into account by transforming the time scale into a spatial scale using the hourly mean in-cloud wind. This step converts the along-range axis to a Lagrangian viewpoint; however, the cross-wind advections are not taken into account, which is necessary to fully transform from an Eulerian viewpoint (radar based) to a Lagrangian (cloud based). In order to accurately analyze the streak long-axis angle with respect to the mean layer winds, a fully-Lagrangian view is necessary. Cross-wind components can result in regions of drizzle that are artificially stretched in the radar domain. For cases of large cross-wind components of the overall wind, relatively small pocket of showers can be elongated in a manner such that it appears in the SWACR gridded product as a stretched, streak-like structure. The smaller the cross-wind component, the less these artificial effects can occur. To account for these changes, the analysis of streak structures was first limited to periods where the mean sub-cloud layer wind was within 35° of the radar along-wind axis (315°/135°) as defined by the climatological wind. Second, by simple geometry, we can remove the horizontal advection of the streaks across the plane by subtracting the wind direction from the radar axis (315°), and adding this value to the measured long axis of the streak measured in the semi-Lagrangian domain. This will result in a fully-Lagrangian long axis angle of the streak. These axis angles were analyzed with respect to the mean sub-cloud wind, mean in-cloud wind, and boundary layer top wind, which was defined as the wind at the top of the boundary layer (White et al. 1996), where wind measurements were analyzed from the closest (temporally) radiosonde launch. In addition, shear through the boundary layer was computed using the near-surface and cloud top wind observations from sounding

data.

Though the mapping of drizzle at cloud base provides important details regarding the spatial distribution of precipitation in marine stratocumulus, of perhaps equal importance is the ability to quantify the strength of the precipitation falling. Regimes were divided into three types: cloud, light drizzle, and heavy drizzle. A cloud regime was considered to have an average maximum in-cloud reflectivity of less than -27 dBZ and a period averaged penetration depth of less than 200 meters. Light drizzle regimes were defined as having an average in-cloud reflectivity between -27 dBZ and -18 dBZ and an average penetration depth between 200 m and 425 m. Finally, heavy drizzle regimes were dictated by an average penetration depth of greater than 425 m and an average in-cloud maximum reflectivity of greater than -18 dBZ.

Chapter 4
Results

The SWACR observations collected at the Azores were the first of its kind for the ARM program. Here, a preliminary analysis of the SWACR observations is presented. Overall, the analysis revealed both opportunities and challenges in the use of scanning cloud radars for cloud and precipitation research. A summary of the main findings will be discussed in the next chapter.

4.1 Comparison to Vertical W-Band ARM Cloud Radar (WACR) Observations

The CW-RHI sampling strategy enables reflectivity observations and documentation of cloud properties across a plane, but does so at the expense of higher temporal resolution due to the reduction in the number of integrated radar samples. To understand the impacts of reduced temporal resolution, the gridded SWACR observations are compared to the WACR profiling observations to first understand how well the gridded radar data resolves the observed cloud field. This is done so we can further categorize potential degradations in the observations with the distance from the radar. An example of such a comparison is shown for the WACR (*Figure 4.1a*) and SWACR (*Figure 4.1b*) for a one-hour period on November 29, 2009. Despite a lower temporal resolution for the SWACR with respect to the WACR, the overall characteristics of cloud base variability, in-cloud reflectivity, and cloud thickness are well resolved by the SWACR. It is apparent that as we increase range from the SWACR, the reduction in radar sensitivity will be an additional factor that will degrade the ability of the SWACR to capture the vertical structure as effectively as the vertically pointing WACR.

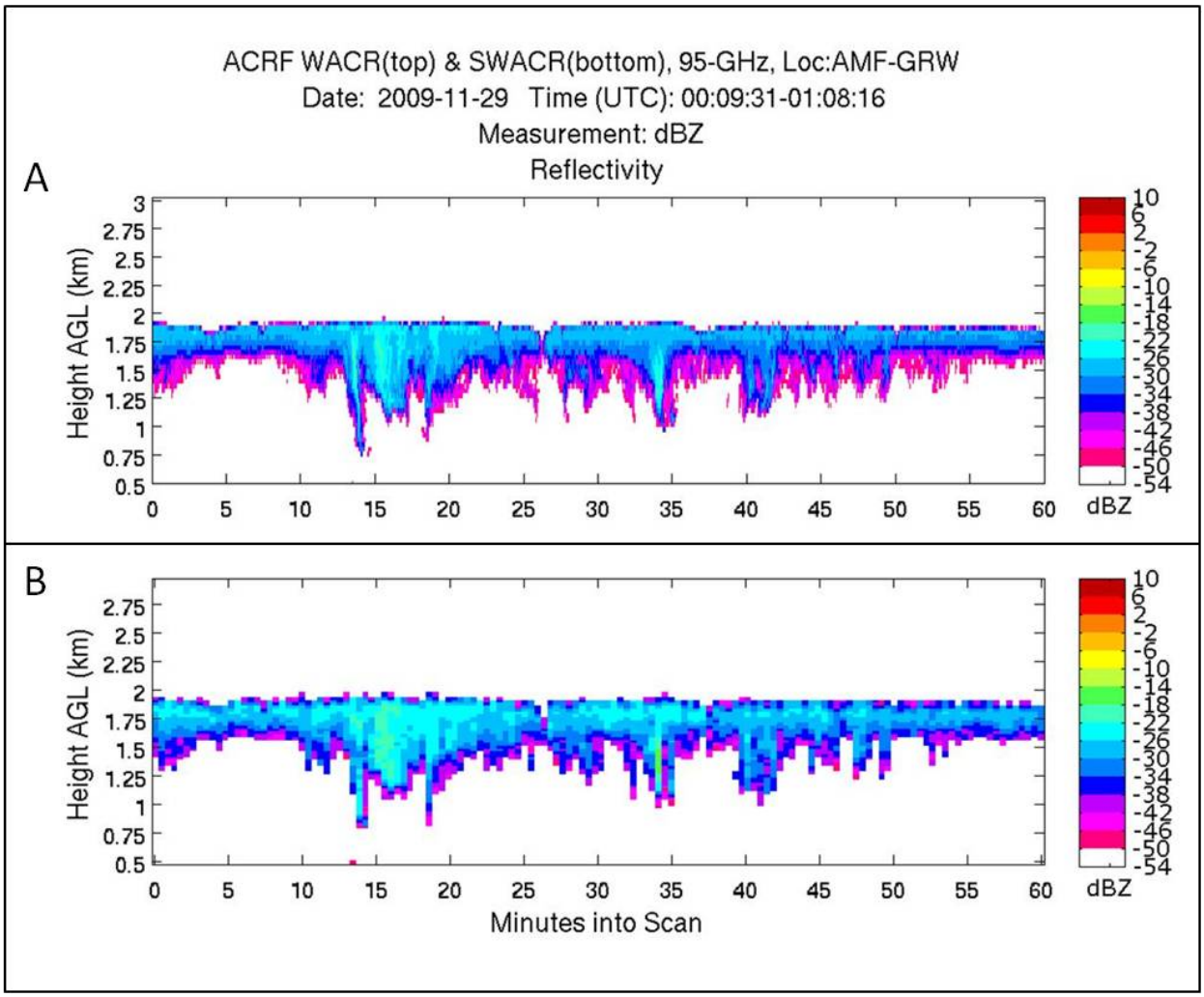

Figure 4.1: WACR (A) and SWACR (B) for 09:31 – 1:08:16 UTC 29 November 2009 located at Graciosa Island, Azores.

This will be discussed in following sections.

The CW-RHI offers information on the structure of clouds and drizzle in a plane expanding 21 km to each side of the column resolved by the profiling WACR. Assuming Taylor's frozen-in turbulence hypothesis, the CW-RHI observations can be used to document the 3D structure of the hydrometeors in the boundary layer. Three typical cloud conditions are observed at Graciosa: a cloud-only, light drizzle, and heavy drizzle case. Examples of such

CW-RHI SWACR observations representative of these regimes are shown in *Figure 4.2* (a-c, respectively). The presence of drizzle particles in volumes sampled by the SWACR increases their radar reflectivity above the SWACR minimum reflectivity detection level, enabling the mapping of the hydrometeor structure at further ranges from the radar. The most extended SWACR returns (both in depth and range) are observed during heavy drizzle conditions. The increase in variability of reflectivity structures can be linked to several causes, including but not limited to a larger distribution of cloud and drizzle particle sizes, increased penetration depths of precipitation particles into the unsaturated sub-cloud layer, and greater

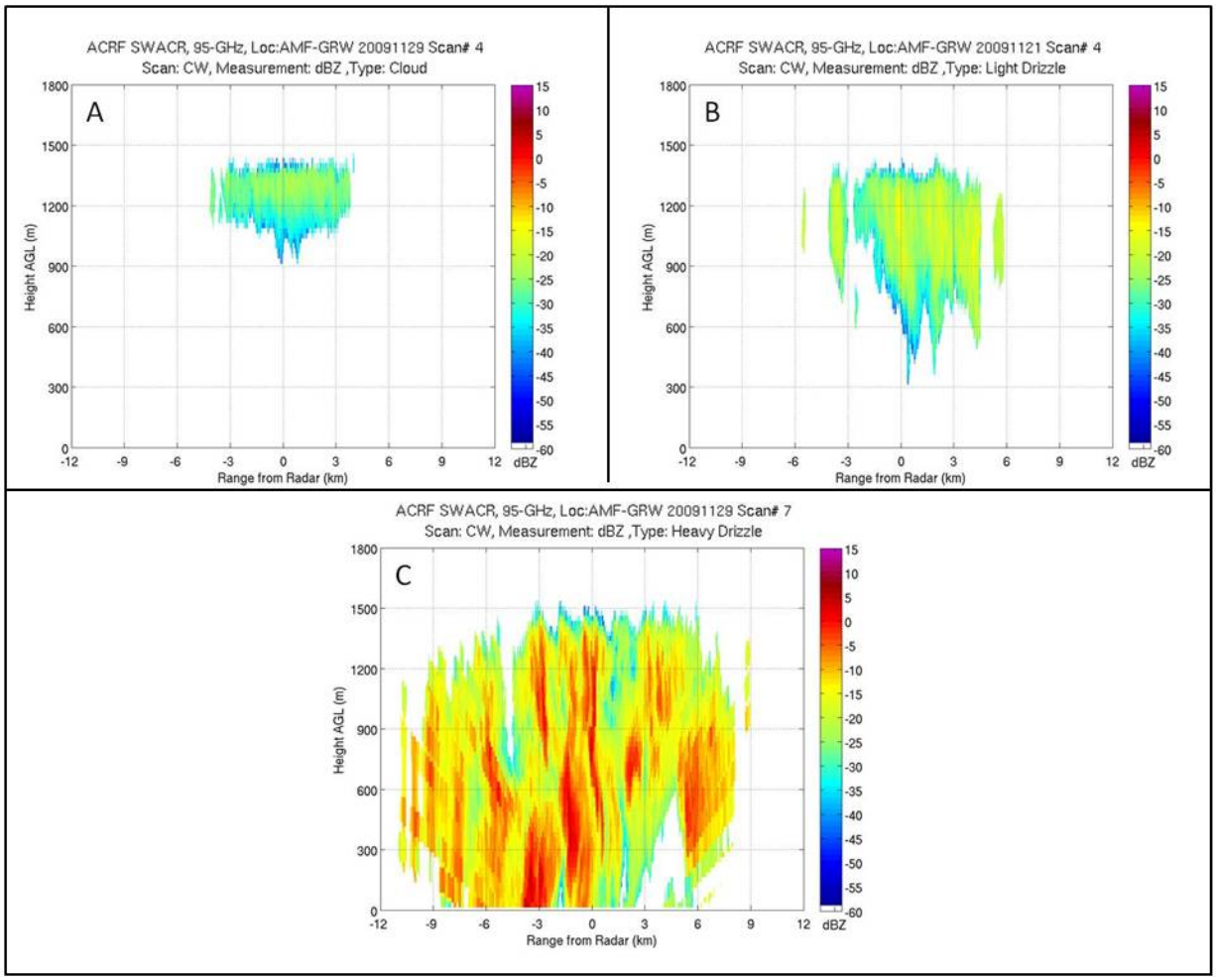

Figure 4.2: SWACR CW-RHI individual along-range scan for (A) cloud-only (Scan 4: 2009/11/29), (B) Light Drizzle (Scan 4: 2009/11/21), and (C) Heavy Drizzle (Scan 7: 2009/11/29) regimes located at Graciosa Island, Azores.

variability in the vertical velocity structure of the cloud from stronger drizzle-producing dynamics and precipitation loading. Furthermore, these sample cases demonstrate that a scanning radar can provide much greater detail in the spatial distribution of drizzle and light precipitation over the domain, which when compiled over an extended scanning period can account for both spatial and temporal evolutions in the field.

The mean of the along-wind component of the mid-cloud wind for each scan was assigned to be the advective wind for the entire SWACR domain. Using Taylor's frozen turbulence hypothesis, we convert the scan time interval to an along-wind spatial dimension and the SWACR data are gridded in a coordinate system with axes: along-wind, cross-wind and height (*Figures 4.3 - 4.6*). The gridded data provide a unique representation of the 3D structure of marine stratocumulus that is not as readily apparent when analyzing column observations. Periods of transition from shallow, non-precipitating clouds to precipitating clouds, or precipitating clouds to non-precipitating clouds or broken fields are noted in several instances (*Fig.4.3 B,C*, *Fig.4.4 D,E,F*, *Fig.4.5 D,E,F*, *Fig.4.6 E,H*) for the full domain. Clearly our ability to detect weak cloud-only structures is severely limited by the sensitivity of the radar; this will be addressed later. Still, these evolutions demonstrate the ability of the SWACR to document changes in the marine boundary layer cloud field with great detail.

4.1.1 Spatial Mapping of Cloud Fraction

Cloud fraction is the first parameter needed in order to quantify the effect of clouds on Earths radiation budget in Global Climate Models (GCMs). Other important parameters include cloud phase, cloud thickness and cloud top height. It is expected that the loss of radar sensitivity with range will bias low the cloud fraction estimates. Here we examine these biases and how they depend on the cloud states of cloud only, light or moderate drizzle as defined in *Section 3.5*. First, using the SWACR gridded data, the cloud occurrence in a

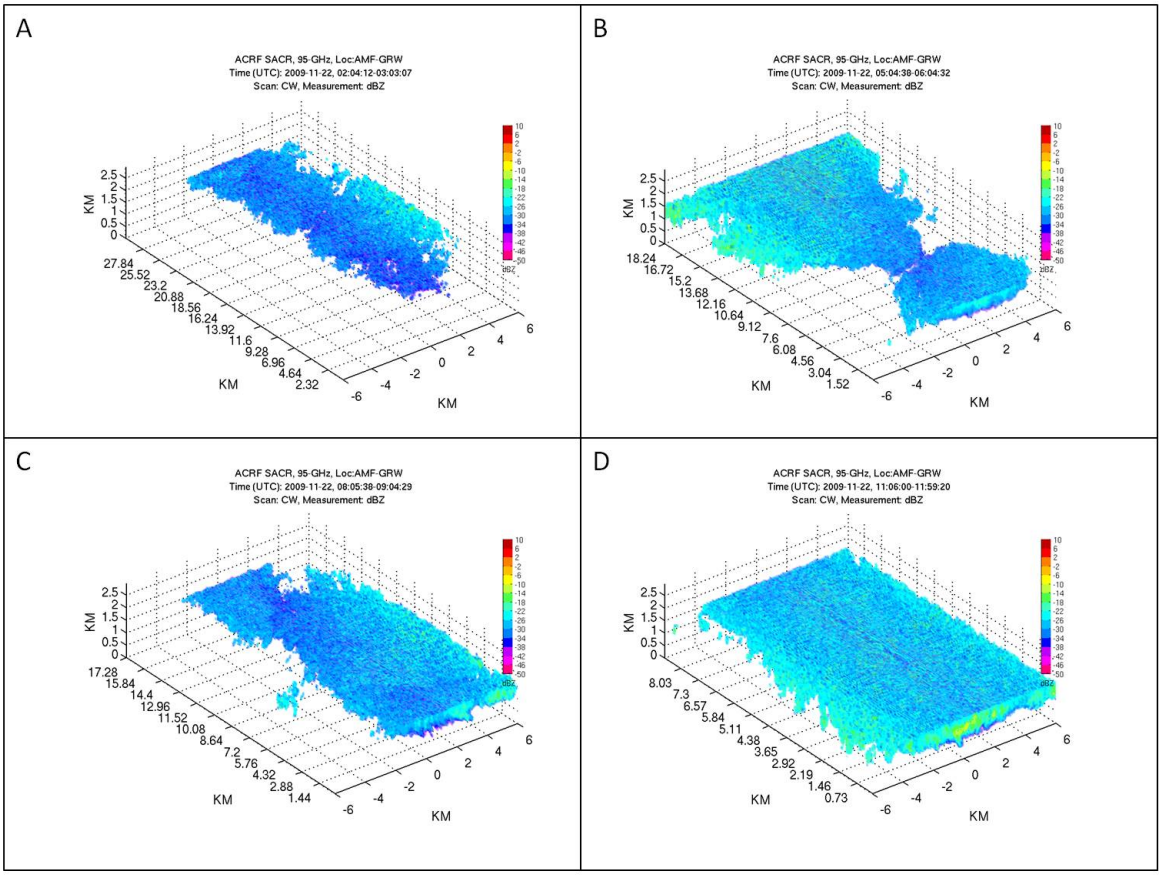

Figure 4.3: SWACR Gridded Radar Reflectivity (dBZ) for 22 November 2009 at Graciosa Island, Azores to +/- 6 km for (A) 02:04:12-03:03:07 UTC, (B) 05:04:38-06:04:32 UTC, (C) 08:05:38-09:04:29 UTC , (D) 11:06:00-11:59:20 UTC, (E) 14:08:09-15:07:53 UTC, (F) 17:11:08-18:10:56 UTC, (G) 20:13:21-21:12:15 UTC, (H) 23:14:21-23:59:42 UTC. Panel (I) shows WACR measured vertical column Radar Reflectivity (dBZ) for 24 hour period (UTC) 22 November 2009 at Graciosa Island, Azores.

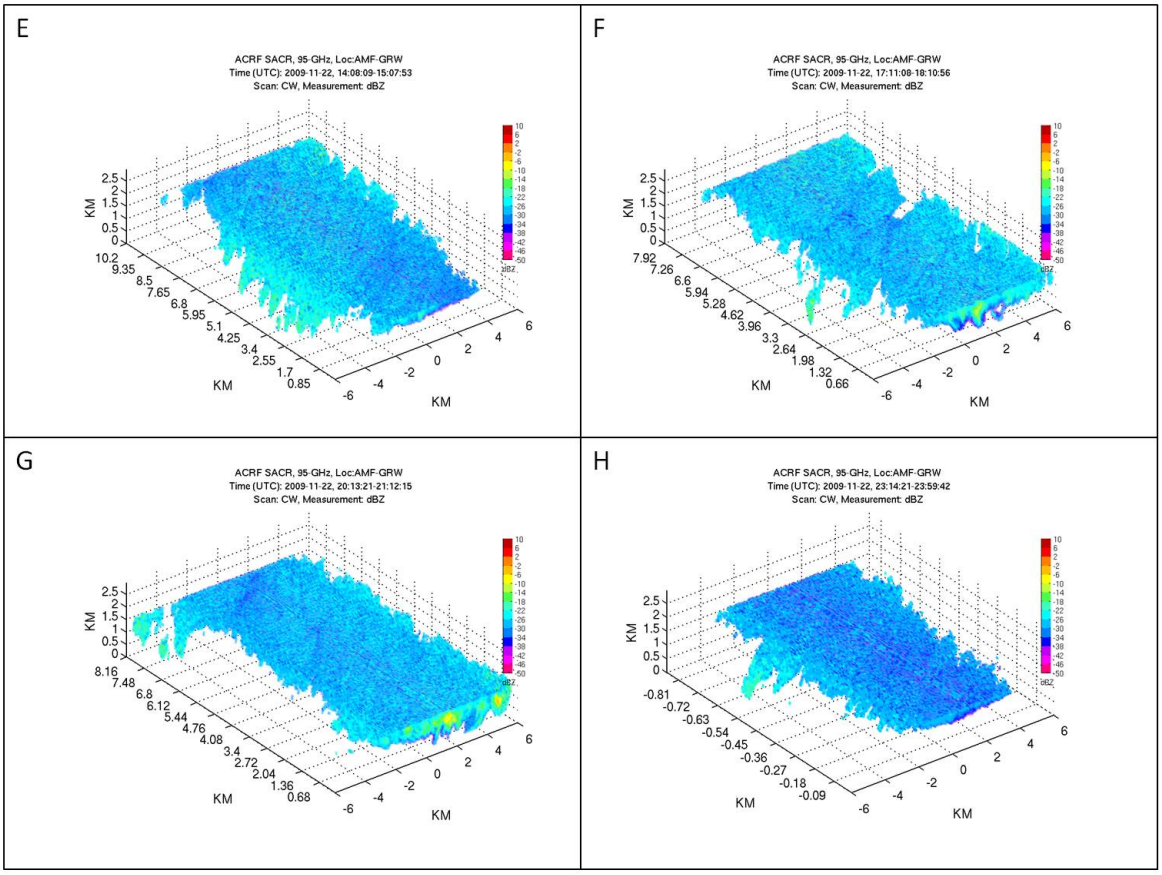

Figure 4.3 (continued)

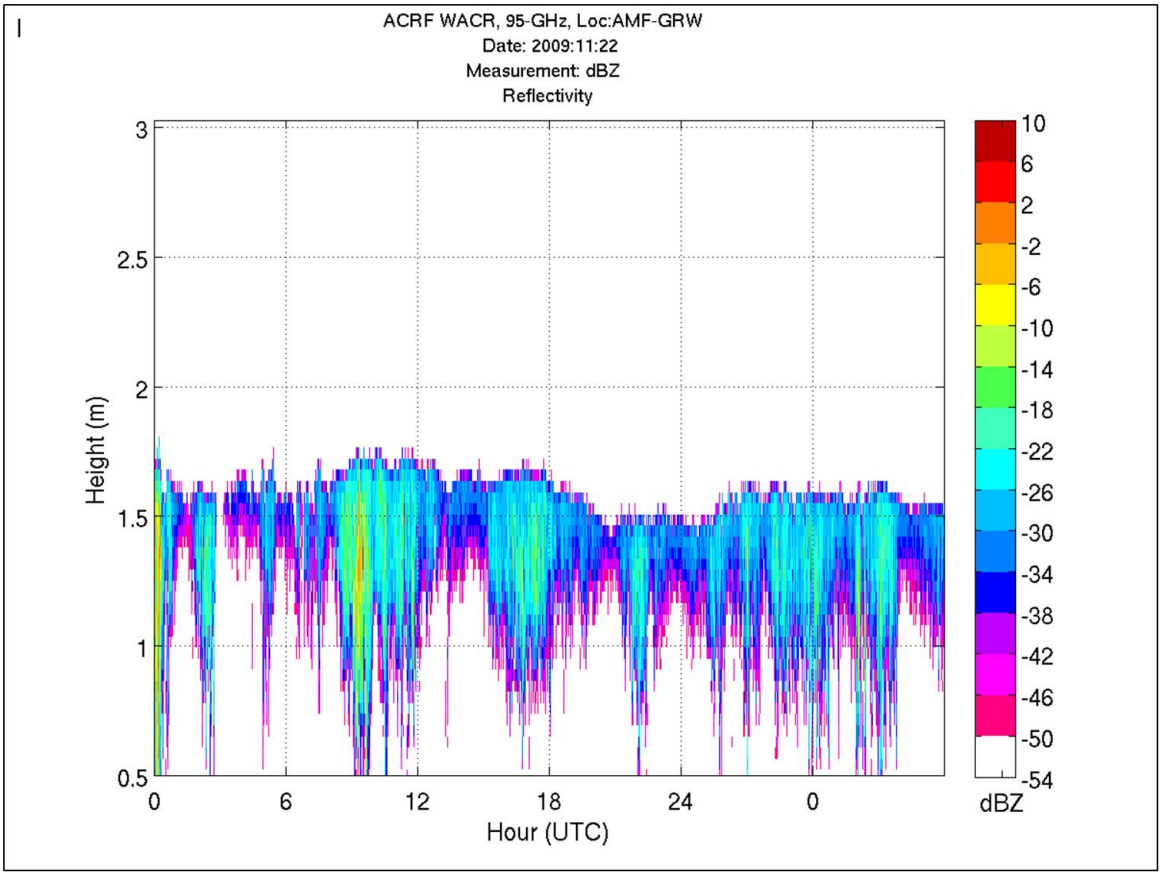

Figure 4.3 (continued)

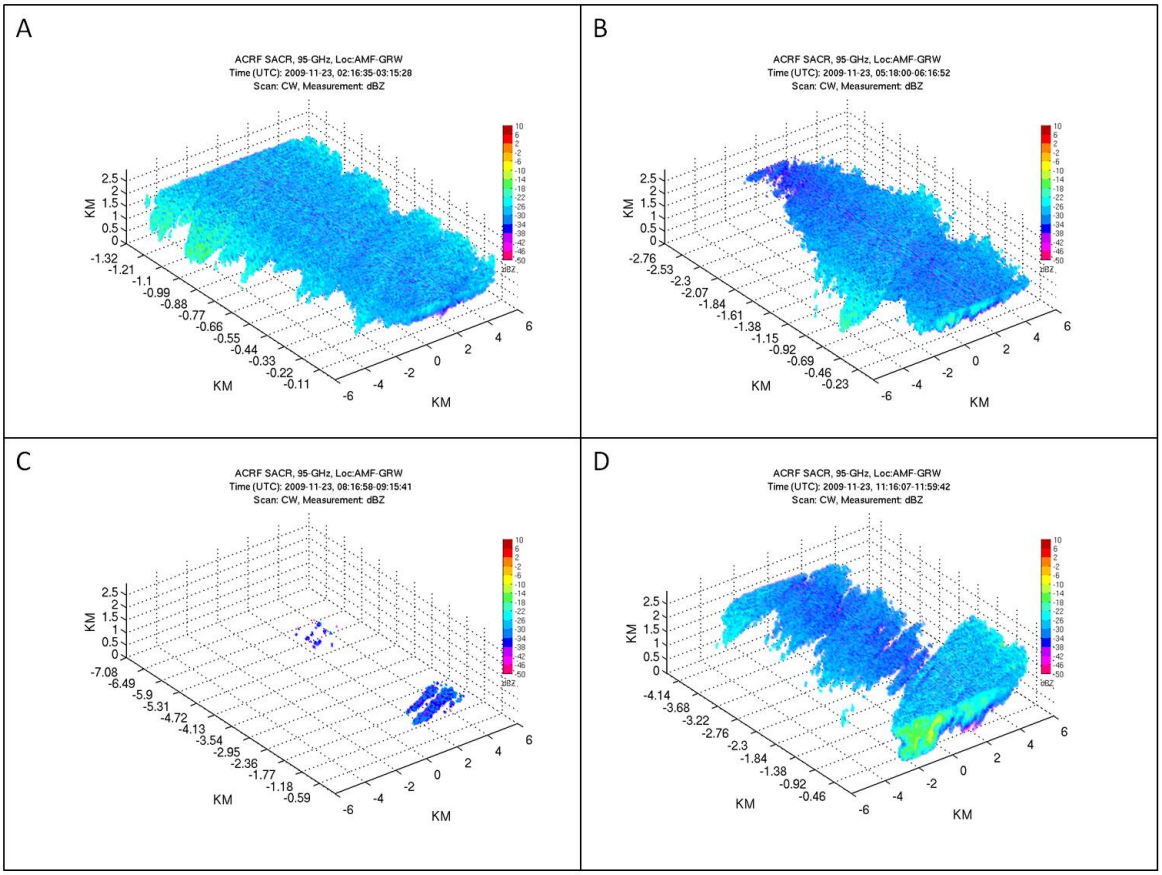

Figure 4.4: SWACR Gridded Radar Reflectivity (dBZ) for 23 November 2009 at Graciosa Island, Azores to +/- 6 km for (A) 02:16:35-03:15:28 UTC, (B) 05:18:00-06:16:52 UTC, (C) 08:16:58-09:15:41 UTC , (D) 11:16:07-11:59:42 UTC, (E) 14:18:17-15:18:43 UTC, (F) 17:22:13-18:22:47 UTC, (G) 20:25:24-21:25:37 UTC, (H) 23:28:37-23:59:32 UTC. Panel (I) shows WACR measured vertical column Radar Reflectivity (dBZ) for 24 hour period (UTC) 23 November 2009 at Graciosa Island, Azores.

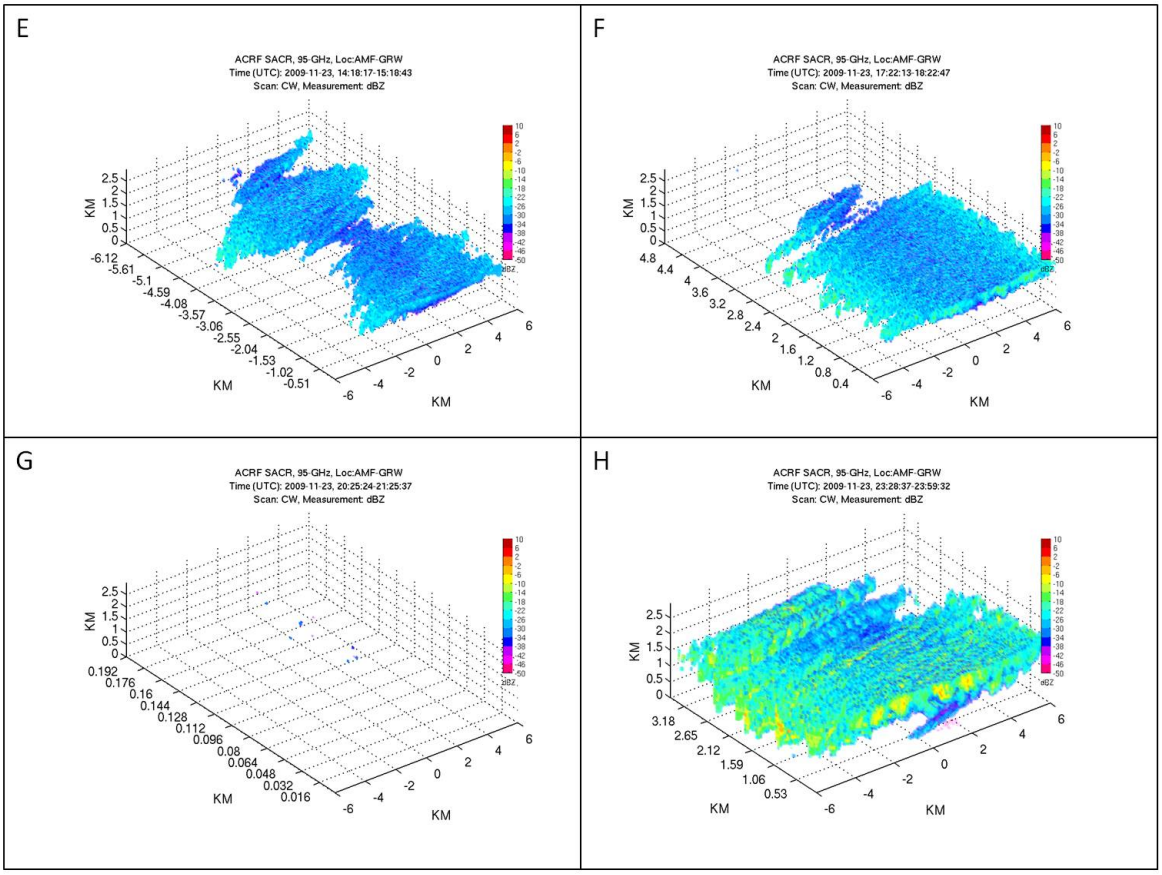

Figure 4.4 (continued)

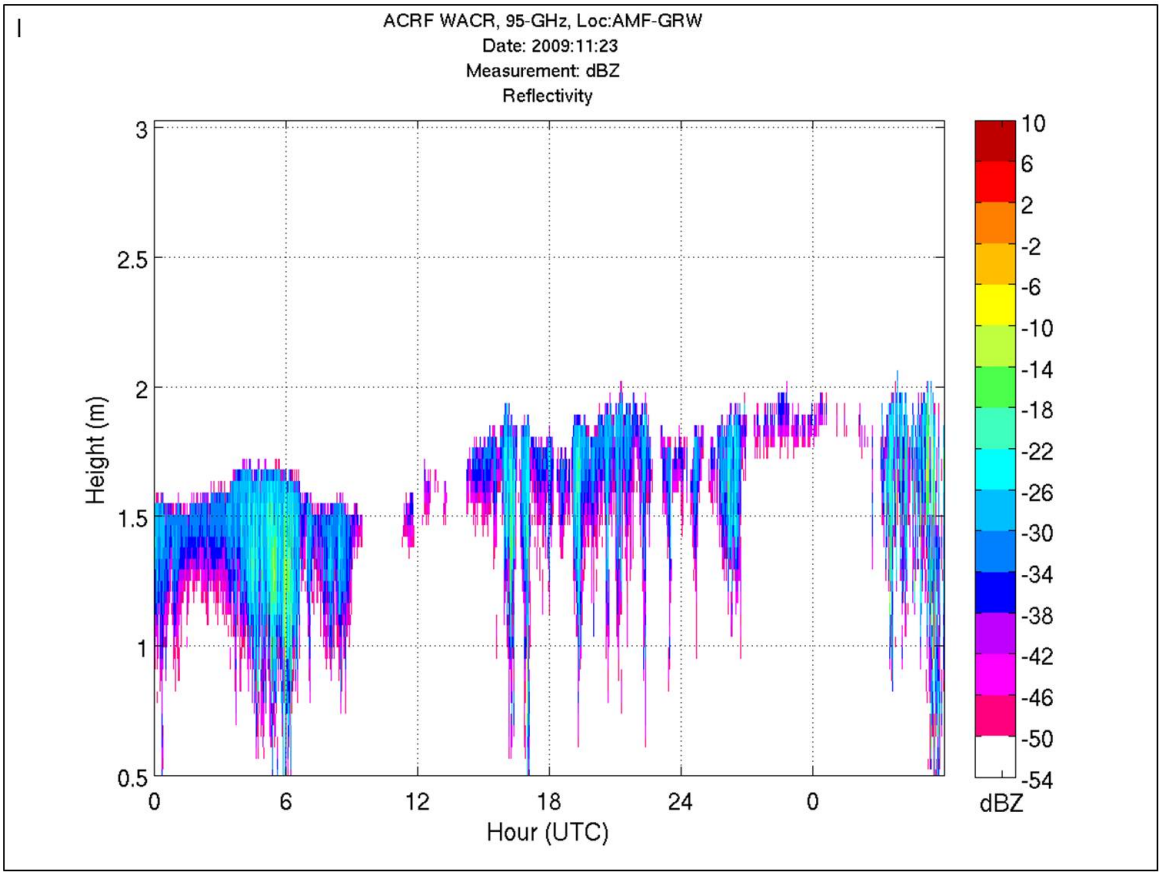

Figure 4.4 (continued)

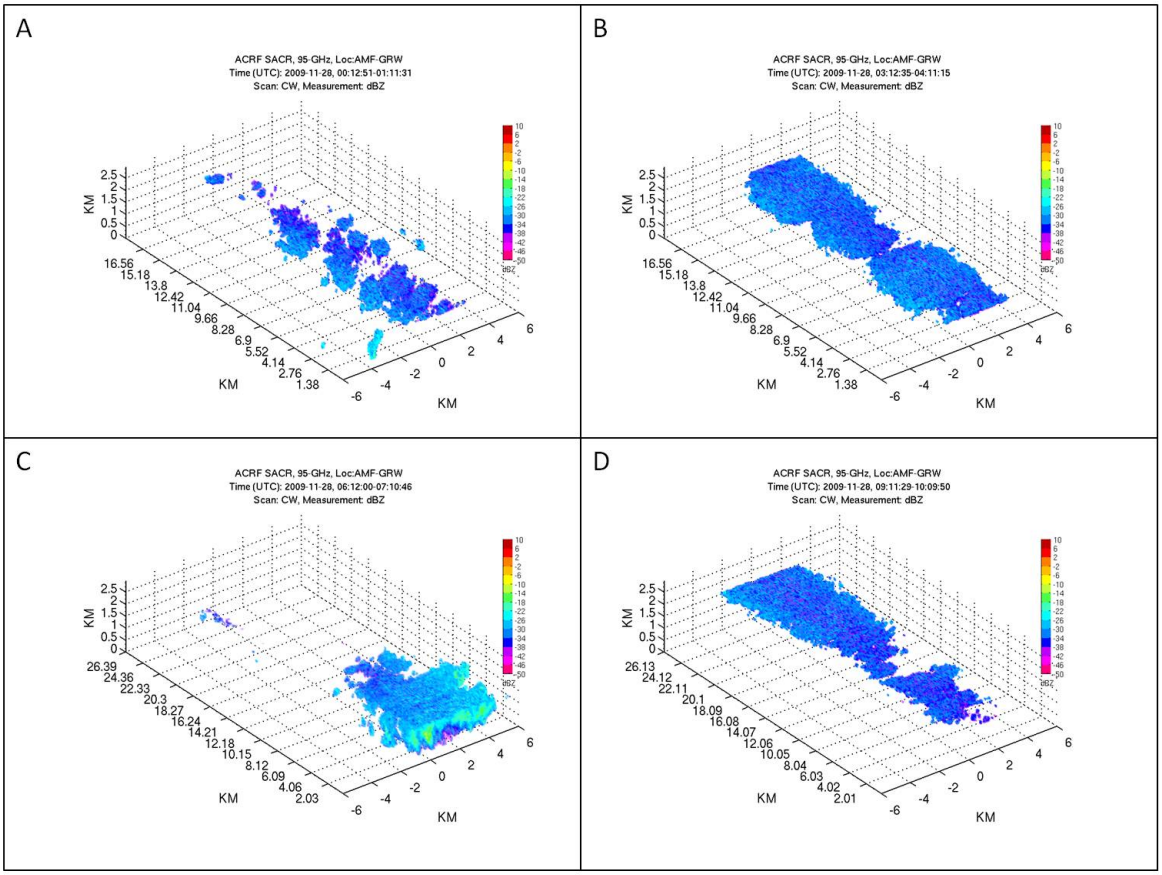

Figure 4.5: SWACR Gridded Radar Reflectivity (dBZ) for 28 November 2009 at Graciosa Island, Azores to +/- 6 km for (A) 00:12:51-01:11:31 UTC, (B) 03:12:35-04:11:15 UTC, (C) 06:12:00-07:10:46 UTC , (D) 09:11:29-10:09:50 UTC, (E) 12:10:54-13:09:40 UTC, (F) 15:11:18-16:10:10 UTC, (G) 18:10:56-19:09:42 UTC, (H) 21:10:14-22:08:32 UTC. Panel (I) shows WACR measured vertical column Radar Reflectivity (dBZ) for 24 hour period (UTC) 28 November 2009 at Graciosa Island, Azores.

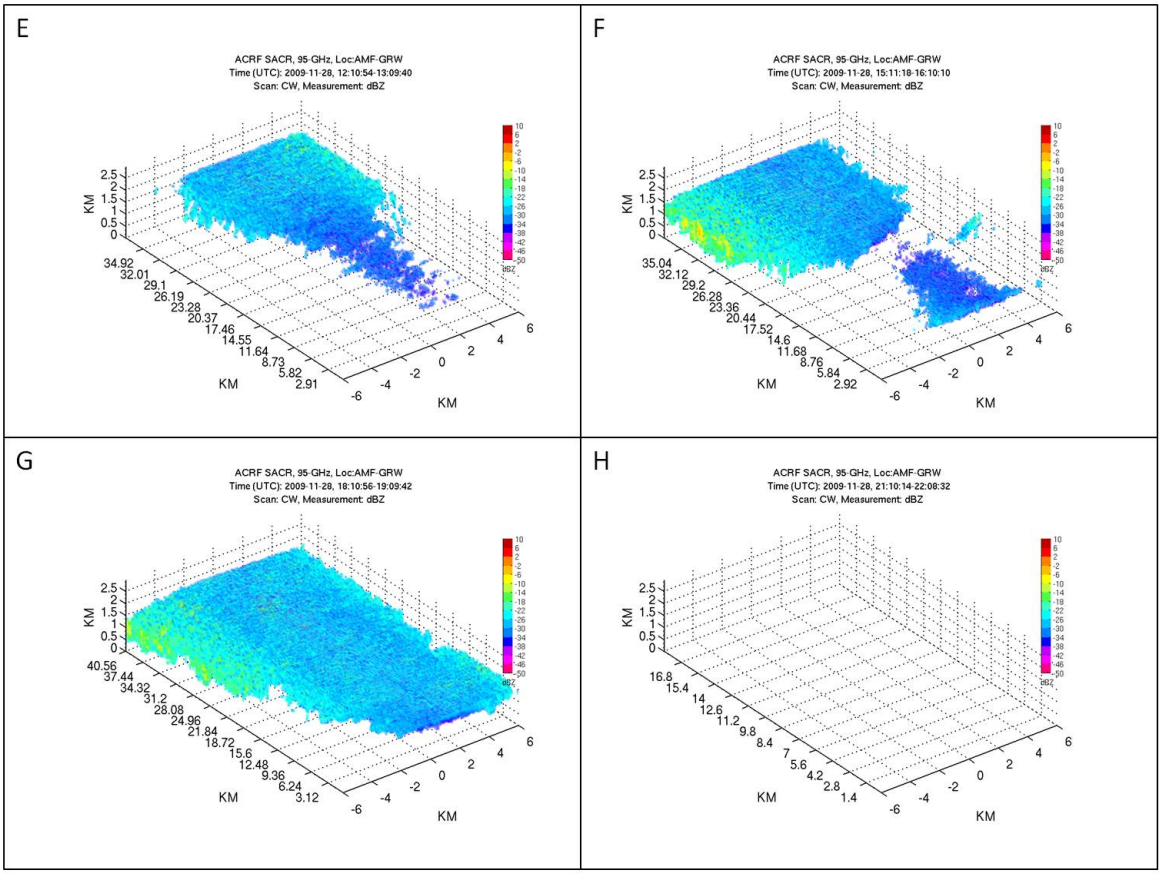

Figure 4.5 (continued)

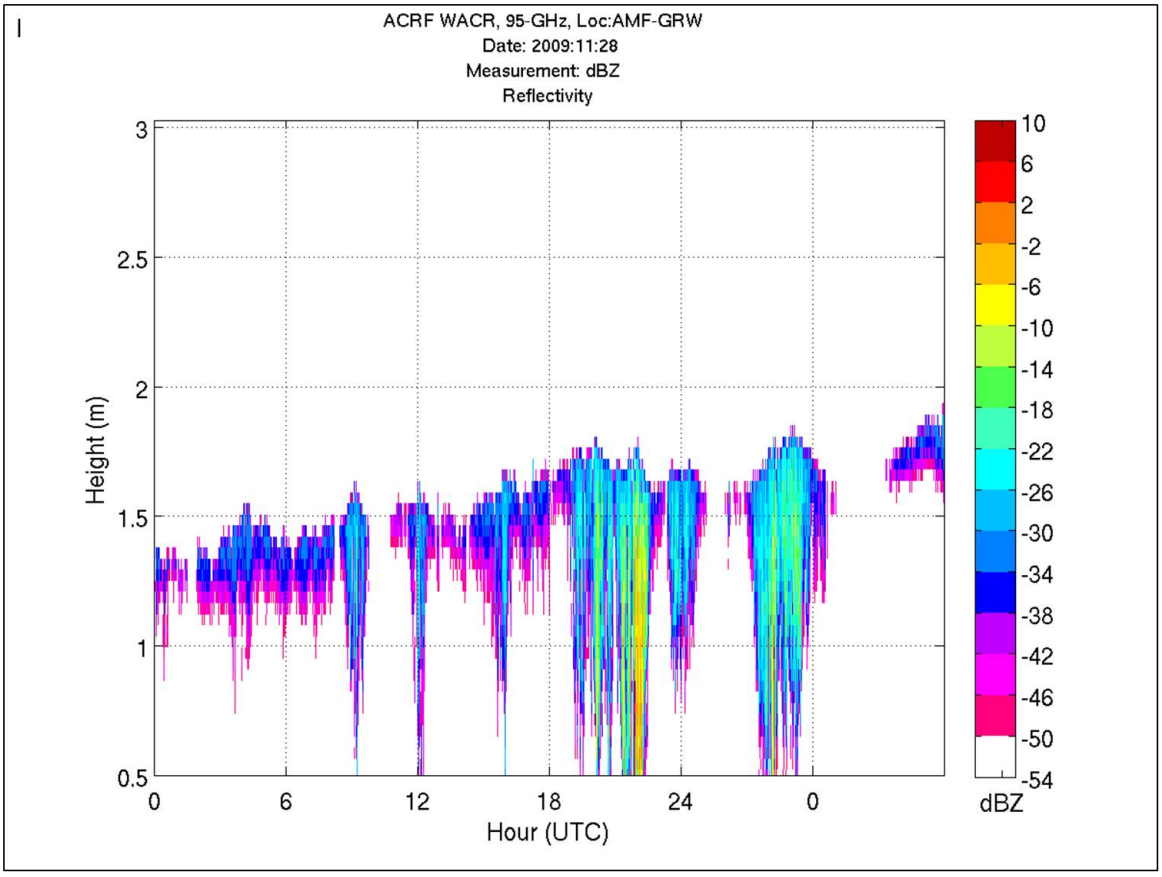

Figure 4.5 (continued)

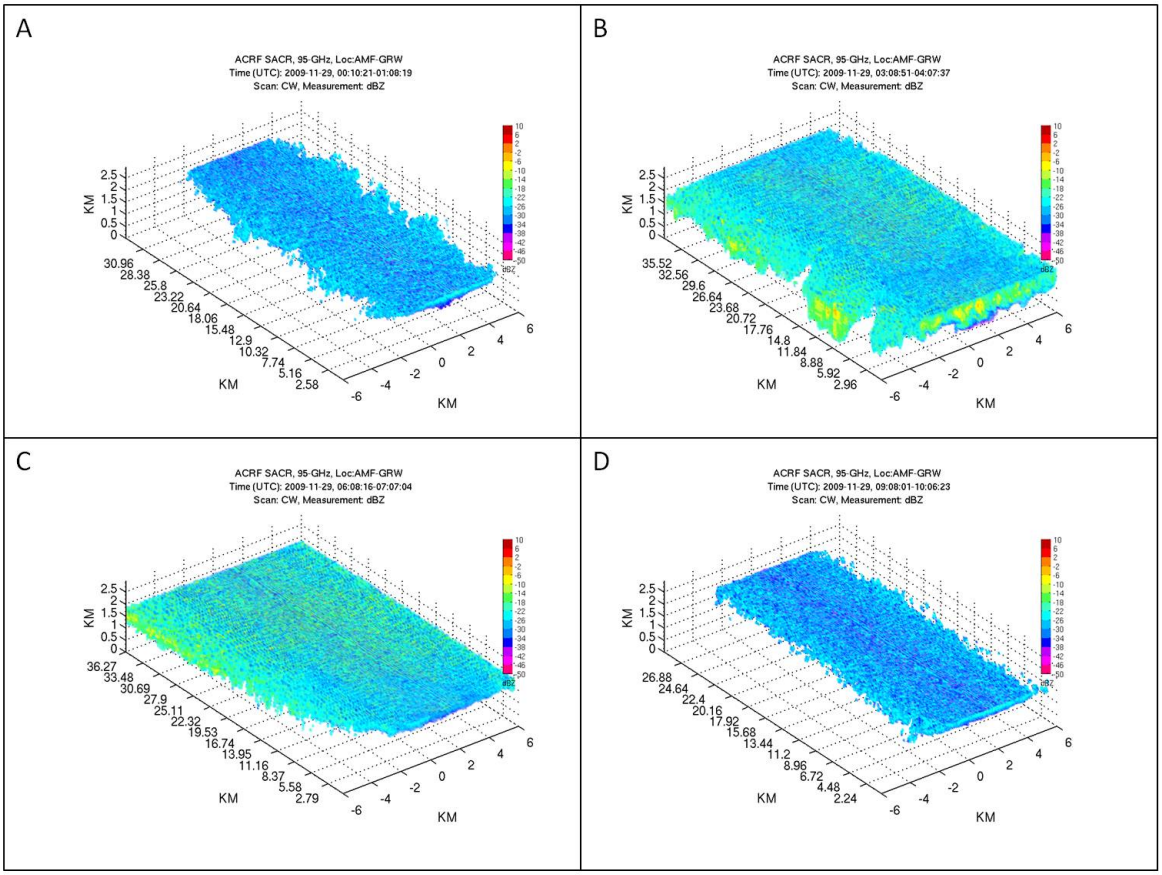

Figure 4.6: SWACR Gridded Radar Reflectivity (dBZ) for 29 November 2009 at Graciosa Island, Azores to +/- 6 km for (A) 00:10:21-01:08:19 UTC, (B) 03:08:51-04:07:37 UTC, (C) 06:08:16-07:07:04 UTC , (D) 09:08:01-10:06:23 UTC, (E) 12:07:25-13:06:16 UTC, (F) 15:09:08-16:09:00 UTC, (G) 18:12:00-19:11:06 UTC, (H) 21:12:02-22:10:25 UTC. Panel (I) shows WACR measured vertical column Radar Reflectivity (dBZ) or 24 hour period (UTC) 29 November 2009 at Graciosa Island, Azores.

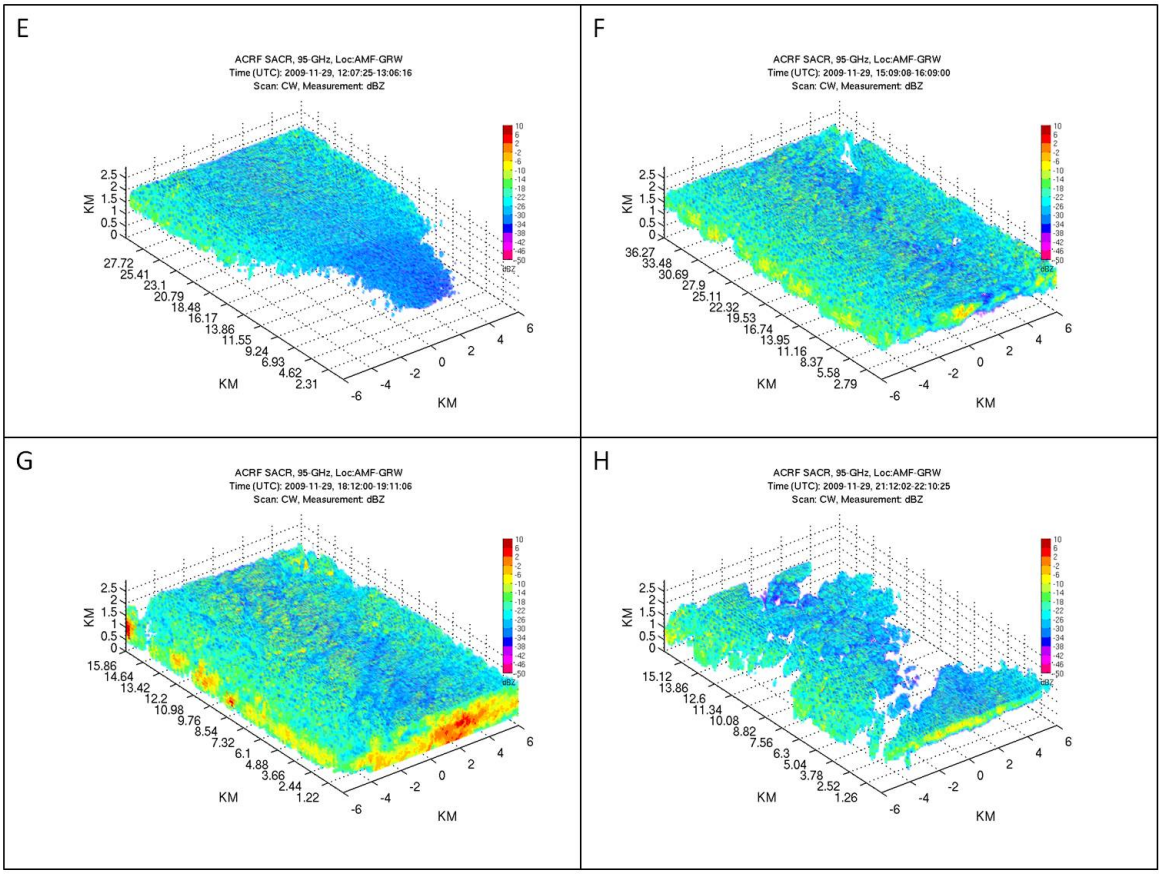

Figure 4.6 (continued)

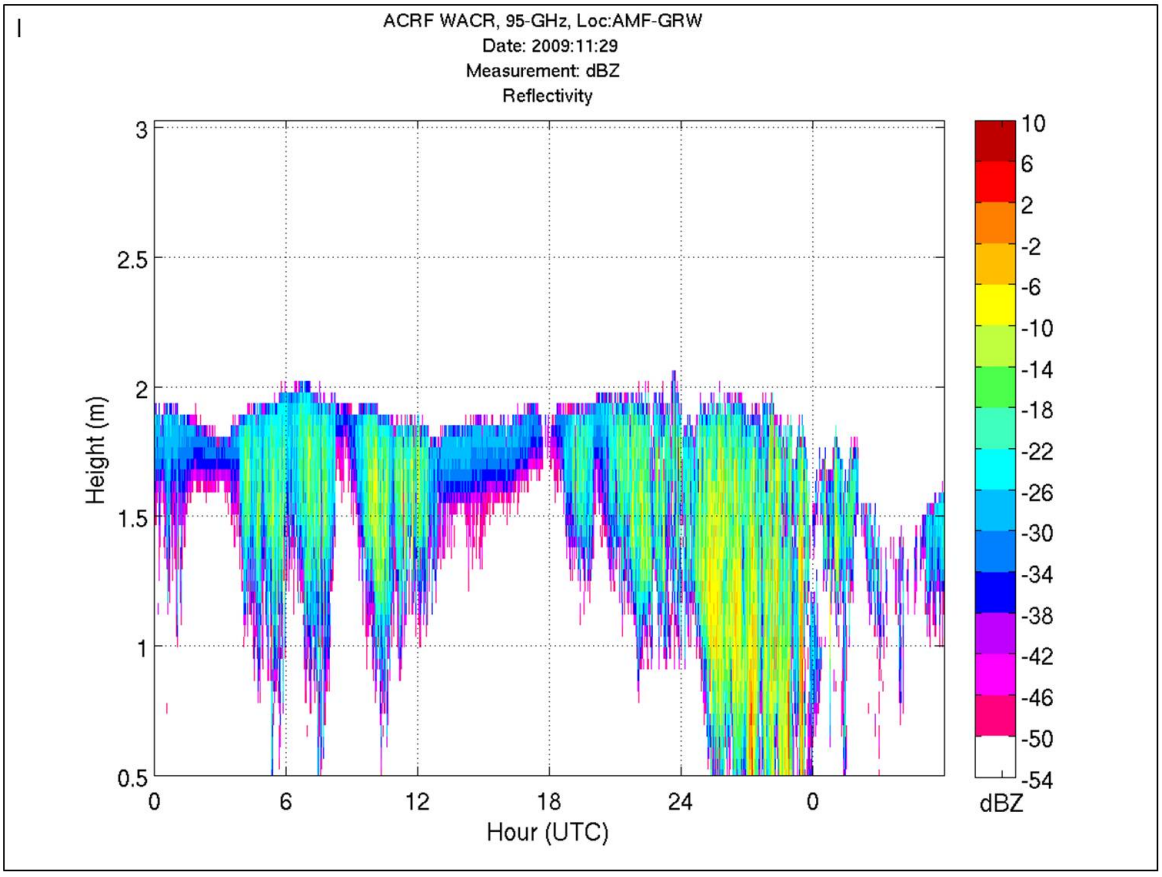

Figure 4.6 (continued)

vertical column is set to 1 if there is at least one vertical grid point containing a significant (greater than -50 dBZ) detection (cloud) and 0 otherwise (no cloud). This procedure generates a 2-D map of cloud occurrences. Second, the cloud occurrences at constant ranges from the radar are used to estimate a cloud fraction at each range point (25 m resolution), defined as the sum of the cloud occurrences divided by the total number of vertical columns at the particular range gate. We further average the cloud fraction over 10 range bins (250 m) to smooth the result for analysis of the spatial variation of cloud fraction with range as measured by the SWACR. This process is repeated for a series of radar reflectivity thresholds (-50, -40, -30, -20, and -10 dBZ) that are applied to the entire SWACR gridded domain to ascertain the impacts of sensitivity.

This process is repeated for six different cloud cases including two cloud-only periods (*Figure 4.7 a-b)*, two light drizzle periods (*Figure 4.7 c-d*), and two heavy drizzle periods (*Figure 4.7 e-f*). Several distinct features are noted throughout the six cases. A reflectivity threshold of -40 dBZ retains the same cloud fraction characteristics as a -50 dBZ threshold for all cases, while for both cloud-only cases, a reflectivity threshold of -20 dBZ reduces cloud fraction to zero. These are important findings, as a 10 dB decrease in the radar sensitivity (e.g., for -50 to -40 dBZ) is equivalent to an increase in unbiased cloud detection range by a factor of 3 by basic MDS arguments (*Eqn. 3.1*).Thus, a cloud radar with radar sensitivity -50 dBZ at 3 km will be able to detect most clouds to a range of 10 km. Furthermore, a cloud radar with sensitivity of -40 dBZ or lower at 3 km will have challenges in detecting unbiased cloud fractions within the first 10 km, as is the case with the SWACR. Cloud fraction for one cloud-only case (*Fig.4.7 a*) diminished by nearly 50% between the -40 dBZ and -30 dBZ reflectivity threshold; for the other cloud-only case (*Fig.4.7 b*), cloud fraction drops to near zero between -30 dBZ and -20 dBZ. The cloud fraction slope was very sharp for both cases in transitioning from cloud to no cloud (4-5 km from radar); we can conclude from our

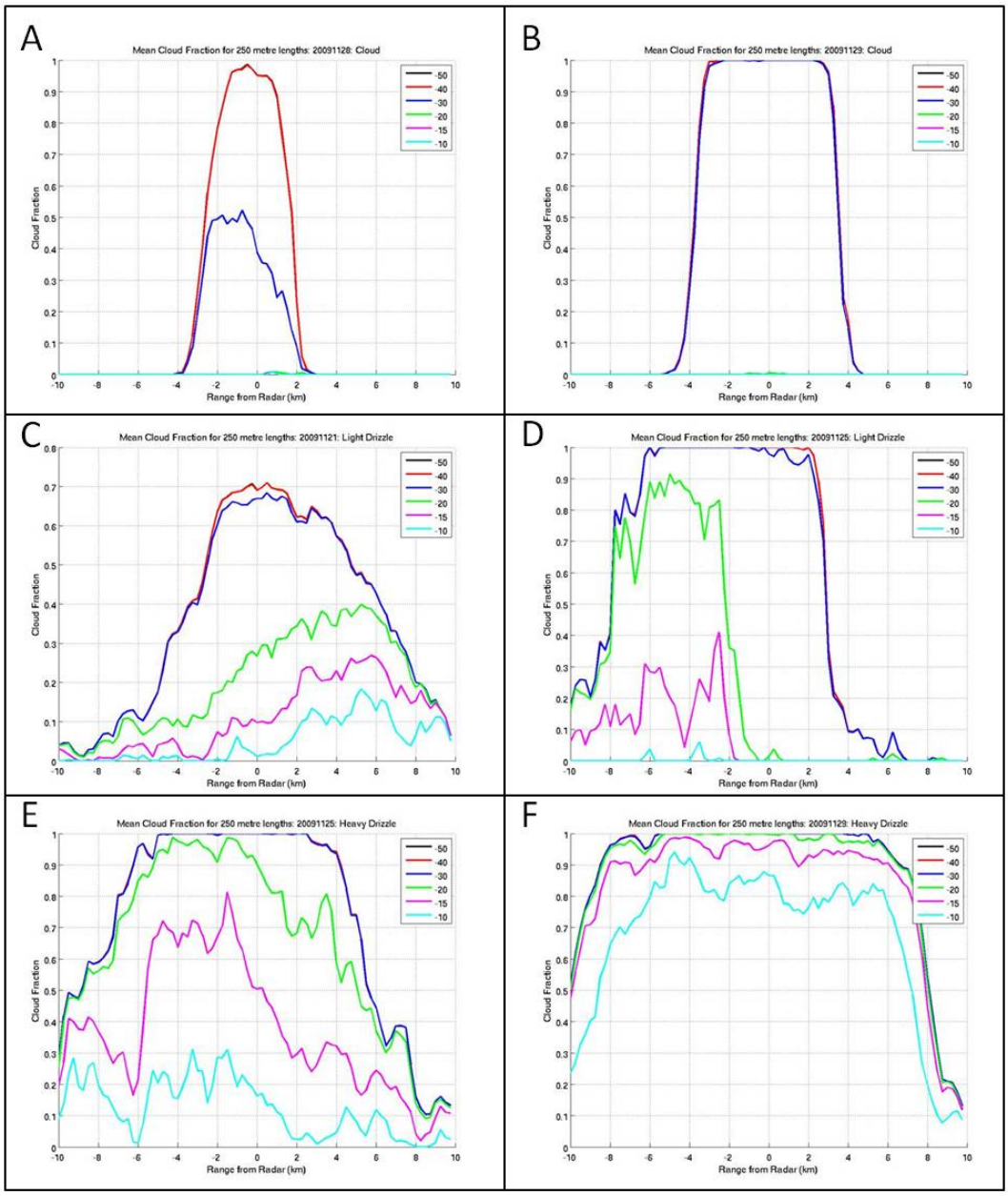

Figure 4.7: SWACR gridded radar reflectivity (dBZ) indicated spatially averaged (250 m) cloud fraction for sample cloud (a-b), light drizzle (c-d), and heavy drizzle (e-f) regimes observed by SWACR CW-RHI in November 2009 at Graciosa Island, Azores.

sensitivity studies that this slope is artificially generated by the inability of the radar to detect smaller particles at range. Cloud fraction measurements for all four drizzle cases reveal a great deal about the distribution and strength of drizzle through the field. We can estimate

the relative strength of the drizzle for regions in the domain by analyzing the cloud fraction measured by the radar for a -15 dBZ threshold (typical radar reflectivity threshold value used to detect drizzle-dominated radar volumes [e.g. Sauvageot and Omar (1987); Löhnert et al. (2001); Kollias et al. (2004)]) relative to the cloud fraction for a -50 dBZ threshold. The light and heavy drizzle examples for 25 November (*Fig.4.7 d-e*) demonstrated more extensive drizzle SW of the radar than NE. The light drizzle case on 21 November (*Fig.4.7 c*) trended toward drizzle NE of the radar, while the 29 November heavy drizzle case (*Fig.4.7 f*) was evenly distributed through the domain.

These examples cases allow us to come to several conclusions regarding the ability of the SWACR to document cloud fraction. Overall, the radar can resolve an accurate cloud fraction for all cases with a MDS of -40 dBZ. In addition, the radar performed relatively well with a limit of -30 dBZ, though some cloud detection is lost. We therefore have confidence that the radar can document cloud fraction with reasonable accuracy at a range of up to 4 km. A cloud fraction of 1 at a range beyond 4 km suggests the existence of widespread drizzle or drizzle-producing clouds. Small-scale peaks and troughs in the cloud fraction can provide some indication to the spatial variability of cloud and drizzle, while larger scale variations suggest extended regions of favourable drizzle environments. Finally, regions of stronger and more widespread drizzle can be identified by finding cases of minimal cloud fraction loss between a -15 dBZ restricted field and a -50 dBZ restricted field.

Observations from the vertically pointing radar (WACR) were analyzed to further determine the impacts of radar sensitivity on cloud fraction, and to ensure that the effects seen in analyzing the SWACR data are not artifacts of the gridding schemes. The WACR-derived hourly-averaged cloud fraction was computed for each scanning period for variable radar reflectivity thresholds (from -50 to +10 dBZ in 1 dB increments). Marine stratocumulus

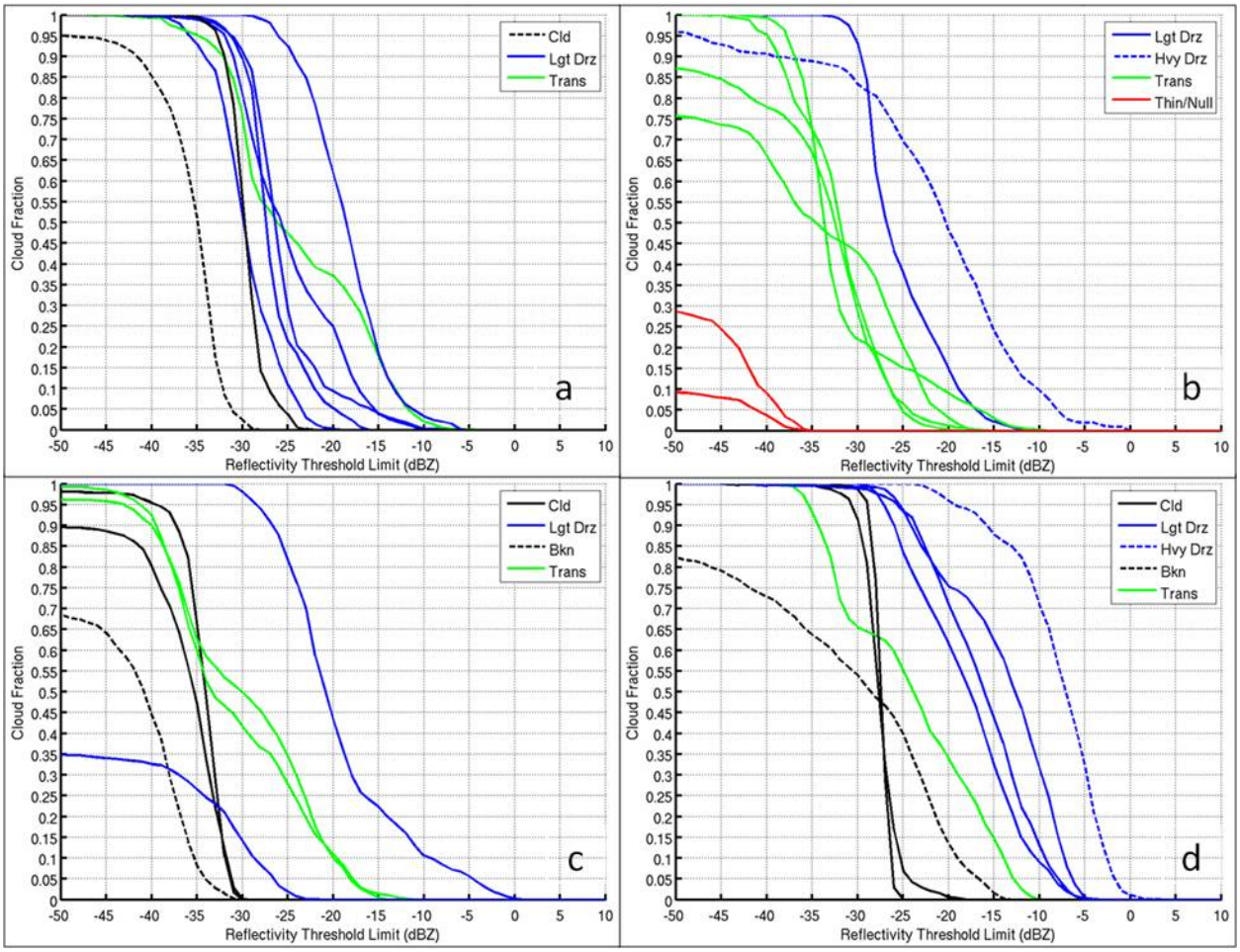

Figure 4.8: WACR Column Cloud Fraction for increased minimum detectable Radar Reflectivity (dBZ) for SWACR scanning hours on (a) 22 November 2009, (b) 23 November 2009, (c) 28 November 2009, and (d) 29 November 2009.

observations from 22, 23, 28, and 29 November, 2009 are considered (*Figure 4.8 a-d*). Clouds exhibit the highest decreases in cloud (or general hydrometeor) fraction with MDS. The majority of cloud cases, as well as several light drizzle and transition cases, demonstrated substantial (greater than 50%) drops in measured cloud fraction over a 5 dB threshold interval; these drop-offs rarely occurred before a MDS of -35 dBZ and were predominantly clustered in the -30 dBZ to -25 dBZ range. Noticeably, drizzle containing layers exhibit two different rates of hydrometeor fraction decrease with MDS with a lower rate of loss of hydrometeor

fraction from 0.3 to 0. These results match well with our SWACR results in *Figure 4.7*.

4.1.2 Spatial Mapping of Cloud Boundaries and Characteristics

The 3D determination of the cloud and precipitation layers (e.g., layer top and layer base) is one of the anticipated observations by the ARM scanning cloud radars. For each gridded vertical column (e.g., fixed horizontal location) cloud top and cloud base were defined as the lowest and highest height, respectively, that SWACR detected significant returns (Reflectivity greater than or equal to -50 dBZ). Using all the available gridded data sets, cloud base height, cloud top height, and cloud thickness are determined for all vertical columns in the gridded domain. Since the radar sensitivity and resolution systematically degrades along the crosswind (range) dimension, all the cloud boundaries estimates that correspond to the same crosswind grid point are averaged. In order to improve the robustness of the mean boundaries estimates we further average them into 250 m resolution crosswind(range) increments. Thus, the results are presented along the crosswind dimension. Finally, these estimates are repeated for different radar reflectivity thresholds (-50; -40; -30; -20; -15; -10 dBZ) applied to the entire SWACR gridded data domain.

Two cases from each of the following conditions are analyzed: cloud-only, light drizzle, and heavy drizzle observations. The regime classification is based on the procedure described in *section 3.5*. The cloud top height as a function of range from the radar for different radar reflectivity threshold values is shown for all six cases in *Figure 4.9*. Both cloud cases (*Figure 4.9 a-b*) demonstrate cloud tops extending 4-6 km from radar zenith, after which there are no more significant returns. The lack of cloud detections beyond this range (4-6 km) is attributed to the lack of sensitivity for the SWACR to detect tenuous cloud radar returns. Drizzle free periods (cloud only) have typically radar reflectivity values below -30 dBZ, with

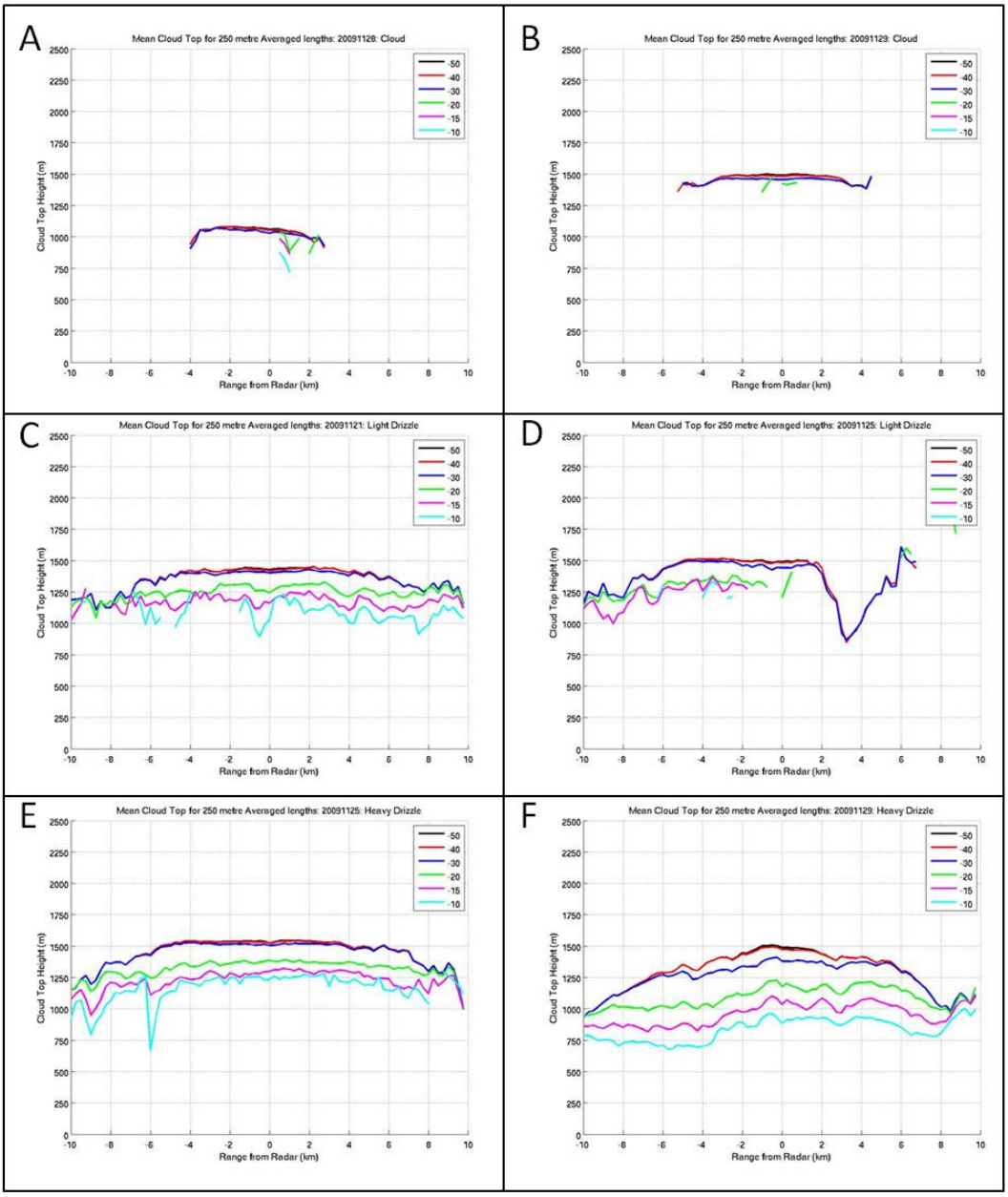

Figure 4.9: SWACR gridded radar reflectivity (dBZ) indicated spatially averaged (250 m) cloud top for sample cloud (a-b), light drizzle (c-d), and heavy drizzle (e-f) regimes observed by SWACR CW-RHI in November 2009 at Graciosa Island, Azores.

maximum reflectivities rarely exceeding -25 dBZ. By virtue of the sensitivity drop in the radar at range, and the generally stable characteristics of cloud-only observations, a sudden drop-off in observations at 4-6 km appears to be purely an artifact of the radar. Furthermore,

the use of high radar reflectivity threshold values (-20 dBZ or higher) results in a complete removal of the cloud layer. Despite the challenge in detecting clouds and their properties (e.g. cloud top height), the SWACR still performs well in resolving unambiguous physical cloud top characteristics out to a range of 5 km away from radar zenith. This is sufficient for most radiative transfer applications and for matching most Large-Eddy Simulations (LES) modeling domains. In the case of drizzling clouds (*Figure 4.9 c-f*), the range detection of the radar is beyond 10 km and the use of a radar reflectivity threshold results in a drop in the cloud top height, but generates range-unbiased statistics. For all six examples (*Figure 4.9 a-f*), the physical cloud top is generally 1.5 km, consistent with the typical height of the marine boundary layer for Graciosa during the month. Assuming cloud top as the top of the PBL, we can conclude that there was little spatial variability in the PBL depth across the radar domain due to a non-varying cloud top height out to 5 km from zenith. From this result, we conclude that any effect by the island topography on the depth of the boundary layer is negligible, as these sample cases are representative of a variety of wind regimes. Finally, the difference between the physical cloud top and drizzle cloud top for all drizzle cases, taken as the difference between cloud top and cloud bottom at zenith and at an 8 km range, averages around 250 m (*Figure 4.9 c-f*).

Similar challenges in the determination of the marine stratocumulus cloud base using the SWACR gridded data as a function of range are found (*Figure 4.10*). For cloud cases (*Figure 4.10 a-b*), the detected boundary is the real cloud base, but its detection beyond 4-6 km is problematic due to the lack of sufficient SWACR sensitivity. For drizzle cases (*Figure 4.10 c-f*), it is important to state that the SWACR is not detecting the true cloud base height, but rather the drizzle particles below the cloud base. The higher radar reflectivity of volumes that contain drizzle particles enable the detection of drizzle bases at far ranges. Evaporation generally occurs as drizzle droplets fall into the sub-cloud atmosphere, decreasing the size of

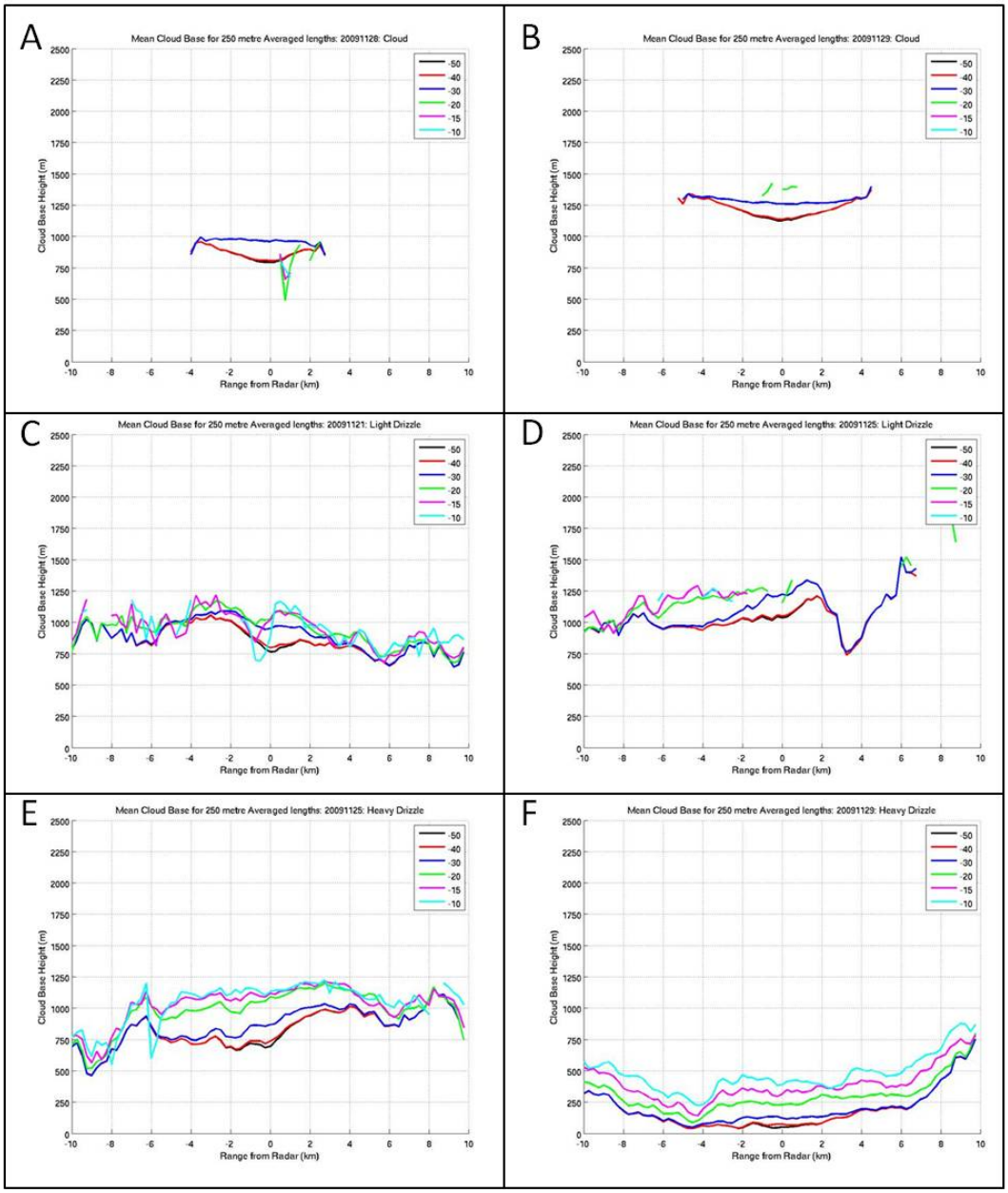

Figure 4.10: SWACR gridded radar reflectivity (dBZ) indicated spatially averaged (250 m) cloud base for sample cloud (a-b), light drizzle (c-d), and heavy drizzle (e-f) regimes observed by SWACR CW-RHI in November 2009 at Graciosa Island, Azores.

the droplets until they either evaporate completely (virga) or reach the ground. The upward concavity in cloud base at lower reflectivity thresholds (less than -30 dBZ) at far ranges suggests that the radar struggles to observe these small drizzle droplets during evaporation

at far ranges from the radar.

Despite the issues with sensitivity in the radar volume, the SWACR presents an interesting depiction of cloud base for all six cases (*Figure 4.10*). Cloud cases (*Figure 4.10 a-b*) exhibit a very stable cloud base, with very little variation because of the lack of larger particles precipitating below cloud base. Precipitating cases (*Figure 4.10 c-f*), on the other hand, demonstrate a noisier cloud base due to the prevalence of drizzle throughout the domain. Large-scale variations in cloud/drizzle base can also be noted, such as in the light drizzle case on 25 November (2 to 6 km, *Figure 4.10 d*), the heavy drizzle case on 25 November (-10 to -8 km and 2 to 8 km, *Figure 4.10 e*) and the heavy drizzle case on 29 November (-6 to -4 km, *Figure 4.10 f*). We can conclude that these are the result of large-scale natural fluctuations in the field, as they do not follow the trend associated with the sensitivity issue. Smaller scale fluctuations, particularly noted in the -10 dBZ threshold contour (*Figure 4.10 c-f*), suggest the impacts of pockets of relatively strong drizzle within the larger domain. These fluctuations are generally small deviations from the overall cloud base trend with range, suggesting these variations (and corresponding drizzle pockets) are more random in nature as opposed to a larger-scale feature.

Finally, the determination of cloud thickness as a function of range for both cloud only and for drizzling cases is examined in *Figure 4.11*. As expected, the erosion of cloud boundaries as a function of range (due to the SWACR drop in sensitivity) results in a cloud thickness that is highly dependent on range. The use of -30 dBZ threshold makes the reported cloud thickness nearly independent of range; however it is biased low due to the inability to resolve smaller particles at cloud edges. For drizzle cases (*Figure 4.11 c-f*), we again find a noisier field than for cloud cases (*Figure 4.11 a-b*), by virtue of the highly varying cloud base from

drizzle.

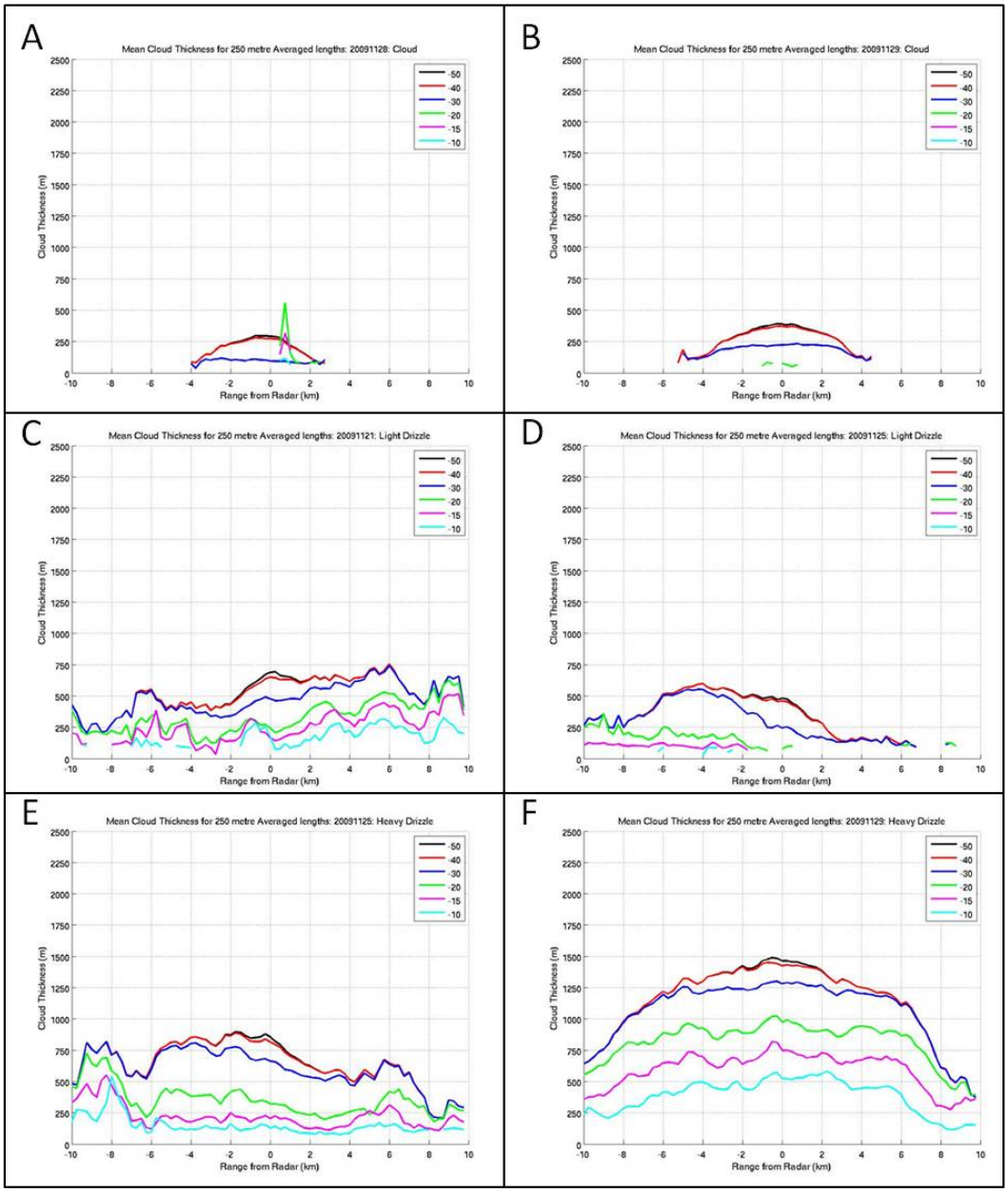

Figure 4.11: SWACR gridded radar reflectivity (dBZ) indicated spatially averaged (250 m) cloud thickness for sample cloud (a-b), light drizzle (c-d), and heavy drizzle (e-f) regimes observed by SWACR CW-RHI in November 2009 at Graciosa Island, Azores.

The overall cloud and drizzle climatology at Graciosa, as observed by the SWACR, revealed several details about the field. For a -50 dBZ threshold (*Figure 4.12*), which represents the maximum sensitivity of the SWACR, we find that cloud top values varied between 900 m and 1800 m, with a frequency peak height around 1700 m (*Figure 4.12 a-c*).

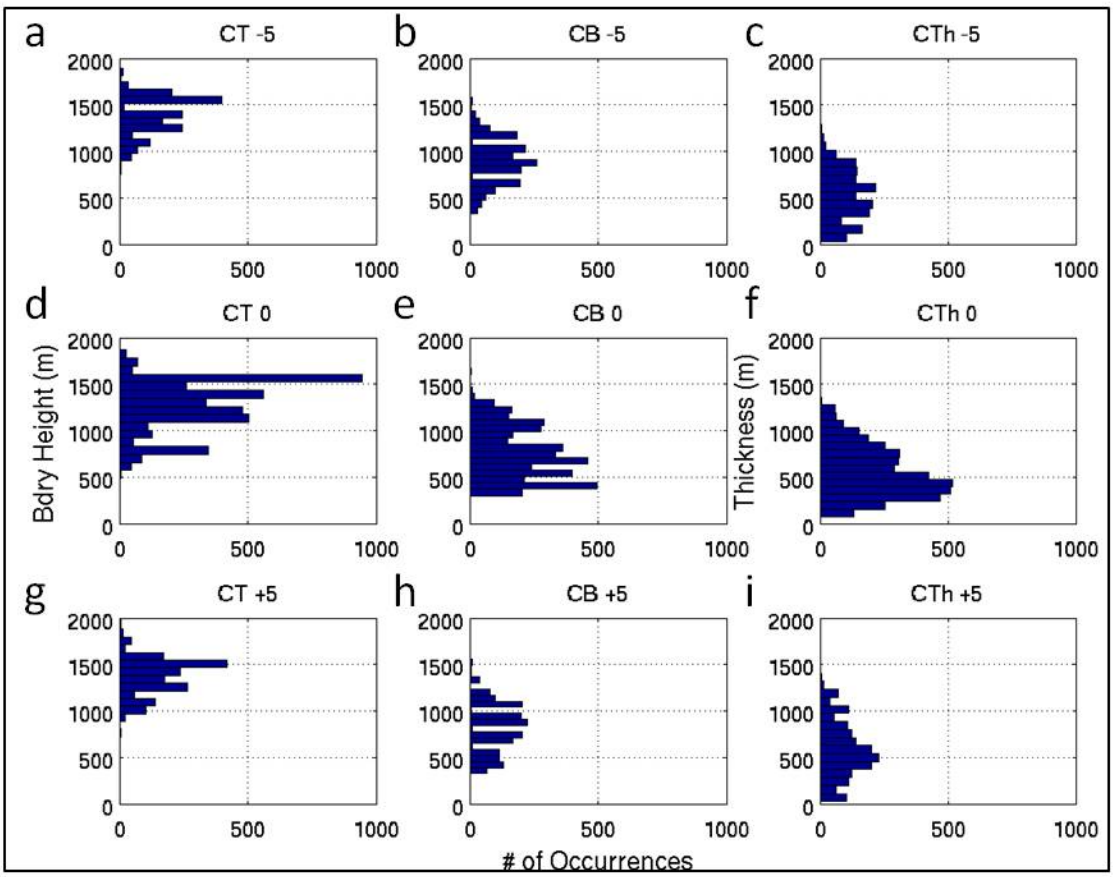

Figure 4.12: SWACR gridded radar reflectivity (dBZ) indicated cloud boundary climatology (probability distribution function) for all scanning periods in November 2009 with an applied -50 dBZ radar reflectivity threshold. Cloud top (a,d,g), cloud base (b,e,h), and cloud thickness (c,f,i) are considered for locations 5 km Southwest (a-c) of the radar, at radar zenith (d-f), and 5 km Northeast (g-i) of the radar.

Further, a secondary frequency peak of ∼800 m is noted directly above the radar (*Figure 4.12 a*); this can be attributed to weak thin clouds that are below the radar sensitivity at 5 km range and are therefore undetectable at this range. Cloud base varied between the

artificially-forced base of 400 m (to remove any radar artifacts) and ∼1200 m, with a general broad frequency peak of observations between 700 m and 1100 m (*Figure 4.12 d-f*). Finally, cloud thicknesses demonstrated a frequency peak of around 400 m within a distribution between 100 m and 1200 m (*Figure 4.12 g-i*). The drizzle field is examined using a -15 dBZ threshold (*Figure 4.13*). Overall, we find a similar drizzle boundary field at all three points. Drizzle top values peaked from 1200 1300 m (*Figure 4.13 a-c*), while drizzle base frequency peaked around 1000 m (*Figure 4.13 d-f*). Finally, drizzle thickness demonstrated a peak

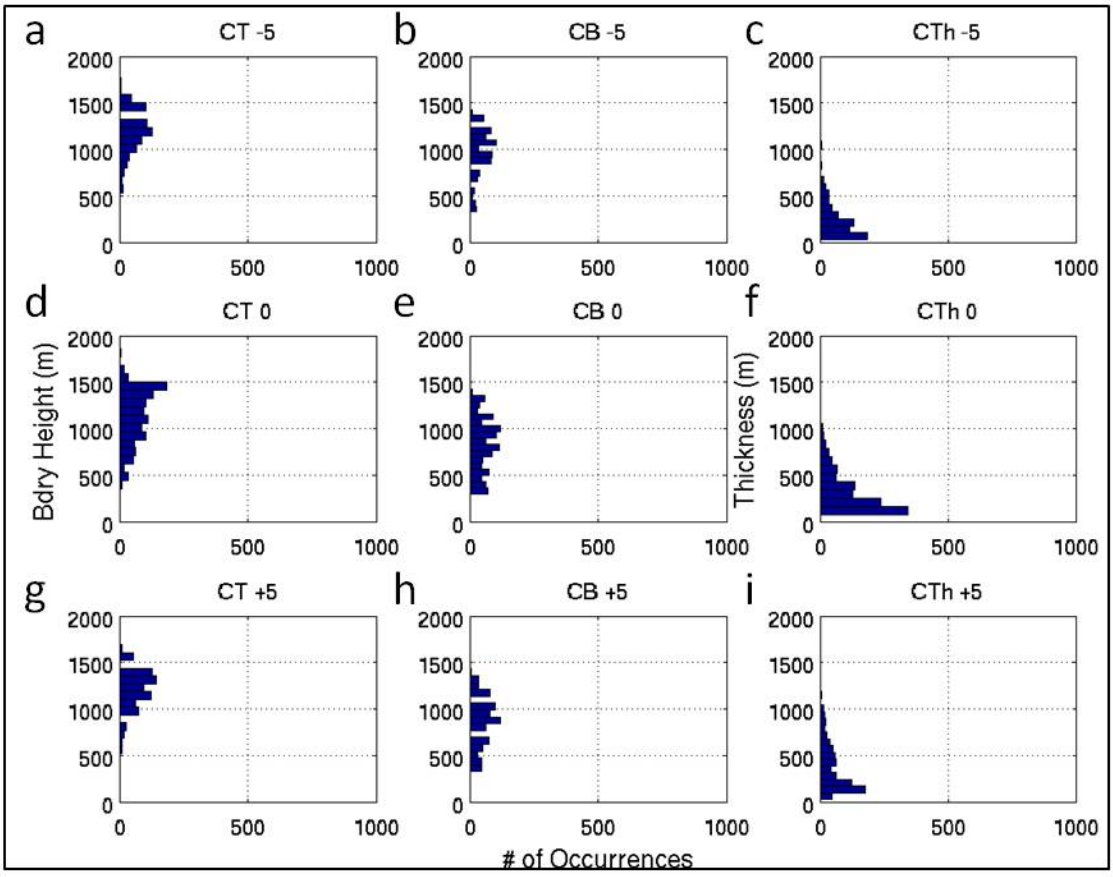

Figure 4.13: SWACR gridded radar reflectivity (dBZ) indicated drizzle boundary climatology (probability distribution function) for all scanning periods in November 2009 with an applied -15 dBZ radar reflectivity threshold. Drizzle top (a,d,g), drizzle base (b,e,h), and drizzle thickness (c,f,i) are considered for locations 5 km Southwest (a-c) of the radar, at radar zenith (d-f), and 5 km Northeast (g-i) of the radar.

frequency of less than 200 m (*Figure 4.13 g-i*), suggesting that the majority of drizzle in the observation field was relatively shallow. For both thresholds (-50 and -15 dBZ), slight differences in the cloud property distributions between the -5 km location (southwest of the radar - over land) and +5 km (northeast of the radar - over ocean) can be seen. These differences may be due to orographic and land-sea contrast effects, though further analysis is required to isolate the causality.

4.2 Observations of Imbedded Roll Structures

Constant height slices of the gridded SWACR data at cloud base, cloud middle, and cloud top can be used to provide insight in the internal structure of marine stratocumulus. Here, the cloud top is defined as the mean cloud top for the full observational domain and the cloud base is defined as the mean ceilometer-indicated cloud base for the scan period. The middle of the cloud layer is defined as the height between cloud base and cloud top height. These divides are applied to the 15:09:08-16:09:00 UTC scan on 29 November, 2009 (*Figure 4.14*), revealing many interesting observations at each height level in the cloud. Maximum reflectivity values generally were measured at cloud base (*Figure 4.14 c*), and diminished to a minimum at cloud top throughout nearly the entire domain, suggesting the occurrence of drizzle and large particle loading at cloud base. Reflectivity values (dBZ) range from -50 to 5 dBZ; the stronger radar returns support the existence of drizzle in the cloud field. Further examination of the 3D gridded radar reflectivity product also suggests the existence of drizzle, wherein several areas of higher reflectivity extend below the apparent cloud base (*Figure 4.14 d*). In addition, a notable decrease in sensitivity to weak radar returns is observed at all three levels with range from the radar, although this effect is most evident at cloud top. Finally, there is a distinct linear streak-type structure evident at all levels of the cloud, though most predominantly at cloud base. These structures occurred in some, but not all,

gridded cases, and were primarily associated with precipitation cases.

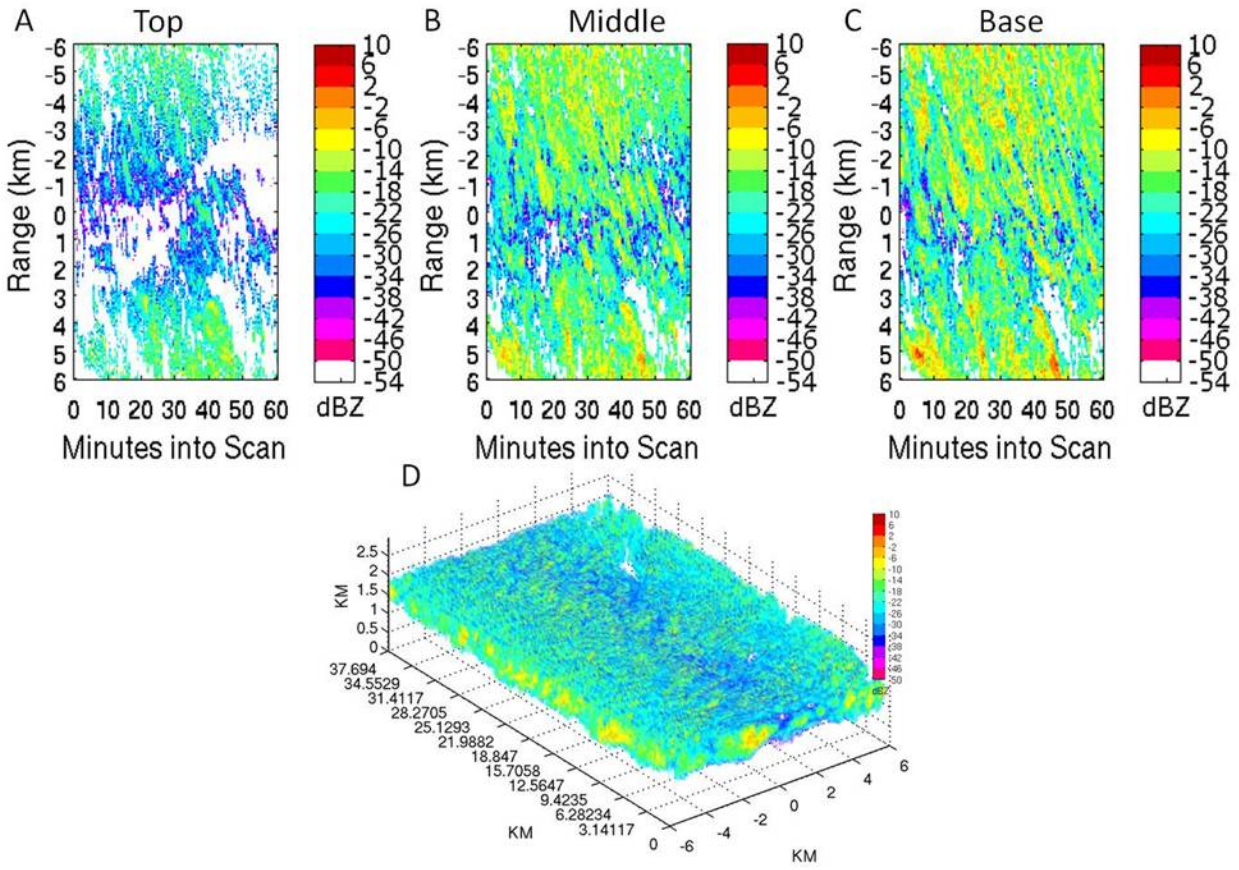

Figure 4.14: SWACR 3D gridded radar reflectivity (dBZ) for 15:09:08-16:09:00 UTC 29 November 2009 at three levels dictated by ceilometer cloud base and radar-indicated cloud top: (a) cloud top, (b) cloud middle, and (c) cloud base. Full 3D gridded domain to +/- 6 km is plotted below (d).

The preferred orientation of the radar reflectivity echoes at the cloud base indirectly suggests the presence of a dynamical organization in terms of boundary layer rolls that is responsible for the drizzle growth. Under this hypothesis, additional analysis was performed to: i) investigate how often such drizzle streaks occur at the cloud base level and ii) what is their orientation relative to the wind direction. Visual inspection of drizzle patterns at cloud base reveal that of 194 sets of SWACR gridded data, 26 exhibited semi-organized streaking structures. Thirteen of these twenty six were removed from analysis by the 35°

criteria proposed in *section 3.5*. The streak types were divided into two categories: unbroken drizzle streaks and loosely-aligned drizzle streaks. Unbroken streaks were considered to be extended (greater than 2 km in length) continuous bands of reflectivity-threshold indicated drizzle and/or non-drizzle that were strongly aligned uni-directionally (less than 3° difference amongst streaks). Loosely-aligned streaks demonstrated similar characteristics to the unbroken streaks, but the alignment of the streaks was not strongly uni-directional (greater than 3° difference between streaks). However, they still demonstrated a general organization along an axis of alignment. *Figure 4.15* demonstrates examples of the criterion outlined above, where (A) is an unbroken case and (B) is a loosely-aligned case. Overall, there were

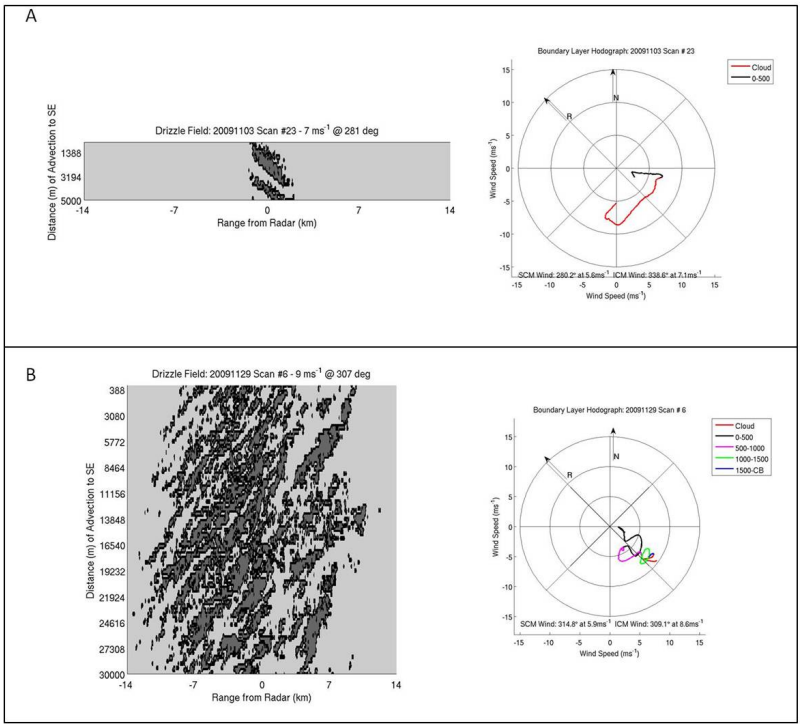

Figure 4.15: Drizzle/No drizzle fields computed using SWACR 3D gridded Radar Reflectivity (dBZ) where dark Gray streaks indicate drizzle, while light gray streaks indicate cloud or no reflectivity. Two streak regimes samples [(A) unbroken streak case (2009/11/03: 11:34:03 11:45:59 UTC) and (B) loosely-aligned streak case (2009/11/29: 15:09:08 16:09:00 UTC)] are presented with corresponding hodographs computed from the nearest radiosonde data [12 UTC (A) and 18 UTC (B)] launched near radar location in Graciosa Island, Azores.

5 unbroken cases and 8 loosely-aligned cases for November 2009. The unbroken case example, 11:34:03-11:46:59 UTC 3 November, 2009 (*Figure 4.15 a*), demonstrates 2 distinct drizzle streaks, separated by roughly 2.5 km. Noting the y-axis points to 315° (northwest), the long axis of the streak is 86°/266°, per our axis definition in *section 3.5*. The loosely-aligned case example, 15:09:08-16:09:00 UTC 29 November, 2009 (*Figure 4.15 b*), shows some evidence of streak alignment, though there is not a clearly organized band, and several of the drizzle bands blend together or vary their axis angle. Despite the noisy streak environment, there is an apparent long axis of 175°/355°. These example cases encompass the general characteristics of their respective regimes.

Analysis was performed to determine if the streaks measured by the SWACR compared well with the results of past studies regarding the streak axis-wind vector alignment, and if preexisting minima for wind speed and shear strength were met. Past studies have utilized several different vertical profiles of wind vectors in the PBL for comparison with the long axis of streaks (e.g. LeMone (1973); Frisch et al. (1976); Kropfli and Hildebrand (1980); Wackerman et al. (1996)). For this study, we considered the mean sub-cloud wind, mean in-cloud wind, and wind at the top of the PBL. Wind measurements at the cloud base height were taken from the nearest sounding. The offset angle, or difference between the mean wind and long axis angle, is shown in *Figure 4.16* for the mean in-cloud wind (a) and mean sub-cloud wind (b). We find the mean sub-cloud wind resolves 64% of cases with an offset angle of 20° or less, in agreement with past observational studies. The mean in-cloud wind performed worse, retaining just 36% of cases within a 20° offset angle. Based on these results, we conclude that the mean sub-cloud wind had the largest influence on the formation of boundary layer rolls for this study. In addition, a minimum wind speed of 3.9 ms^{-1} was noted for all 13 cases, exceeding criteria proposed several past studies of a minimum speed

of 3.5 ms^{-1} required to support organization of roll structures (e.g. Kropfli and Hildebrand (1980); Lohou et al. (1998)).

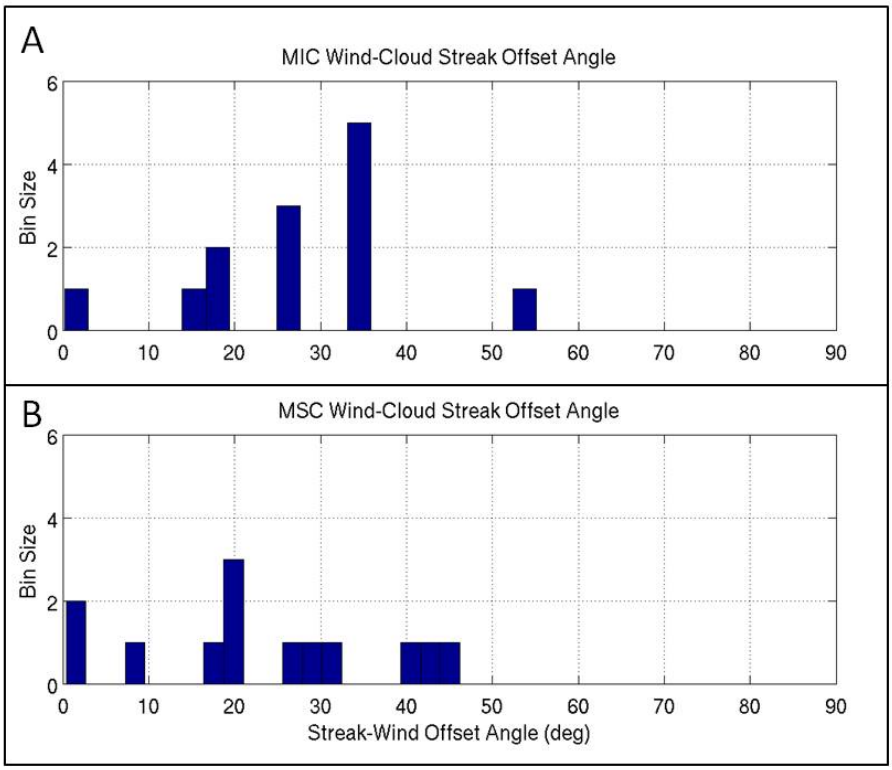

Figure 4.16: Histogram of difference between SWACR-indicated drizzle streak long-axis angle and radiosonde measured averaged sub-cloud wind or in-cloud wind (offset angle) for November 2009 documented drizzle streak events at Graciosa Island, Azores. Bin size represents number of documented cases for a given offset angle.

Horizontal wind shear in the boundary layer has also been utilized to define a minimum threshold for rolls to occur. To determine the influence of PBL shear at Graciosa, surface to PBL-top shear was computed for each case using sounding observations, and is plotted in *Figure 4.17* with respect to wind-roll offset angle. Shear was computed as the vector difference between the surface wind and the PBL-top wind. Despite substantial noise in the result, cases of unbroken streaks trend toward shear values greater than 7.5 x 10^{-3} s^{-1}, while loosely-aligned cases are predominantly clustered below 7.5 x 10^{-3} s^{-1}. Past studies have

shown that higher shear values are associated with rolls in the PBL, and Weckwerth et al. (1997)

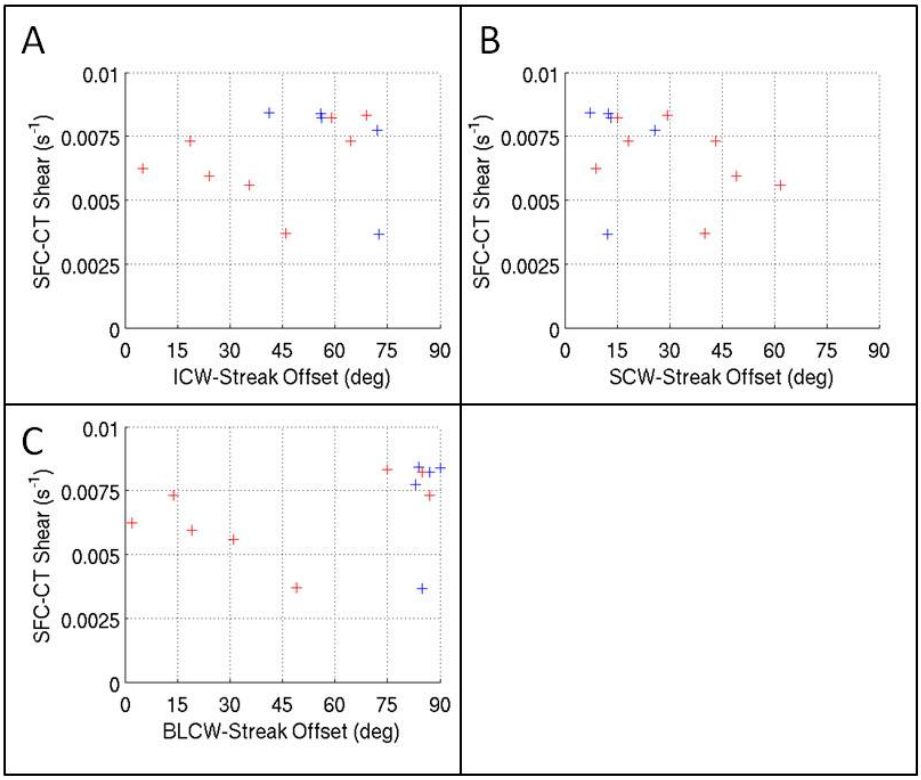

Figure 4.17: Computed surface-to-cloud top shear (s^{-1}) corresponding to drizzle streak-mean in-cloud wind direction offset angle (A), drizzle streak-mean sub-cloud wind direction offset angle (B), and drizzle streak-mean PBL-top wind direction offset angle (C) for November 2009 documented drizzle streak events at Graciosa Island, Azores; presented are unbroken cases (blue) and loosely-aligned cases (red).

suggested a minimum shear of 2 x 10^{-3} s^{-1} to form and sustain coherent roll structures. This criteria was met by all streak cases (*Figure 4.17*). It should be noted that sonde wind data can lead or lag radar data by as much as 3 hours, inciting an unknown amount of error into the analysis of shear correlation. Future field studies utilizing the SWACR and sounding data should consider a higher temporal resolution for sounding launches to better analyze these correlations.

Unbroken cases had a mean offset angle of 18.1° with a mean wind speed of 5.3 ms^{-1}. Loosely-aligned cases had a mean offset angle of 27.5° with a mean wind of 4.9 ms^{-1}. Mean shear values were 7.3 x 10^{-3} s^{-1} for unbroken cases and 6.6 x 10^{-3} s^{-1} for loosely-aligned cases. In general, we conclude that the environment for unbroken rolls exhibit many characteristics of boundary layer rolls, and we can therefore conclude that boundary rolls were occurring at cloud base, and were well documented by the SWACR. The other two cases were not as apparent, though both seem to demonstrate some organized circulations in the PBL that are orienting the drizzle field along a common axis. We propose that the greatest source of error in the results stems from the lower temporal frequency of wind observations relative to the SWACR observations. It should also be noted that all of these cases were instances of drizzle structures (rolls) imbedded in a widespread cloud field, restricting the likelihood of visible satellite detection. The SWACR, however, successfully demonstrated the ability to detect these rolls in the drizzle field to ranges exceeding 10 km from the radar over an extended observation period.

4.3 Determination of Cloud Liquid Water Content in 3D Volumes

Although first-order radar science products (radar reflectivity, cloud fraction, cloud boundaries) can provide important information about marine stratocumulus cloud properties, many second-order products such as cloud liquid water content (LWC) and liquid water path (LWP) derived from radar observations are of great interest to the science community. There have been several concerted efforts in the past to determine LWC from radar reflectivity (e.g. Atlas (1954); Sauvageot and Omar (1987); Fox and Illingworth (1997); Wang and Geerts (2003)) following the fundamental formula:

$$Z = \alpha LWC^{\beta} \tag{4.1}$$

where Z is radar reflectivity (mm^6m^{-3}), LWC is measured liquid water content (gm^{-3}), and α and β are constants. It is important to note that the presence of drizzle in the radar sampling volume greatly reduces the applicability and accuracy of such simple relationships derived analytically or empirically, as these larger drizzle droplets contain substantially less liquid water than that which would be required of cloud droplets to generate similar radar returns. If coinciding LWP measurements are available from a microwave radiometer and the radar reflectivity profile is dominated by cloud-only contributions, the profile of the cloud LWC(h) can be derived using the following formula:

$$LWC(h) = \frac{(LWP * Z(h)^{\frac{1}{2}})}{\sum_{t=1}^{M}(Z(h)^{\frac{1}{2}}\Delta h)} \tag{4.2}$$

where Z(h) is the measured radar reflectivity (mm^6m^{-3}) at each height, Δh is the range gate width (25 m), and M is the number of in-cloud gates (Frisch et al. 1998). Overall, if LWP measurements are available (only in zenith pointing) and drizzle has negligible impact on the measured radar reflectivity, then the technique has demonstrated reasonable success in retrieving the LWC profile. However, in scanning mode, no LWP measurements are available away from zenith. In order to address this limitation, the following approach was followed: First, the vertically pointing measurements (Z(h) and LWP) are used to retrieve the LWC profile using *Eqn.4.2*. Second, regression analysis is applied to the LWC(h)-Z(h) dataset to derive the coefficients in expression *Eqn.4.1*. Finally, the empirically derived LWC = f(Z) relationship (*Eqn.4.1*) is applied to all the SWACR gridded data. This approach was applied at each above-radar range gate for 30 scans in November 2009, where a co-located microwave radiometer provided measurements of LWP. Using the measured reflectivity and estimated in-cloud LWC, we trained an α of 0.0342 and β of 1.2882 for application to *Eqn.4.1*.

Using *Equation 4.1*, LWC could be calculated for the 3D volume; summing for each vertical column, we also can determine column LWP values (*Figure 4.18 a-b*). The apparent presence of high LWC values near the edges of the gridded data is caused by the drop in

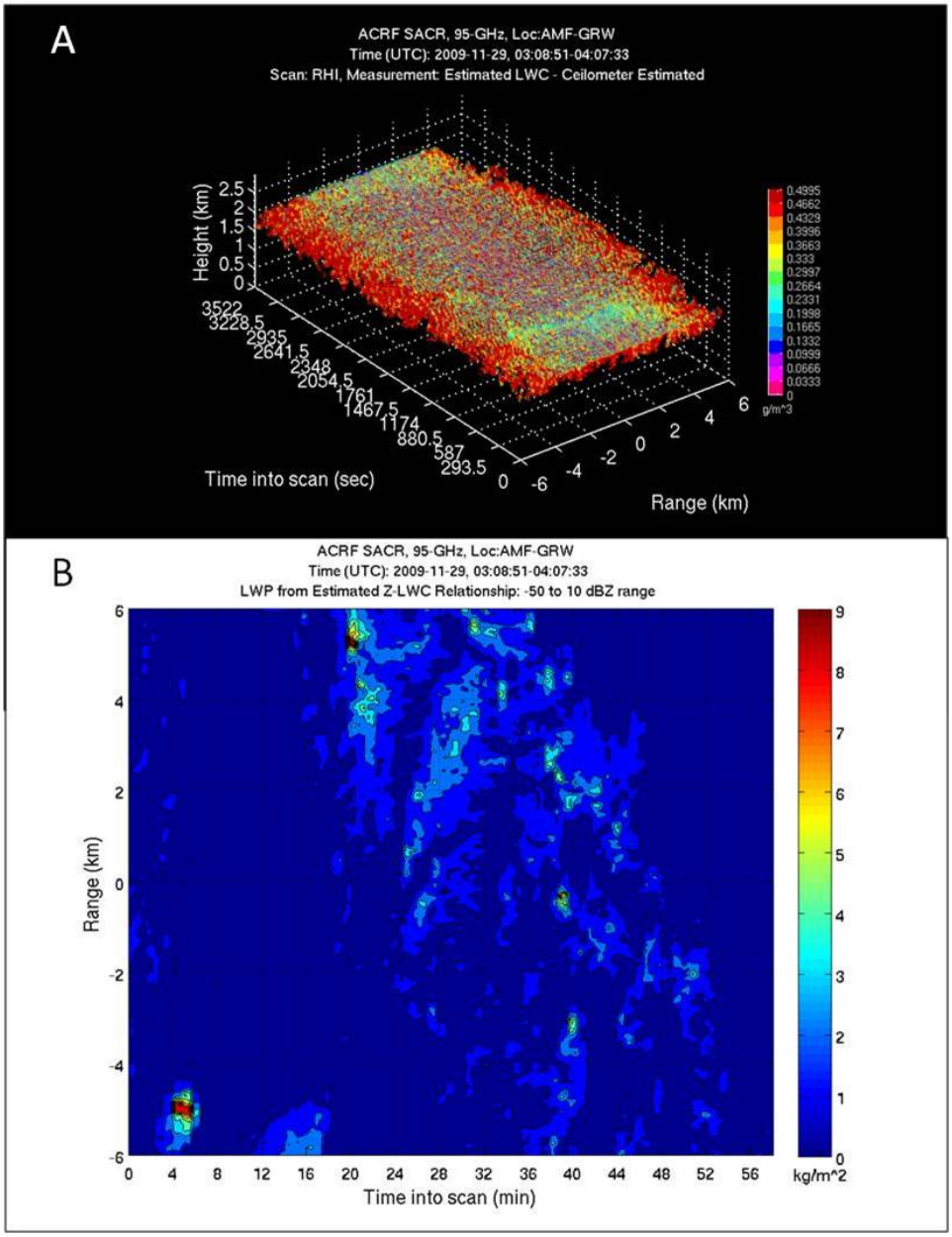

Figure 4.18: SWACR gridded LWC (gm^{-3}) for 2009/11/29 03:08:51-04:07:33 UTC (A) and corresponding summed gridded LWP (kgm^{-2}) at Graciosa Island, Azores. LWC values computed with $\alpha = 0.0342$ and $\beta = 1.2882$ (trained from co-located radiometer).

sensitivity that results from the detection of only high radar reflectivity values, thus biasing the LWC computed values high. No direct verification of the performance of the approach is available; however, we can get some insight on its performance by looking the LWP(x,y) field derived by integrating the LWC(x,y,z) values in each column. Although the values for α and β were trained using local, zenith data it is immediately evident that in certain areas LWP fields are biased abnormally high. These unrealistic values for LWC and LWP computed from the radar reflectivity field demonstrate the difficulties in applying algorithms trained for column measurements to a 3D field and the sensitivity of this retrieval to the presence of drizzle in the radar sampling volume. This is because drizzle particles have a strong radar reflectivity relative to cloud particles, but contribute little to the liquid water content of a cloud. Therefore, an algorithm designed for a cloud-only field will resolve unreasonably high LWC values for these stronger drizzle returns. In addition, the radar sensitivity issue results in a reflectivity field that is biased high at further ranges from the radar, which artificially biases the LWC and LWP field high at distance from the radar.

Chapter 5
Summary

The purpose of this study was to evaluate the observation capabilities of the U.S. Department of Energy (DOE) Atmospheric Radiation Measurement (ARM) Climate Research Facilitys Scanning W-Band (95 GHz) Cloud Radar (SWACR). The SWACR is the first of many scanning cloud radars that the ARM program will deploy at its fixed and mobile sites. These deployments will lead to systematic 3D cloud and precipitation observations and signal a shift from a multi-instrument vertically pointing (soda straw) observation technique to a radar-centric scanning 3D observation technique. Scanning radars have been used for decades for weather monitoring and warning, and the bulk of their volume coverage is based on a sequence of fixed elevation scans (PPI). This approach has been found ineffective for narrow beam cloud radars and cloud detection. This study used data provided from a Cross-Wind Range Height Indicator (CW-RHI) pattern developed for the SWACR. The primary metric of performance for a cloud radar is its ability to detect weak clouds and its high reliability for long-term, unattended operations (Moran et al. 1998). This study focused on the ability of the SWACR to detect not only weak marine stratocumulus clouds, but also drizzle associated with marine stratocumulus for an extended period as part of the CAP-MBL field campaign at Graciosa Island, Azores. In addition to the SWACR, data from the W-Band ARM Cloud Radar (WACR), Vaisala Ceilometer, and Sounding Balloons from the Graciosa campaign were also used for analysis.

Using the calibrated radar reflectivities reported in the data files, we determined that the SWACR radar constant during nominal scanning operations was -42.66 dBZ, and had

absolute sensitivity to -52 dBZ at 1 km range. This information was used to compute the MDS for the SWACR at all ranges from the radar, indicating the amount of sensitivity loss with range for this instrument by virtue of the square of the distance relation.

Overall, the radar performed well in documenting radar reflectivity and cloud characteristics for an extended observation period in November 2009. Over 190 individual CW-RHI scanning periods were analyzed. Radar reflectivity values demonstrated a reduced temporal resolution when compared with WACR observations, but the spatial details of in-cloud and sub-cloud observations away from the zenith column proved a substantial gain over the column observation approach of the WACR. A drizzle mask applied to cloud base measurements revealed several instances of drizzle fields organized into streaks or rolls. Structures were classified as unbroken rolls and loosely-aligned rolls, with 5 and 8 cases documented, respectively. Using sounding wind observations, we found that $\sim$64% of streak cases were aligned within 20° of the mean sub-cloud wind, while just 36% aligned within 20° of the mean in-cloud wind. We concluded, based on these results and past studies, that the mean sub-cloud wind was most directly driving the dynamics controlling the observed rolls. Further results included a minimum wind speed for roll-like formations of 3.9 ms^{-1}, and all roll cases exceeding the shear threshold of 2 x 10^{-3} s^{-1} proposed by Weckwerth et al. (1997). Unbroken cases had a mean sub-cloud wind-streak axis offset angle of 18.1° and a mean wind of 5.3 ms^{-1}, supporting the hypothesis of boundary layer rolls. The study of these streaks also had considerable error and spread in the data; this is thought to be a function of the low temporal resolution of the wind data (6 hours) relative to the scanning speed of the radar ($\sim$30 seconds), wherein wind measurements were extrapolated up to 3 hours from their observed time for study. Other sources of error include the natural variability in the field, as well as the technique used to combine scan-to-scan periods. The latter of these issues can be addressed in future studies by adaptively shifting each individual CW-RHI scan

to account for horizontal advections by the layer wind, creating a fully-Lagrangian (cloud based) viewpoint. This type of shift, coupled with the transform of the time coordinate to a spatial coordinate in the along-wind direction, should resolve the most accurate cloud field possible with this radar scanning technique.

The radar proved a strong ability to document realistic cloud boundaries and cloud fraction to a range of ∼4 km from the radar. Beyond 4 km, the sensitivity loss of the radar severely reduced the ability to document weaker cloud-only features, though drizzle and very large cloud particles could be documented to ranges exceeding 10 km. The overall cloud and drizzle field suggested that many of the sharp cloud boundaries documented in the radar domain were a function of the radar sensitivity; however, the radar documented a strong ability to also document naturally-occurring cloud and drizzle boundaries. Cloud top measurements tended to decrease in height with range, while cloud base measurements tended to increase in height with range. These artificial effects were due to the inability to document small cloud particles at cloud top and cloud base, and an inability to measure small evaporating drizzle droplets at cloud base for far ranges from the radar. For a sampling of six radar volumes representing cloud, light drizzle, and heavy drizzle, three distinct cloud thickness regimes were documented above the radar, and two distinct regimes at 5 km from radar. Cloud thicknesses of ∼250 m, ∼750 m, and ∼1500 m were measured at radar zenith, and were associated with cloud-only, light drizzle, and heavy drizzle cases, respectively; at 5 km, only the drizzle case thicknesses were present. A further climatology of all CW-RHI scanning periods demonstrated a well-distributed cloud thickness regime, with a peak frequency of slightly lower thickness at radar zeith as opposed to 5 km for a -50 dBZ reflectivity threshold; this was due to the inability of the radar to detect weak thin clouds at more than 4 km range. Although the cloud boundaries demonstrated many instances of natural variability, the overall appearance of cloud thinning was primarily an artifact of the

radar due to sensitivity loss and attenuation. Fractional cloudiness was impaired in a similar way with respect to sensitivity and attenuation issues. Natural variations in the strength and spatial extent of drizzle were evident for a reflectivity field limited to -20 dBZ or greater. Heavy drizzle cases generally had more widespread strong drizzle than light drizzle cases, demonstrated by the ability to retain high cloud fraction with a field limited to -15 dBZ with respect to a field limited to -50 dBZ.

The prevalence of drizzle and inability to identify it in the 3D domain, coupled with a loss of low-reflectivity measurements at range due to sensitivity loss, was detrimental to an accurate realization of cloud Liquid Water Content (LWC) and total Liquid Water Path (LWP). A concerted effort was made to utilize the works to Frisch et al. (1998) in application to a 3D domain. Column SWACR data and co-located microwave radiometer data allowed for the determination of an equation relating radar reflectivity to LWC. In general, the greatest source of error was the prevalence of drizzle in the domain biasing measurements to high reflectivity values. A broad reflectivity-based drizzle mask was considered for application to the data, but it was decided that there was not enough observational information to make an accurate drizzle mask for proper retrieval of LWC and LWP. In addition, the widespread prevalence of drizzle during the campaign raises questions to the ability to resolve LWC and LWP with the Graciosa data.

Overall, 3D gridded SWACR reflectivity exhibited a strong enhancement in our understanding of the horizontal extent and structure of uniform and broken marine stratocumulus clouds as they passed over the observation domain. In particular, several distinct regimes were noted, including cloud, broken cloud, cloud-to-drizzle transition, light drizzle, and heavy drizzle. Broken cloud regimes and transitional regimes offered the most gain in horizontal understanding over the column-based technique offered by the WACR, though variations in

all structures exhibited the gains offered by these scanning techniques. In addition, reflectivity values greater than -15 dBZ, the estimated threshold for drizzle, showed distinct streak structures at cloud base in some cases, suggesting the existence of along-wind boundary layer rolls embedded in the cloud structure, enhancing precipitation. Despite these advances, the radar was limited by sensitivity at range from the radar, resulting in an effective range of $\sim$4 km for detection of weak clouds. However, the long-term observational capabilities of this radar, combined with sensitivity to weak clouds at closer ranges, meet the base ARM metrics of success for the instrument and poses a significant gain for GCMs in modeling boundary layer cloud and drizzle structures. Though not addressed in this study, the radar can adequately measure velocity and spectrum width fields, though new approaches need to be developed to isolate individual parts of these fields such as vertical velocity and differential fall speed contributions to the spectrum width. The isolation of these types of fields will aid in creating 3D drizzle masks, further enhancing our ability to derive second-order products such as LWC and LWP with reasonable accuracy. The Scanning W-Band Cloud Radar provides an exciting new technology to apply toward a better understanding of lower tropospheric clouds and their radiative properties. Its ability to provide a three dimensional field of cloud observations can push the science toward the desired regional understanding required for advancing Global Climate Models. This study has demonstrated some of the gains and losses associated with this radar and its gridded data, and further development of the techniques used to analyze this data will certainly yield greater advances in the understanding of marine stratocumulus and other low clouds.

Bibliography

Ackerman, T. and G. Stokes, 2003: The atmospheric radiation measurement program. *Physics Today*, **56**, 38–44.

Albrecht, B., 1989: Aerosols, cloud microphysics, and fractional cloudiness. *Science*, **245**, 1227–1230.

Albrecht, B., C. Bretherton, D. Johnson, W. Scubert, and A. Frisch, 1995a: The atlantic stratocumulus transition experiment – astex. *Bulletin of the American Meteorological Societ*, **76**, 889–904.

Albrecht, B., M. Jensen, and W. Syrett, 1995b: Marine boundary layer structure and fractional cloudiness. *Journal of Geophysical Research*, **100 (D7)**, 14 209–14 222.

Albrecht, B., D. Randall, and S. Nicholls, 1988: Observations of marine stratocumulus clouds during fire. *Bulletin of the American Meteorological Society*, **69 (6)**, 618–626.

Anagnostou, E. N., C. A. Morales, and T. Dinku, 2001: The use of trmm precipitation radar observations in determining ground radar calibration biases. *Journal of Atmospheric and Oceanic Technology*, **18**, 616–628.

Atlas, D., 1954: The estimation of cloud parameters by radar. *Journal of Meteorology*, **11**, 309–317.

Baeck, M. L. and J. A. Smith, 1998: Rainfall estimation by the wsr-88d for heavy rainfall events. *Weather and Forecasting*, **13**, 416–436.

Bretherton, C., et al., 2004: The epic 2001 stratocumulus study. *Bulletin of the American Meteorological Society*, **85**, 967–977.

Brown, R., 1980: Longitudinal instabilities and secondary flows in the planetary boundary layer: A review. *Reviews of Geophysics and Space Physics*, **18 (3)**, 683–697.

Clothiaux, E., M. Miller, B. Albrecht, T. Ackerman, J. Verlinde, D. Babb, R. Peters, and W. Syrett, 1995: An evaluation of a 94-ghz radar for remote sensing of cloud properties. *Journal of Atmospheric and Oceanic Technology*, **12**, 201–229.

Clothiaux, E. E., T. P. Ackerman, G. G. Mace, K. P. Moran, R. T. Marchand, M. A. Miller, and B. E. Martner, 2000: Objective determination of cloud heights and radar reflectivities using a combination of active remote sensors at the arm cart sites. *Journal of Applied Meteorology*, **39**, 645–665.

Cressman, G. P., 1959: An operational objective analysis system. *Monthly Weather Review*, **87 (10)**, 367–374.

Doviak, R. J. and D. S. Zrnic, 1993: *Doppler Radar and Weather Observations*. Second edition ed., Dover Publications, Inc., Mineola, New York.

Fox, N. and A. Illingworth, 1997: The retrieval of stratocumulus cloud properties by ground-based cloud radar. *Journal of Applied Meteorology*, **36**, 485–492.

Frisch, A., R. Chadwick, W. Moninger, and J. Young, 1976: Observations of boundary-layer convective cells measured by dual-doppler and echosonde, and by microbarograph array. *Boundary-Layer Meteorology*, **10**, 55–68.

Frisch, A., C. Fairall, and J. Snider, 1995: Measurements of stratus cloud and drizzle parameters in astex with a ka-band doppler radar and a microwave radiometer. *Journal of the Atmospheric Sciences*, **52**, 2788–2799.

Frisch, A., G. Feingold, C. Fairall, T. Uttal, and J. Snider, 1998: On cloud radar and microwave radiometer measurements of stratus cloud liquid water profiles. *Journal of Geophysical Research*, **103**, 23 195–23 197.

Harrison, D., S. Driscoll, and M. Kitchen, 2000: Improving precipitation estimates from weather radar using quality control and correction techniques. *Meteorological Applications*, **6**, 135–144.

Harrison, E., P. Minnis, B. Barkstrom, V. Ramanathan, R. Cess, and G. Gibson, 1990: Seasonal variation of cloud radiative forcing derived from the earth radiation budget experiment. *Journal of Geophysical Research*, **95**.

Keenan, T., 2003: Hydrometeor classification with a c-band polarimetric radar. *Australian Meteorological Magazine*, **53**, 23–31.

Klein, S. and D. Hartmann, 1993: The seasonal cycle of low stratiform clouds. *Journal of Climate*, **6**, 1587–1606.

Kollias, P. and B. Albrecht, 2000: The turbulence structure in a continental stratocumulus cloud from millimeter wavelength radar observations. *Journal of Atmospheric Science*, **57**, 2417–2434.

Kollias, P., E. Clothiaux, B. Albrecht, M. Miller, K. Moran, and K. Johnson, 2005: The atmospheric radiation measurement program cloud profiling radars: An evaluation of signal processing and sampling strategies. *Journal of Atmospheric and Oceanic Technology*, **22**, 930–948.

Kollias, P., E. Clothiaux, M. Miller, B. Albrecht, G. Stephens, and T. Ackerman, 2007: Millimeter-wavelength radars: New frontier in atmospheric cloud and precipitation research. *Bulletin of the American Meteorological Society*, **88 (10)**, 1608–1624.

Kollias, P., C. Fairall, P. Zuidema, J. Tomlinson, and G. Wick, 2004: Observations of marine stratocumulus in se pacific during the pacs 2003 cruise. *Geophysical Research Letters*, **31**, 22110, doi:10.1029/2004GL010751.

Kollias, P., J. Rémillard, E. Luke, and W. Szyrmer, 2011: Cloud radar doppler spectra in drizzling stratiform clouds: 1. forward modeling and remote sensing applications. *Journal of Geophysical Research*, **116 (D13201)**, 1–14, doi:10.1029/2010JD015237.

Kropfli, R. and P. Hildebrand, 1980: Three-dimensional wind measurements in the optically clear planetary boundary layer with dual-doppler radar. *Radio Science*, **15 (2)**, 283–296.

Kuettner, J. P., 1971: Cloud bands in the earth's atmosphere: Observations and theory. *Tellus XXIII*, **4**.

LeMone, M., 1973: The structure and dynamics of horizontal roll vorticies in the planetary boundary layer. *Journal of the Atmospheric Sciences*, **30**, 1077–1091.

Leon, D., Z. Wang, and D. Liu, 2008: Climatology of drizzle in marine boundary layer clouds based on 1 year of data from cloudsat and cloud-aerosol lidar and infrared pathfinder satellite observations (calipso). *Journal of Geophysical Research*, **113 (D00A14)**, 1–15, doi:10.1029/2008JD009835.

Liebe, H. J., 1985: An updated model for millimeter wave propagation in moist air. *Radio Science*, **20 (5)**, 1069–1089.

Liu, Y., B. Geerts, M. Miller, P. Daum, and R. McGraw, 2008: Threshold radar reflectivities for drizzling clouds. *Geophysical Research Letters*, **35**, 1–5, doi:10.1029/2007GL031201.

Löhnert, U., S. Crewell, and C. Simmer, 2001: Profiling cloud liquid water by combining active and passive microwave measurements with cloud model statistics. *Journal of Atmospheric and Oceanic Technology*, **18**, 1354–1366.

Lohou, F., B. Campistron, A. Druilhet, P. Foster, and J. Pages, 1998: Turbulence and coherent organizations in the atmospheric boundary layer: a radar-aircraft experimental approach. *Boundary-Layer Meteorology*, **86**, 147–179.

Moran, K. P., B. E. Martner, M. Post, R. A. Kropfli, D. C. Welsh, and K. B. Widener, 1998: An unattended cloud-profiling radar for use in climate research. *Bulletin of the American Meteorological Society*, **79 (3)**, 443–455.

Ramanathan, V., R. Cess, E. Harrison, P. Minnis, B. Barkstrom, E. Ahmad, and D. Hartmann, 1989: Cloud-radiative forcing and climate: Results from the earth radiation budget experiment. *Science*, **243 (4887)**, 57–63.

Sauvageot, H. and J. Omar, 1987: Radar reflectivity of cumulus clouds. *Journal of Atmospheric and Oceanic Technology*, **4**, 264–272.

Schumann, U. and C.-H. Moeng, 1991: Plume fluxes in clear and cloudy convective boundary layers. *Journal of the Atmospheric Sciences*, **48 (15)**, 1746–1757.

Serpetzoglou, E., B. Albrecht, P. Kollias, and C. Fairall, 2008: Boundary layer, cloud, and drizzle variability in the southeast pacific stratocumulus regime. *Journal of Climate*, **21**, 6191–6214.

Stevens, B., G. Vali, K. Comstock, R. Wood, M. C. vanZanten, P. H. Austin, C. S. Bretherton, and D. H. Lenschow, 2005: Pockets of open cells and drizzle in marine stratocumulus. *Bulletin of the American Meteorological Society*, **86 (1)**, 51–57, doi:10.1175/BAMS-86-1-51.

Stokes, G. and S. Schwartz, 1994: The atmospheric radiation measurement (arm) program: Programmatic background and design of the cloud and radiation test bed. *Bulletin of the American Meteorological Society*, **75 (7)**, 1201–1221.

Takano, T., et al., 2010: Development and performance of the millimeter-wave cloud profiling radar at 96 ghz: Sensitivity and spatial resolution. *Electronics and Communications in Japan*, **93 (3)**, 42–49.

vanZanten, M., B. Stevens, G. Vali, and D. Lenschow, 2005: Observations of drizzle in nocturnal marine stratocumulus. *Journal of the Atmospheric Sciences*, **62**, 88–106.

Wackerman, C. C., C. L. Rufenach, R. A. Shuchman, J. A. Johannessen, and K. L. Davidson, 1996: Wind vector retrieval using ers-1 synthetic aperture radar imagery. *IEEE Transactions on Geoscience and Remote Sensing*, **34 (6)**, 1343–1352.

Wang, J. and B. Geerts, 2003: Identifying drizzle within marine stratus with w-band radar reflectivity. *Atmospheric Research*, **69**, 1–27, doi:10.1016/j.atmosres.2003.08.001.

Weckwerth, T. M., J. W. Wilson, R. M. Wakimoto, and N. A. Crook, 1997: Horizontal convective rolls: Determining the environmental conditions supporting their existence and characteristics. *Monthly Weather Review*, **125**, 505–526.

White, A., C. Fairall, A. Frisch, B. Orr, and J. Snider, 1996: Recent radar measurements of turbulence and microphysical parameters in marine boundary layer clouds. *Atmospheric Research*, **40**, 177–221.

White, A. B., J. R. Jordan, B. E. Martner, F. M. Ralph, and B. W. Bartram, 2000: Extending the dynamic range of an s-band radar for cloud and precipitation studies. *Journal of Atmospheric and Oceanic Technology*, **17**, 1226–1234.

Widener, K. and K. Johnson, 2006: W-band arm cloud radar (wacr) handbook. Doe-arm.

Wood, R., 2009: Clouds, aerosol, and precipitation in the marine boundary layer (cap-mbl) science plan for the 2009/2010 deployment of the arm mobile facility to graciosa island, the azores, ne atlantic. DOE/SC-ARM 02.

Wood, R. and C. Bretherton, 2006: On the relationship between stratiform low cloud cover and lower-tropospheric stability. *Journel of Climate*, **19**, 6425–6432, doi: 10.1175/JCLI3988.1.

Zecchetto, S., P. Trivero, B. Fiscella, and P. Pavese, 1998: Wind stress structures in the unstable marine surface layer detected by sar. *Boundary-Layer Meteorology*, **86**, 1–28.